
Increasing Phase Transformation Rate in Advanced High Strength Steel Applications

Dissertation
zur Erlangung des Grades
des Doktors der Ingenieurwissenschaften
der Naturwissenschaftlich-Technischen Fakultät
der Universität des Saarlandes

von
Farnoosh Forouzan
Saarbrücken
2019

Tag des Kolloquiums: 10. Mai 2019
Dekan: Prof. Dr. Gregor Jung
Berichterstatter: Prof. Dr.-Ing. Frank Mucklich
Prof. Dr.-Ing. Christian Boller
Prof. Dr. Esa Vuorinen
Vorsitz: Prof. Dr. Marta-Lena Antti
Akad. Mitarbeiter: Dr.-Ing. Flavio Soldera
Weitere Mitglieder: Prof. Dr. Maria Santofimia Navarro
Prof. Dr. Annika Borgenstam
Prof. Dr. David Porter

To my Family

Preface

This work is accomplished within the framework of the joint Ph.D. project in the European School of Materials (EUSMAT) through the Doctoral Programme in Materials Science and Engineering (DOCMASE) between January 2015 to January 2019.

It has been carried out under the supervision of Associate professor Dr. Esa Vuorinen at Luleå University of Technology as the main supervisor and Prof. Dr.-Ing. Frank Mücklich at Saarland University as the second university.

This work has been focused on study of the Quenching and Partitioning (Q&P) process by assessing involved mechanisms, microstructure and mechanical properties, aiming at an acceleration of phase transformation rate to shorten the process time in addition to improving properties in service to the industry.

A part of the work has been performed together with students in different case study projects during these 4 years, who are mentioned as co-authors of different journal or conference papers.

The results acquired have been presented in peer-review scientific journals, which are appended at the end of this book.

Farnoosh Forouzan
Jan 2019, Luleå

Popular Science Summary

Demands from society and industry to develop lighter components in order to reduce the required energy and environmental impact of specially vehicles and equipment subjected to moving, have resulted in a huge interest in development and improvement of advanced high strength steels (AHSS). Enhancement of the merit indexes as yield strength/density ($R_{0.2}/\rho$) ratio in addition to other properties of importance for the specific application, is the principle goal in this strive.

In this work, one low-carbon low-silicon and one high-carbon high-silicon steel were subjected to a special heat treatment named as “Quenching and Partitioning” (Q&P). The main goal was to use the Q&P technique to produce ultra-high strength steels with their required properties in a very short time. Besides, this technique has been tested directly after laser welding and in these tests not only reduced the risk of brittle martensite formation but also shortened the post welding treatment time in comparison with regular methods.

To evaluate the feasibility, limitations and advantages of this method, the microstructural evolution, as well as mechanical properties of the samples were investigated. The promising results have shown that this method can be applied successfully for different applications and save a lot of time, cost and energy.

Populärvetenskaplig sammanfattning

Krav som ställs av samhället och industrin på utveckling av lättare komponenter för framför allt fordon men även annan rörlig utrustning har medfört ett stort intresse för utveckling och förbättring av existerande avancerade höghållfasta stål (AHSS) i syfte att minska energiförbrukning och miljöpåverkan. Målet är att förbättra olika materialindex som kvoten mellan förlängningsgräns och densitet [$R_{p0.2}/\rho$] eller egenskaper som utmattningshållfasthet, allt efter vad som är viktigast för den specifika tillämpningen.

I detta arbete har ett lågkolhaltigt stål med låg kiselhalt och ett högkolhaltigt stål med hög kiselhalt utsatts för värmebehandlingsmetoden ”quenching and partitioning” (Q&P), vilket blir ungefär ”släckning och omfördelning” på svenska. Huvudsyftet har varit att utveckla ultrahöghållfasta stål som uppfyller de krav som ställs på dessa genom en process som är betydligt snabbare än vad som vanligtvis är möjligt. Därtill så har den föreslagna tekniken testats i direkt anslutning till lasersvetsning och då inte enbart gett en minskad risk för bildning av spröd martensit utan även en betydligt kortare behandlingstid efter svetsningen.

För att utvärdera teknikens möjligheter, begränsningar och fördelar har mikrostrukturförändringar och de mekaniska egenskaperna för materialen undersökts. De lovande resultaten har visat att denna behandlingsmetod (Q&P) kan användas på ett framgångsrikt sätt för olika applikationer och genom det kan man spara tid, kostnader och energi.

Populäre Wissenschaftszusammenfassung

Steigende Anforderungen seitens der Gesellschaft und Industrie, leichtere Werkstoffe zu entwickeln, um deren Auswirkungen auf Energieverbrauch und Umwelteinfluss zu reduzieren, führten zu einem großen Interesse, hochfeste unlegierte Stähle (Advanced High Strength Steels – AHSS), zu entwickeln und verbessern. Das Hauptziel dieser Arbeit ist die Erhöhung von Leistungsindikatoren wie der spezifischen Festigkeit (Fließspannung $R_{0,2}$ /Dichte ρ) zusätzlich zu anderen einsatzabhängigen Eigenschaften.

In der vorliegenden Arbeit wurden jeweils ein niedrigkohliges siliziumarmes und ein hochkohliges siliziumreiches Stahl einem Prozess namens „Quenching and Partitioning“ (Q&P) unterworfen. Das Hauptziel war, die Erzeugung ultra-hochfester Stähle mittels Q&P-Prozess mit den geforderten Eigenschaften nach kurzen Prozesszeiten zu erreichen. Daneben wurde diese Technik direkt im Anschluss an Laserschweißen angewendet und es wurde gezeigt, dass nicht nur das Risiko der Bildung spröden Martensits reduziert wurde, sondern auch die Nachbearbeitungszeit insgesamt im Vergleich zum regulären Schweißen verringert werden konnte.

Die Untersuchung der Mikrostrukturentwicklung sowie der mechanischen Eigenschaften hergestellter Proben dienten dazu, die Anwendbarkeit, Grenzen und Vorteile dieser Prozessmethode zu evaluieren. Die Ergebnisse haben gezeigt, dass der Q&P-Prozess erfolgreich für mannigfaltige Anwendungen geeignet ist und ein großes Einsparungspotential für Zeit, Kosten und Energie hat.

Acknowledgment

This thesis would never have been possible to accomplish without the support, guidance, motivation, and encouragement of many people.

First, I would like to express my gratitude to my principal supervisor Prof. Esa Vuorinen at LTU, who has taught me a lot in materials science and also in life. You allowed me to develop myself as an independent researcher in the best possible way. You are always kind, patient and open for long fruitful discussions about steels! I would also like to sincerely acknowledge Prof. Marta-Lena Antti, although she was my supervisor only the first year of my Ph.D., she supported me all these four years of study.

I greatly appreciate my second supervisor Prof. Frank Mücklich at Saarland University and Dr. Flavio Soldera for their support before starting my Ph.D. till now and your kind hospitality when I was in Saarbrücken, Germany.

I am grateful of EUSMAT organization who gave me this opportunity to start my Ph.D. in Europe, in the fantastic family of DocMASE.

Special thanks to Lars Frisk and Johnny Grahn for their daily help and guidance with a kind smile! Your kind support is invaluable.

I am thankful to all colleagues and friends at the division of Materials Science at LTU and the chair of functional materials at UDS for providing a pleasant work environment. Special thanks to Pia Åkerfeldt, Rosa Pineda, Johannes Webel, Agustina Guitart, Dominik Britz, Ali Hedayati, Luciano Borasi, Per Rubin, Prof. Erik Navara and Prof. Sir Harry Bhadeshia for all your assistance, productive discussions, nice criticizes and useful recommendations.

In addition, the heartfelt thanks go to my old supervisors at Isfahan University of Technology, Prof. Kermanpur, Prof. Nirumand and Prof. Najafizadeh, for all their kind support and unforgettable lessons that they taught me and my dearest friends in Iran and Sweden for keeping company through all these years which brightened my dark nights and kept my heart warm!

I would like to thank my family for their endless love, encouragement, and support; my beloved wonderful Mom, my kind sister Sholeh, and brothers Mohammad Reza and Amir Reza and fantastic family of Ali, who always supports us by their great heart. Undoubtedly, I could not have done this without you.

Finally, I would like to express my deepest and dearest gratitude to my beloved Ali. Nothing could be done without your endless love and support. Thank you for helping me in every single second of my Ph.D. Thank you, my wonderful Armin! I am very happy to have you, you grew up during the years that I worked on this thesis. Thank you for all your smiles and the happiness that you brought to our life.

Contents

1	Introduction	25
1.1	Development of Advanced High Strength Steels (AHSS)	25
1.2	Strengthening Mechanisms	27
1.3	Development Methods for 3rd Generation AHSS	28
1.3.1	Improvement of Dual Phase (DP) Steels	28
1.3.2	Modified TRIP Steels	28
1.3.3	Ultrafine Carbide Free Bainite (CFB)	29
2	Quenching and Partitioning	31
2.1	Chemical Composition of Q&P steels	32
2.2	Overview of mechanisms in the Q&P process	34
2.2.1	Martensite formation	37
2.2.2	Martensite morphology	38
2.2.3	Stability of retained austenite	40
2.3	Constrained carbon equilibrium (CCE) model	40
3	Scope of the present work	43
3.1	The increase of phase transformation rate	44
3.2	Using Q&P in industrial applications	46
3.2.1	Press Hardening	46
3.2.2	Welding	47
3.2.3	Bearing steels	49
3.3	Objectives	49
4	Materials and Methods	51
4.1	Materials	51
4.2	Heat Treatment	53
4.2.1	Q&P treatment of Domex 960	54
4.2.2	Q&P treatment of 06CV	55

4.3	Material characterization techniques.....	58
4.3.1	Light Optical Microscopy.....	58
4.3.2	Microhardness.....	59
4.3.3	SEM, EDX, and EBSD	59
4.3.4	XRD Analysis.....	60
4.3.5	Charpy-V impact toughness	60
4.3.6	Tensile Testing	60
5	Results and discussion:	63
5.1	Thermal Treatments:	63
5.2	Microstructure.....	64
5.2.1	The microstructure of Domex 960	64
5.2.2	The microstructure of 06CV	66
5.3	Mechanical properties.....	68
5.3.1	Mechanical properties of Domex 960	68
5.3.1	Mechanical properties of 06CV	69
6	Summary of appended papers	71
7	Conclusions and Future work.....	77
7.1	Imporant conclusions.....	77
7.2	Future work	79
8	References	81

Appended papers:

Paper I.....	
Paper II.....	
Paper III.....	
Paper IV.....	
Paper V.....	

Abstract

The bainite transformation rate has been shown to increase by starting the heat treatment with partial martensite transformation after austenitization. Based on this fact, a process very similar to “Quenching and Partitioning” (Q&P) is used to produce a fine-grained complex microstructure of martensite, bainite and retained austenite with outstanding mechanical properties in a very short time. During this process, different mechanisms including bainite transformation, carbon partitioning, carbide precipitation, grain growth may occur. All these mechanisms can affect the mechanical properties such as strength, ductility and toughness. Investigation of the different mechanisms influencing the properties and subsequent optimization of these is important. In this work, different mechanisms of the Q&P heat treatment process and its practical industrial applications have been investigated.

Firstly, the implementation of a Q&P method directly after laser welding for a few seconds to substitute any post welding treatment has been studied. To investigate the feasibility, limitations, and advantages of this method for a low-carbon low-silicon high strength steel, the microstructure and mechanical properties by both modelling and experimental approach were studied. Promising results show that this method can decrease the ordinary post-welding treatment time from a few minutes to a few seconds, and in addition improve the mechanical properties of the fusion zone and the heat affected zone to the same or even higher values in comparison with the base material.

In the second part of this work, the effect of quenching and partitioning on the microstructure and mechanical properties of a high carbon steel has been studied. The aim with this part was to optimize the phase transformation rate for production of ultra-high strength steel by controlling its microstructural evolution. The results show that it is possible to get good strength values also for high carbon steels by Q&P treatment. In addition, the approach with process control maps can give a good overview of which properties can be achieved by this method. Hardness value of over 700 HV, and tensile strength of up to 2.5 GPa with a relatively good ductility of 4–6% has been achieved by quenching

to room temperature and partitioning for less than one minute at 400 °C resulting in a microstructure consisting of martensite and retained austenite. In a nutshell, the approach to bainite transformation with pre-existing martensite shorten the processing time for development of advanced high strength steels significantly. This method is also possible to be used in industrial processes as in welding.

Keywords: Advanced high strength steel; Quenching and partitioning; Welding

Sammanfattning

Omvandlingen av austenit till bainit kan påskyndas genom att inleda värmebehandlingen genom att först omvandla en del av austeniten till martensit. Baserad på detta faktum, har en process som är mycket lik den så kallade ”Snabbkylning och Omfördelningen” (“Quenching and Partitioning”, (Q&P)) använts för att skapa en finkornig komplex mikrostruktur bestående av martensit, bainit och restaustenit med utmärkta mekaniska egenskaper på mycket kort tid. Under denna process kan olika mekanismer innefattande bainitomvandling, kolomfördelning, karbidutskiljning och korntillväxt förekomma. Dessa kan påverka de mekaniska egenskaperna som hållfasthet, duktilitet och seghet. En undersökning av de olika mekanismerna som påverkar egenskaperna och den efterföljande optimeringen av dessa är viktig. I detta arbete har olika mekanismer som påverkar Q&P värmebehandlingsprocessen och dess praktiska industriella tillämpningar undersökts.

I första delen av detta arbete har med denna utgångspunkt implementeringen av en Q&P metod direkt efter lasersvetsning för några sekunder för att ersätta andra efterbehandlingsmetoder studerats. För att studera möjligheterna, begränsningarna och fördelarna av denna metod för ett lågkolhaltigt höghållfast stål med låg kiselhalt har mikrostrukturen och de mekaniska egenskaperna studerats genom såväl modellering som experimentellt. Resultaten är lovande och visar att den vanliga efterbehandlingstiden kan minskas från några minuter till några få sekunder, och därtill kan de mekaniska egenskaperna för den smälta zonen och den värmepåverkade zonen förbättras och kan vara lika bra eller till och med bättre i jämförelse med grundmaterialet.

I den andra delen av detta arbete har effekten av Q&P på mikrostrukturen och de mekaniska egenskaperna för ett högkolhaltigt stål studerats. Målet med denna del var att optimera omvandlingshastigheten för att tillverka ultrahöghållfast stål genom att styra mikrostrukturens utveckling. Resultaten visar att det är möjligt att erhålla goda hållfasthetsegenskaper även för högkolhaltiga stål genom Q&P behandling. Därtill, ger ansatsen med processtyrningskartor en bra översikt över vilka egenskaper som kan erhållas med denna metod. Hårdhetsvärde på över 700 HV och brottgräns

på upp till 2.5 GPa med relativt god duktilitet på 4-6 % har erhållits genom snabbkyllning till rumstemperatur och omfördelning vid 400 °C under mindre än en minut resulterade i en mikrostruktur bestående av martensit och restaustenit.

I ett nötskal kan ansatsen att genomföra bainitomvandling med hjälp av en viss andel martensit som skapas i förväg förkorta tiden avsevärt för processer för att utveckla avancerade höghållfasta stål. Metoden är också möjlig att använda för industriella processer som svetsning.

Keywords: Advanced high strength steel; Quenching and partitioning; Svetsning

Zusammenfassung

Die Rate, mit der Austenit zu Bainit umwandelt, wurde erhöht, wenn bereits teilweise Martensit nach der Austenitisierung gebildet wurde. Basierend darauf wurde ein Prozess entwickelt, der sehr ähnlich mit dem „Quenching & Partitioning“-Prozess ist und der mit kurzer Prozesszeit ein feines und komplexes Stahlgefüge bestehend aus Martensit, Bainit und Restaustenit mit exzellenten mechanischen Eigenschaften produziert. Während dieses Prozesses treten mehrere Mechanismen auf, unter anderem die Bainitumwandlung, Kohlenstoffpartitionierung, Karbidausscheidung und Kornwachstum. All diese Mechanismen beeinflussen die mechanischen Eigenschaften wie Festigkeit, Duktilität und Zähigkeit. Die Untersuchung und anschließende Optimierung dieser Wirkweisen hinsichtlich der genannten Eigenschaften sind sehr wichtig. In der vorliegenden Arbeit wurden die verschiedenen Mechanismen des Q&P-Prozesses auf ihre industrielle Anwendbarkeit hin untersucht.

Als erstes wurde der Einsatz von Q&P über wenige Sekunden direkt nach dem Laserschweißen untersucht, um jegliche Schweißnachbehandlungen zu ersetzen. Sowohl Modellierung, als auch Charakterisierung der entstehenden Mikrostruktur und der mechanischen Eigenschaften eines niedrigkohligen siliziumarmen hochfesten Stahls wurden herangezogen, um die Anwendbarkeit, Grenzen und Vorteile dieser Methode zu untersuchen. Die Ergebnisse zeigen, dass diese Methode die Schweißnachbearbeitungszeit, die üblicherweise mehrere Minuten beträgt, auf Sekunden reduzieren kann. Zusätzlich werden die mechanischen Eigenschaften der Schweißzone und der Wärmeeinflusszone derart verbessert, dass sie den Level des Ausgangsstahls erreichen oder sogar übersteigen.

Im zweiten Teil wird der Einfluss von Q&P auf die Mikrostruktur und mechanischen Eigenschaften eines hochkohligen Stahls untersucht. In diesem Fall war das Ziel die Optimierung der Umwandlungsrate zur Erzeugung eines ultra-hochfesten Gefüges. Es zeigte sich, dass auch für hochkohlige Stähle gute Festigkeitswerte mittels Q&P erzeugt werden können. Darüber hinaus liefern Karten zur Prozesskontrolle eine gute Übersicht, welche Eigenschaften durch diese Methode erzielt werden

können. Härtewerte über HV700, und Zugfestigkeiten bis zu 2,5 GPa mit verhältnismäßig guten Duktilitäten von 4-6 % wurden erreicht, indem auf Raumtemperatur abgeschreckt („Quenching“) und für weniger als eine Minute bei 400 °C gehalten wurde („Partitioning“). Das resultierende Gefüge bestand daraufhin aus Martensit und Restaustenit. Zusammengefasst lässt sich die Prozesszeit deutlich verkürzen, wenn die Bainitumwandlung in einem Gefüge der Austenit bereits teilweise zu Martensit umgewandelt ist. Diese Methode besitzt daher auch großes Potential bei der Anwendung in industriellen Schweißprozessen.

Keywords: Advanced high strength steel; Quenching and partitioning; Schweißen

Appended Papers

Paper I:

F. Forouzan; S. Gunasekaran; A. Hedayati, E. Vuorinen; F. Mücklich, "*Microstructure Analysis and Mechanical Properties of Low Alloy High Strength Quenched and Partitioned Steel*", **Solid State Phenomena**, 258, 574-578, 2017.

Paper II:

F. Forouzan, E. Vuorinen, F. Mücklich, "*Post weld-treatment of laser welded AHSS by application of quenching and partitioning technique.*", **Materials Science and Engineering: A.**, 698, 174-182, 2017.

Paper III:

F. Forouzan, A. Guitar, E. Vuorinen, F. Mücklich, "*Effect of carbon partitioning, carbide precipitation and grain size on brittle fracture of Ti-alloyed steel during welding and Q&P process*", **Metals** 8 (10), 747, 2018.

Paper IV:

F. Forouzan, L. Borasi, E. Vuorinen, F. Mücklich, "*Optimization of quenching temperature to minimize the micro segregation induced banding phenomena in quenching and partitioning (Q&P) steels*", **Steel Research International**, 90 (1), Article ID 1800281, 2019.

Paper V:

F. Forouzan, L. Borasi, E. Vuorinen, F. Mücklich, "*Process Control Maps to Design an Ultra-High Strength-Ductile Steel*", under review in **Materials Science and Technology**, Accepted for Publication, May 2019.

Conference Contributions

1. **F. Forouzan**, L. Borasi, E. Vuorinen, F. Mücklich, “*Effect of Mn and Cr micro segregation on microstructure after quenching and partitioning*”, THERMEC2018, July 8–13, **2018**, Paris, France.
2. **F. Forouzan**; H. Zhang, E. Vuorinen, F. Mücklich, “*Study of The Kinetics of Precipitation in an AHSS steel after Laser Welding and Quenching and Partitioning*”, International Materials Research Meeting in The Greater Region, April 6–7, **2017**, Saarbrücken, Germany.
3. **F. Forouzan**; E. Vuorinen, F. Mücklich, “*Application of Quenching and Partitioning Process on Advanced High Strength Steels*” LIGHTer International Conference, Nov 21–22, **2017**, Gothenburg, Sweden.
4. **F. Forouzan**; N. Strandqvist; E. Vuorinen; E. Navara, F. Mücklich,” *Effect of Tempering on Microstructure and Mechanical Properties of Laser Welded and Post-Weld Treated AHSS Specimens*”, 16th International Symposium on Metallography and Materials Science, Stará Lesná, High Tatra Mountains, Slovak Republic, April 20–22, **2016**.
5. **F. Forouzan**; S. Gunasekaran; A. Hedayati, E. Vuorinen; F. Mücklich,” *Microstructure Analysis and Mechanical Properties of Low Alloy High Strength Quenched and Partitioned Steel*”, 8th International Conference on Materials Structure & Micromechanics of Fracture, Brno, Czech Republic, June 27–29, **2016**.

Abbreviations

AHSS	Advanced High Strength Steel
B	Bainite
BCC	Body-Centered Cubic
BCT	Body-Centered Tetragonal
CCE	Constrained carbon equilibrium
CFB	Carbide Free Bainite
CP	Complex Phase
DP	Dual Phase
EBSD	Electron Back Scattered Diffraction
FCC	Face Centered Cubic
FM	Fresh Martensite
HSLA	High strength low alloyed
K-S	Kurdjumov-Sachs relation
L-IP	Lightweight steels with induced plasticity
LOM	Light optical microscope
M	Martensite
M_f	Martensite finish temperature
M_s	Martensite start temperature
Pct.	Percent
PT	Partitioning Temperature
Pt	Partitioning time
Q&P	Quenching and Partitioning
QT	Quenching Temperature
RA	Retained Austenite
SEM	Scanning Electron Microscopy
SIP	Shear band strengthened
TM	Tempered Martensite
TRIP	TRansformation Induced Plasticity
TWIP	Twinning Induced Plasticity
Wt%	Weight percent

1 Introduction

1.1 Development of Advanced High Strength Steels (AHSS)

Throughout the world, there is increasing interest in the development of new Advanced High Strength Steels (AHSS) with enhanced combination of strength and ductility to reduce the weight of components in order to reduce the environmental impact of fuel consumption and gas emissions and to increase the safety of vehicles [1]. Mechanical properties, industrial feasibility and cost-effectiveness are also critical aspects that must be considered. For these reasons, the improvement of the high strength steel grades does not only represent an important area of study but also a challenging one that must be carefully analyzed. The average use of AHSS in car body design from both mass percentage and also the variety of available grades has increased significantly over the past 20 years [2]. Most of the current commercially applied AHSS steels have been developed from Dual-Phase (DP) steel [3]. Starting from the late 1970s the increase in strength without losing or even improving the ductility generated

significant interest and extensive research on DP steels [4,5]. One important finding was the contribution of retained austenite on the elongation of DP steels. It was observed that the ductility of DP steels increased with an increase in retained austenite [6].

In addition to DP steels, Complex Phase (CP) and TRansformation Induced Plasticity (TRIP) steels are other AHSS grades that are currently being used or under investigation by steel suppliers. These grades are referred to as “first generation” AHSS as shown in the overview of their tensile properties in comparison with other grades in Figure 1-1. While the first generation of AHSS contains low alloy steels, the “second generation” was developed by adding higher amounts of alloying elements, such as manganese, nickel or chromium which led to the introduction of the austenitic stainless steels, Twinning Induced Plasticity (TWIP) steels, lightweight steels with induced plasticity (L-IP) and shear band strengthened steels (SIP). Despite providing an excellent combination of strength and ductility, the cost and difficulties in the industrial processing made the use of this group limited [7].

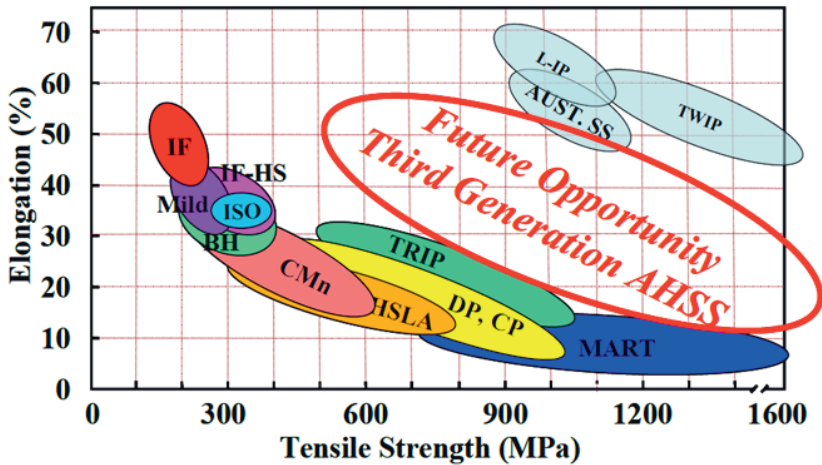


Figure 1-1 Overview of tensile strength vs elongation for various classes of conventional and advanced high strength sheet steel (AHSS) grades [3].

The first generation AHSS concepts are mostly ferritic-based multi-phase microstructures. DP steels are still the most applied AHSS grades. Interest in DP steels results from improved strength and formability, good weldability, relative ease of processing, and availability [8].

The current area of research is focused on the “third generation” of AHSS in order to enhance the tensile strength/ductility combinations without adding high amount of expensive elements. At this time, the effort is mainly dedicated to improving the processing of the already developed steels using new heat treatments or low additions of special elements. In the following subsections a few of the most attractive new methods to develop 3rd generation AHSS will be described shortly and finally “quenching and partitioning” methodology which is the main concept of this work, will be explained more in detail in chapter 2.

1.2 Strengthening Mechanisms

Strength in steels comes from several phenomena, which is why they are able to offer such a wide range of properties. The heat treatment of steels allows a great variation in microstructure to be produced so that a wide range of mechanical properties can be obtained even in plain carbon steels. The addition of alloying elements provides even better control over microstructure and consequently mechanical properties, as a result of their influence on the phase diagram and kinetics of transformations. The most important strengthening mechanisms are:

- Work hardening (dislocation strengthening)
- Solid solution strengthening by interstitial atoms
- Solid solution strengthening by substitutional atoms
- Refinement of grain size
- Precipitate strengthening

The only method which results not only in increasing of the strength but also ductility is the decrease of the grain size by different means. So, this technique is the main method for production of AHSS today. In this regard, thermo-mechanical treatments can be used in order to control the size and shape of the austenite grains. Besides, controlling the cooling cycle from austenite to give the possibility for a finer structure is another common method.

1.3 Development Methods for 3rd Generation AHSS

1.3.1 Improvement of Dual Phase (DP) Steels

The dual phase steels are low-alloy steels consisting of two major phases. One is soft and the other one is considerably harder. To produce DP steels, samples are heated to the ferrite-austenite region to transform part of structure to austenite. The subsequent quenching to room temperature transforms austenite to martensite.

Increasing the martensite fraction by changing the carbon content and/or intercritical annealing temperature resulted in a stronger still formable structure such as DP780 and DP980 which are now available commercially [3]. In addition, grain refinement by special hot deformation to increase the strength has been successfully practiced for this kind of steel [9-12].

1.3.2 Modified TRIP Steels

The TRIP steels developed to have a major or minor fraction of austenite by using different quantities of austenite-stabilizing solutes. During plastic deformation, austenite transforms to martensite. Having retained austenite as micro-constituent in microstructure not only increases the ductility but gives also a TRIP effect and a blocking of crack propagation (BCP) which has been defined by Zackayetal [13] around 50 years ago. The production of TRIP is similar to DP steels with the difference that the sample is quenched to a temperature above M_s and hold at this temperature until carbon inside bainitic ferrite diffuse out to austenite and stabilizes by that some retained austenite at room temperature. During the last quench, some austenite will transform to martensite, so the structure consists of ferrite, austenite, and martensite.

Primary TRIP steel grades have had higher carbon contents than currently used in commercially available grades. In addition, grain refinement of TRIP steels by microalloying has also been investigated [14,15]. Tensile strengths of up to 1 GPa with elongation level around 20 % has been obtained as can be seen in Figure 1-2.

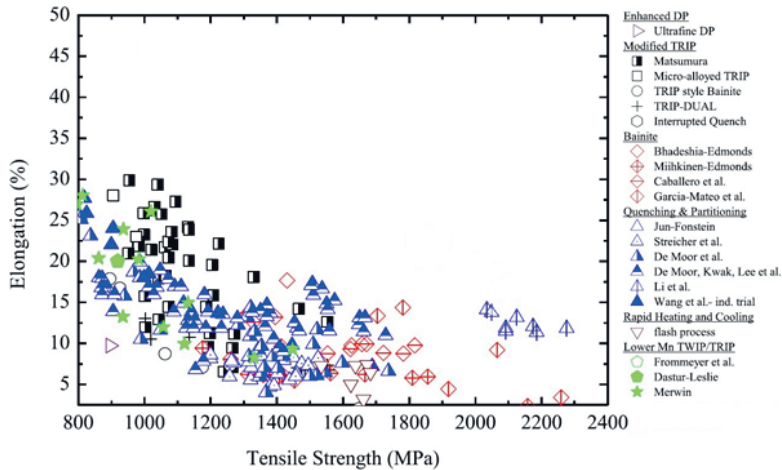


Figure 1-2 Overview of mechanical properties obtained by different approaches to producing the 3rd generation of AHSS [16].

1.3.3 Ultrafine Carbide Free Bainite (CFB)

Numerous works have been conducted to create ultrafine bainitic microstructures over the last decade [17–21]. The difference between CFB in comparison with bainitic steels starts from their chemical composition. CFB steels contain a certain amount of silicon and/or aluminum which are elements that suppress the formation of carbides and stabilize the austenite. So that the resulting microstructure consists of fine sheaves of ferritic bainite laths and thin austenitic films. By using low enough transformation temperatures for austempering at 200 °C, very fine laths in the thickness range of 20–40 nm can be achieved, which improves the properties significantly. For instance, the strength of 2.5 GPa with 600 HV hardness is achieved after 15 days heat treatment of a 0.98C–1.89Mn–1.46Si–1.26Cr (in wt%) steel [21]. Although the properties are very good, the time seems to be too long for industrial purposes and thus further work has been done on increasing bainite kinetics, reducing heat treatment to hours rather than days by alloying with Al and/or Co [20,22].

2 Quenching and Partitioning

The quenching and partitioning (Q&P) represent an original heat treatment to achieve a martensitic matrix with a minor fraction of retained austenite. The process starts from a full or partial austenitization of the steel and subsequently controlled quenching between the martensite start (M_s) and martensite finish temperatures (M_f) in order to obtain a desired fraction of martensite in the microstructure. Finally, holding at a certain temperature for a specific time (normally a few minutes) called partitioning step, followed by the cooling down to room temperature. The partitioning stage can be performed at the same temperature as the quenching stage, named as “one-step Q&P”, or at a higher temperature “two-step Q&P”. The process is schematically illustrated in Figure 2-1. The partitioning step promotes the carbon enrichment in the retained austenite due to the carbon diffusion from martensite formed during the first quench to austenite [4]. As a result, the austenite that is not sufficiently enriched in carbon transforms into martensite during the final

quenching. So, martensite transformed during the first quenching has lower carbon content due to the tempering effect and it is usually termed as “initial martensite”. Depending on partitioning conditions, tempering of martensite to increase the toughness without a too great loss of the strength of martensite could be performed. Since the martensite formation is a shear transformation, the fraction of initial martensite must be controlled by adjusting the quenching temperature.

On the other hand, by high enough carbon enrichment of the austenite which has not been transformed at the first quenching, retained austenite (RA) will stabilize during the partitioning stage. After the final cooling, despite the austenite has been carbon-enriched, if its M_s temperature is still above room temperature because of an insufficient stabilization, the martensitic transformation could take place. This martensite is usually called “fresh martensite” or “untempered martensite”. It has a higher dislocation density and it is supersaturated in carbon.

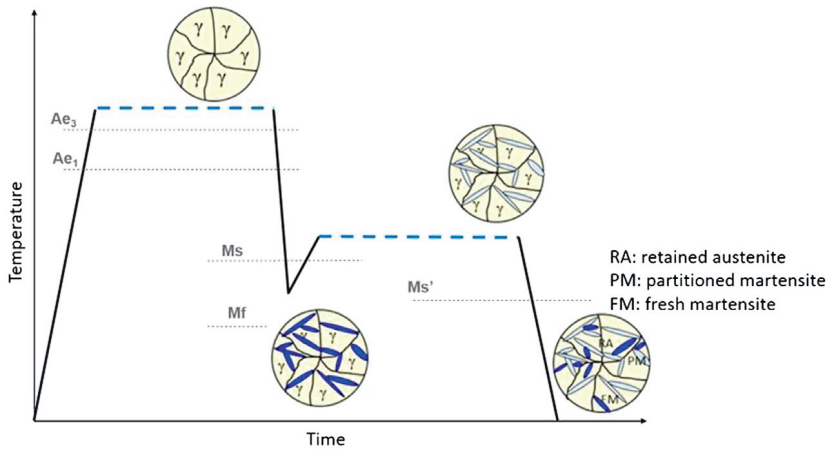


Figure 2-1 Schematic Temperature vs. Time representation of the quenching and partitioning thermal cycle with corresponding microstructure evolution [23].

2.1 Chemical Composition of Q&P steels

The chemical composition design of typical Q&P steels is based on generating the optimal conditions to achieve retained austenite, and to avoid the carbide formation or any diffusive transformation. Because competing reactions decompose retained austenite to other phases (i.e. bainitic ferrite) or reduce the amount of carbon available to stabilize the austenite by carbide precipitation or coarsening. Consequently, these

reactions will reduce the possibility to achieve the required mechanical properties.

Silicon, aluminum and phosphorous represents suitable alloying elements to hinder diffusive transformations and thus, retard the cementite formation (see Figure. 2-2) [24-26]. Since it is not possible for these elements to dissolve in cementite, it is required for the cementite to reject them in order to grow, and it represents the main cause for the delay of this transformation [24,27].

Recently, the effect of Si on the acceleration of bainite transformation was investigated [24,28]. It has been shown that the addition of silicon stabilizes the austenite phase during the partitioning stage and retards the austenite decomposition into bainite.

Among these elements, silicon appears to be more effective for Q&P treatment [27], because although Al could suppress the carbide formation it is associated with faster austenite decomposition into bainite [25]. Thus, its utilization in steels for Q&P is limited in contrary to CFB steel.

However, steels with silicon additions have shown problems related to the galvanizing process because of the formation of an adherent oxide [27]. Therefore, it is necessary to replace Si by Al or P in steels which need to be galvanized.

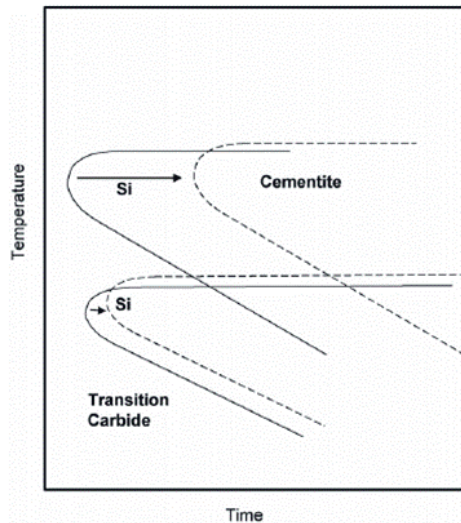


Figure 2-2 Schematic C-curve emphasizing the delaying effect of silicon on the kinetics of carbide formation [29].

Adding manganese (Mn) decreases the driving force for transformation and resulting in slower transformation [30]. Nickel (Ni), is also effectively stabilizing austenite for longer times at higher partitioning temperatures. The use of manganese has been more popular because it is economically convenient compared to nickel but it will increase the degree of segregation in the steel [31]. On the other hand, the addition of Cr, which increases the hardenability and reduces C diffusivity in austenite and slows down the austenite decomposition, has been recently reported as more effective than Ni in the stabilization of retained austenite after Q&P [32]. Molybdenum is potential of importance in hot-dip coated sheet products -where partitioning is accomplished in conjunction with coating- since it could effectively stabilize austenite for longer times at higher partitioning temperatures in Si-added steels [16].

At last but not least, selection of the carbon content could play a critical role in the mechanical properties of the steel after Q&P. Because the M_s temperature drops considerably with the addition of carbon and thus an austenite stabilization can be reached easier. Moreover, the carbon content affects significantly the mechanical properties due to its interstitial nature in steel and the effect of solid solution strengthening.

2.2 Overview of mechanisms in the Q&P process

An ideal microstructure after two step Q&P process consist of tempered martensite retained austenite and frequently fresh martensite. However, other competing reactions were reported in numerous publications. These competing reactions include bainite transformation and growing, tempering of martensite and carbide precipitation formation [28,33-37]. Typical microstructure of Q&P treated steel can be seen in Figure 2-3 and 2-4 [38,39].

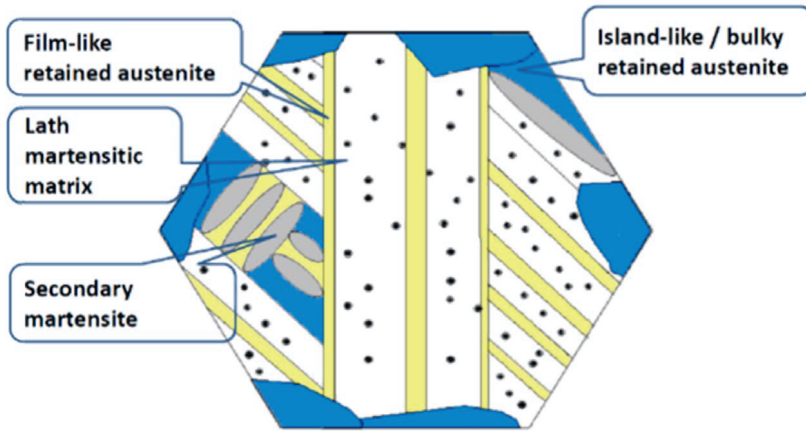


Figure 2-3 Schematic of a typical microstructure of Q&P treated grain including submicron-scale lath martensite or bainite matrix within which uniformly distributed fine carbides with an average size of several nanometers plus submicron-scale island-like metastable retained austenite (RA) or polygonal ferrite and film-like RA with film width of dozens of nanometers [39].

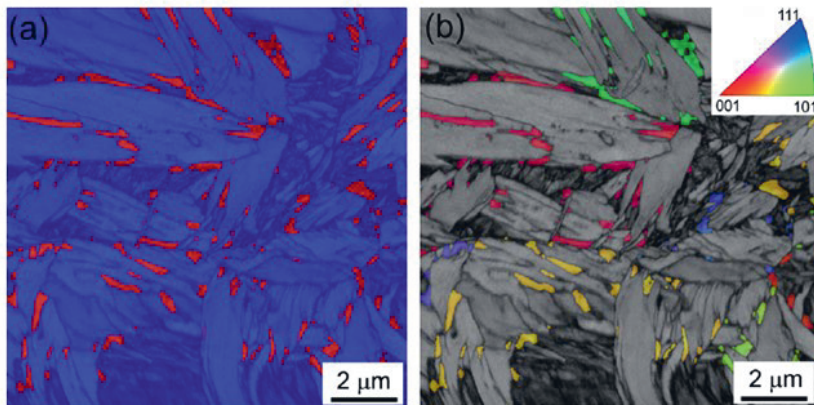


Figure 2-4 The microstructure observed by EBSD analysis of a 0.2%C steel a) Combination of image quality map and phase map where blue corresponds to martensite and red corresponds to retained austenite -Darker bands are associated with fresh martensite. b) Combination of the inverse pole-figure map and band contrast map on austenite- bright areas correspond to martensite, dark areas are associated with fresh martensite and austenite is shown colorful depending on its orientation [38].

Depending on the chemical composition, an almost instantaneous transitional carbide precipitation after quenching could occur in martensite before the partitioning stage. Nevertheless, as the formation of

cementite is supposed to be inhibited, an increase in the partitioning time or partitioning temperature may lead to a resolution of these transitional carbides providing, a “new” source of carbon to enrich the austenite carbon content during partitioning. For example, as shown in Figure 2-5 by prolonging the partitioning time an increment in the austenite fraction is observed as a second peak when different partitioning times are considered [29]. The possible explanation for this behavior is due to the difference between the carbon content of RA achieved after a short partitioning time (first peak) and after longer time. Although the amount of RA after short time is higher its carbon content is low, and it has lower stability. By prolonging the holding time, some of the RA will decompose to other phases such as ferritic bainite. When the partitioning time is longer than approximately 1800 seconds, the austenite has gotten high enough carbon content so that the austenite will not transform to martensite at quenching to room temperature.

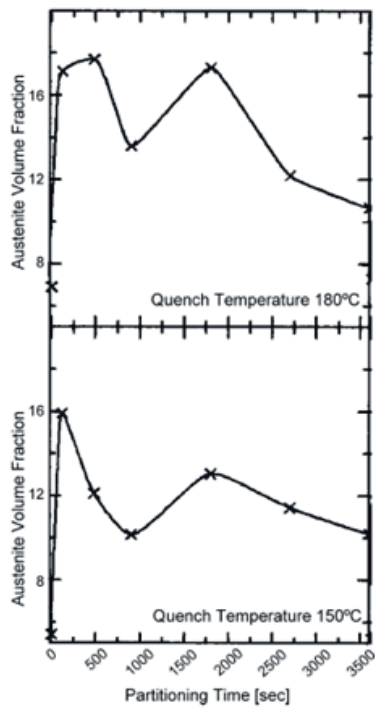


Figure 2-5 Analysis of volume fraction of austenite as a function of partitioning time for quenching temperatures of 180°C and 150°C. [29].

It is clearly revealed that isothermal martensite and bainite form at or close to the partitioning temperature. While isothermal martensite formation begins almost immediately after quenching, the formation of bainite seems to follow TTT diagram predictions [33]. Additionally, the quenching temperature influences the kinetics of the bainitic transformation. Higher quenching temperatures involve a higher initial fraction of austenite and thus, lower carbon content present within the austenite. Hence, as a result of the lower carbon content stabilizing the austenite, the bainite formation occurs faster when the quench temperature is increased [33].

It is important to notice that the fresh, high-carbon, martensite has been reported as high strength and brittle microconstituent because of its carbon content [40,41]. Therefore, its low capability to deform leads to potential sites for voids or cracks nucleation in interfaces of fresh martensite/initial martensite or fresh martensite/austenite [42].

2.2.1 Martensite formation

Martensite forms when steel quenches from austenite to an appropriately low temperature. The cooling must be rapid enough so that there is no time for a diffusion-controlled phase transformation to ferrite. The driving force for the transformation increases with decreasing temperature, resulting in a shear transformation of the face centered cubic (FCC) lattice of austenite to body-centered tetragonal [43,44]. The transformation occurs as a series of small-scale displacements of atoms across a moving semicoherent interface. The result is the formation of lenticular martensitic laths inside the parent austenite grains. As the transformation progresses, new laths are formed inside the parent austenite grains until all austenite has transformed.

Finding the critical temperatures of phase transformations, specially martensite start transformation temperature (M_s) is crucial with regard to Q&P heat treatment design. Several empirical and physical models for predicting the M_s temperature have been proposed over the past 70 years.

Table 2-1 Different formulas for estimation of the M_s temperature.

Formula	Reference
772-316.7C-33.3Mn-11.1Si-27.8Cr-16.7Ni-11.1Mo-11.1W	[45]
811-361C-38.9Mn-38.9Cr-19.4Ni-27.8Mo	[46]
772-300C-33.3Mn-11.1Si-22.2Cr-16.7Ni-11.1Mo	[47]
834.2-473.9C-33Mn-16.7Cr-16.7Ni-21.2Mo	[48]
812-423C-30.4Mn-12.1Cr-17.7Ni-7.5Mo	[49]
785-453C-16.9Ni-15Cr-9.5Mo+217(C)2-71.5(C)(Mn)-67.6(C)(Cr)	[49]
838-600[1-exp(-0.96C)]	[50]

In the above Equations mentioned in Table 2-1, the variables stand for the mass fractions of the respective alloying elements in wt%. However, all these empirical equations are typically limited to only a narrow composition range of alloys and an experimental verification should always be carried out.

2.2.2 Martensite morphology

The morphology of martensite varies according to the chemical composition and mainly the carbon content of the steel, i.e. lath martensite in low carbon steels and plain (lenticular) martensite in high carbon steels [51]. Normally, the lath martensite in low carbon steels is with high-density dislocations as the substructure, in contrast to twin substructure in lenticular high carbon martensite [52].

For low carbon steels with a total carbon content of approximately 0.2 weight percent, the laths are grouped together into blocks. A cluster of blocks will form a packet when sharing the same (111) γ to which the

corresponding $(001)\alpha'$ is almost parallel [44]. It is shown that by increasing the carbon content, the sizes of both packet and block decrease [53]. In low carbon steels, a block which is observed as having different contrasts under optical microscopy contains two groups (sub-blocks) of laths which are of two K-S variants with a misorientation degree of around 10. On the other hand, in the high carbon alloy, a block consists of laths of a single K-S variant, as shown in Figure 2-6.

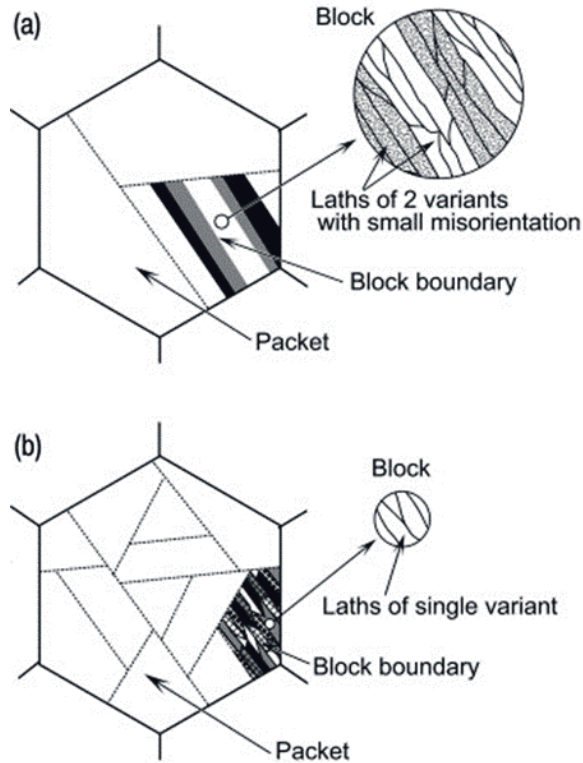


Figure 2-6 Schematic illustrations showing lath martensite structure in (a) low carbon (0–0.4%C) and (b) high carbon (0.6%C) alloys[53].

The high-angle boundaries between the packets and the blocks act as obstacles to dislocation movement, granting improved tensile strength and fracture toughness of the material. Morito et al. [53] categorized certain martensitic variant combinations as “sub-blocks” because of their low mutual misorientation angle. In any case, fully martensitic microstructures are typically characterized by a high strength but relatively low uniform elongation.

2.2.3 Stability of retained austenite

It has been shown [40,54-56] that the stability of retained austenite (RA) is mainly affected by i) the chemical composition (principally local carbon content) of the retained austenite ii) the grain size iii) the morphology of the retained austenite iv) the constraint generated by phases surrounding the austenite and v) there is also a small effect of dislocation density and the crystallographic orientation of the austenite with respect to the loading direction.

As it is well defined, carbon is the element which provides austenite with the highest stability. However, the high carbon content is not the only factor to ensure the stability of the austenite. It is shown that the morphology of retained austenite can strongly affect the austenite stability [55,56]. Since the blocky retained austenite regardless of its carbon content presents lower mechanical stability than filmy austenite. Two different mechanisms have been used to explain this.

The first one correlates the stability of RA to its adjacent microconstituents. Since filmy austenite is located between martensite laths and austenite must deform in order to accommodate the volume expansion of the martensitic transformation during TRIP effect, the strength of martensite surrounding the film austenite could avoid/delay the martensite transformation in this morphology [56]. The second explanation for the higher stability of the filmy-austenite refers to the residual stresses i.e. volume expansion during martensitic transformation that compress the retained austenite. Subsequently, this hydrostatic pressure may hinder or postpone the TRIP effect as the martensitic transformation contains a volume expansion [56].

2.3 Constrained carbon equilibrium (CCE) model

Designing the Q&P heat treatment, based on optimization of both strength and elongation mainly depends on the amount and morphology of different micro-constituents, i.e. FM, TM, RA, B, and precipitates. Among them retained austenite (RA) play a key role in Q&P steels.

It has been proposed that the carbon partitioning from martensite into austenite is controlled by the constrained carbon equilibrium (CCE) principle. The aim of this model is to predict the carbon concentration in

austenite under the condition where: (i) Competing reactions, such as cementite or transition carbide formation or bainite transformation, are suppressed; (ii) An identical carbon chemical potential exists in both ferrite (or martensite) and austenite; and (iii) The carbon partitioning proceeds under the assumption that the interface between ferrite and austenite does not migrate. However, carbide precipitation in martensite is often observed during the partitioning step of low or high carbon steels, even if they contain a high amount of Si. As a result, this carbide consumes some of the carbon and consequently reduces the amount of available carbon to enrich austenite during partitioning. Hence, the carbon concentration of the austenite after the partitioning step is supposed to be lower than that predicted under the CCE conditions excluding carbide precipitation.

In order to estimate the RA, a theoretical model to determine the optimum quench temperature based on CCE conditions has been proposed and used extensively [25,29,57]. The basis of this method is described below:

Firstly, it is required to estimate the fraction of martensite (and also austenite) based on the quench temperature by Koistinen and Marburger relationship (Eq. 2-1) [58].

$$f_M = 1 - e^{-\alpha_m(M_s - QT)} \quad (\text{Eq. 2 - 1})$$

$$\alpha_m = 10^{-3} (27.2 - \sum_i S_i X_i - 19.8 (1 - e^{-1.56x_c})) \quad (\text{Eq. 2-2})$$

$$\sum_i S_i x_i = 0.14x_{Mn} + 0.21x_{Si} + 0.11x_{Cr} + 0.08x_{Ni} + 0.05x_{Mo} \quad (\text{Eq. 2-3})$$

Where f_M refers to the austenite fraction transformed into martensite at the quench temperature (QT), α_m is the rate parameter which can be calculated from (Eq.2-2) and depends on the chemical composition (Eq. 2-3), while M_s is the martensite start temperature of the steel.

Since the initial austenite after the quenching stage can be described as $1 - f_M$, assuming that all carbon partitions from martensite to austenite and that other competing reactions are precluded (bainite growth, carbide precipitation, etc.), the carbon content in austenite ($\%C^V$) after the partitioning step is obtained by (Eq. 2-4):

$$\%C^{\gamma} = \frac{\%C^{alloy}}{1 - f_M} \quad (\text{Eq. 2 - 4})$$

At the final cooling, if the austenite is not completely stabilized (which means that the carbon content is not high enough and its M_s temperature is above room temperature) part of this retained austenite transforms into “fresh martensite” following Koistinen and Marburger relationship (Eq. 2-1).

Figure 2-7 illustrates the differences between the retained austenite fraction measured by X-ray diffraction analysis and the predicted according to the model described above in steel grade 9260 (0.6% C–0.95%Mn–1.96%Si (wt.%)). So, it is clear that despite the lower amount of austenite achieved, the shape of the curve and the optimum quench temperature to obtain the maximum austenite fraction do not change very much, which means that the method could be used to get a good estimation of optimum QT. The alteration on the final austenite can be explained by considering the presence of competing reactions which either decrease significantly the carbon available to partition and stabilize the austenite or reduce the austenite volume due to a transformation (carbide precipitation, and bainite growth respectively) (Section 2.2).

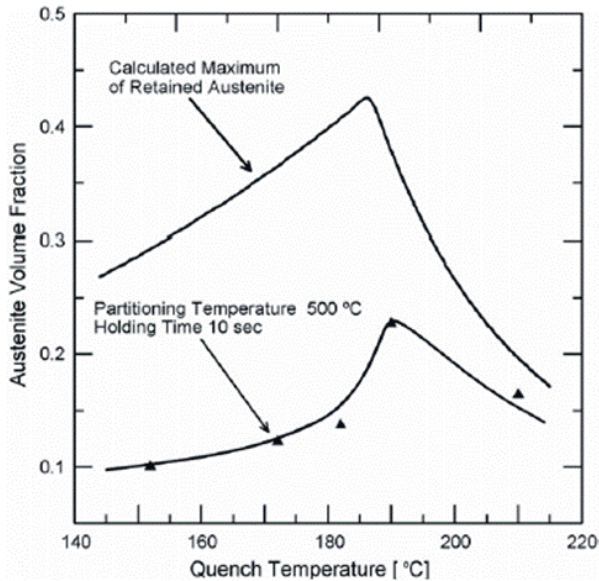


Figure 2-7 Comparison between the measured and predicted RA fraction for steel grade 9260 (0.6% C–0.95%Mn–1.96%Si (wt.%))[29].

3 Scope of the present work

As mentioned earlier, development of advanced high strength steels is of great importance for industry and society. The goal is to reduce the environmental impact from industrial processes and products. Although many of the AHSS were proposed already in the 1970s and 1980s, the use of some of them in different applications are still limited. This is mainly due to the feasibility and the cost of production of such steels, as for example the very long heat treatment time required for CFB steels or because some steels as stainless steels, TWIP steels and Maraging steels are highly alloyed with expensive elements such as Ni, Cr, Mn. The other reason is the practical limitation of them in service. Because most of the AHSS are produced by a controlled thermal or thermo-mechanical treatment, the microstructure and properties could change significantly after high temperature heating for instance, after welding or hot forming processes.

3.1 The increase of phase transformation rate

Different kinds of ferritic-austenitic microstructures (i.e. DP, CFB) shows the best toughness and strength properties. But normally the diffusional phase transformation takes a long time to reach the steady state condition. For example, the duration to reach steady-state for the bainite reaction in low temperature austempering of high carbon high silicon steels is typically longer than 10 h at a temperature of 250°C. The transformation duration can exceed 100 h for lower temperatures [19,21,59].

Conventional tempering temperatures for hypereutectoid steels in order to achieve high hardness are typically within 160–230°C.

Therefore, decomposition of retained austenite after quenching to bainite take tens if not hundreds of hours [60]. This problem makes this kind of heat treatments very difficult and costly for industry.

Ko and Cottrell showed in 1952 [61] that pre-existing martensite shortens the required duration for an incubation time of bainite transformation to 1/3. Recent investigations have also confirmed this observation that the effect of preliminary martensite is the same as if the same amount of bainite exist in the system before the final bainite transformation [62,63]. Based on this fact, comparing schematic heat treatment “A” and “B” in Figure 3-1 illustrates that although both of them are multiphase microstructures containing bainite and martensite, in combination with probably retained austenite and carbides, heat treatment “B” takes much longer time to create the stable condition for final quenching and minimum amount of fresh martensite (FM).

The thermal treatment “A” is very close to the ideal Q&P process which also starts with the transformation of part of austenite to martensite.

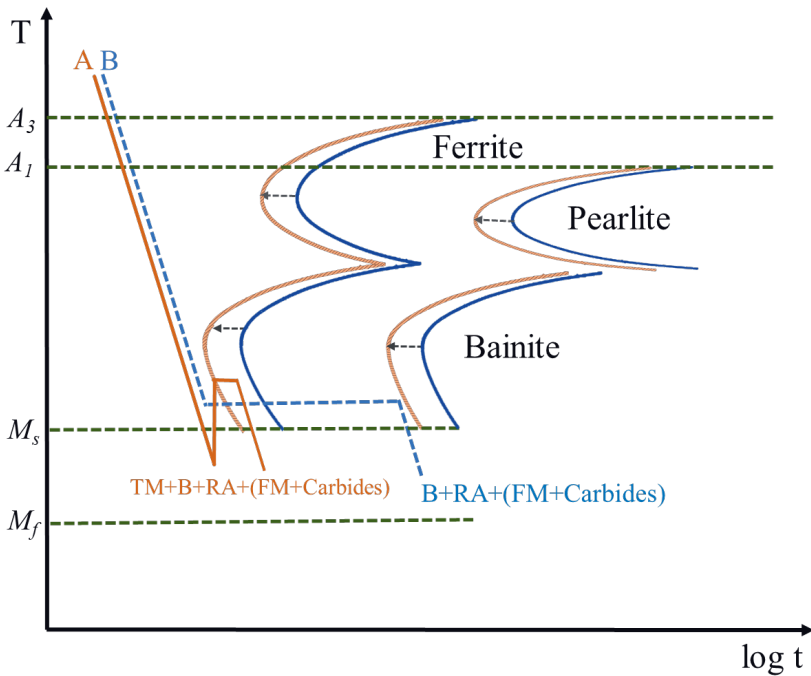


Figure 3-1 Schematic of two heat treatments on a general CCT-diagram for hypoeutectoidic steel. Blue curve is shifted to the left (red curve) after partial martensite formation. In cooling cycle, A: martensite is followed by bainite, in cooling cycle B: Bainite is followed by martensite.

So, if the steel contains enough alloying elements such as Si for retarding the diffusional transformations, the process could avoid the formation of bainite during the heat treatment as it is originally aimed for Q&P process. However, the process provides the possibility for (carbide-free) bainite formation during the partitioning step, i.e. in the presence of martensite. This overlap between the process of carbon partitioning from initial martensite and the formation of bainite, lead to an enhanced carbon enrichment of the austenite by both mechanisms. Therefore, the increase of the carbon concentration in the austenite through the carbon partitioning from martensite would accelerate the rate that austenite reaches the maximum carbon content at which the formation of bainite is stopped[64].

On the other hand, thermal treatment “B” is very close to the austempering process to produce CFB, but in that case depending on the

austempering temperature it takes tens if not hundreds of hours to enrich the stable fully carbide free bainite and carbon enriched austenite[65].

3.2 Using Q&P in industrial applications

Generally, AHSS are produced by using special thermal and/or mechanical treatments which could be affected during the last production steps for different applications. For example, for different hot forming processes the microstructure and mechanical properties of all or some parts of the component could significantly change. Below are three possible application areas for which a Q&P treatment could be added at the end of the process presented.

3.2.1 Press Hardening

The advantage of using the Q&P process directly during the press hardening is proposed by Vuorinen [18,66] in 2012. Although the process is not as quick as conventional press hardening of boron steels, it showed the higher quality of the product. The schematics of the process is shown in Figure 3-2. Although this subject is still relatively new, many researchers are working to establish the methodology and its cons and pros [67-70].

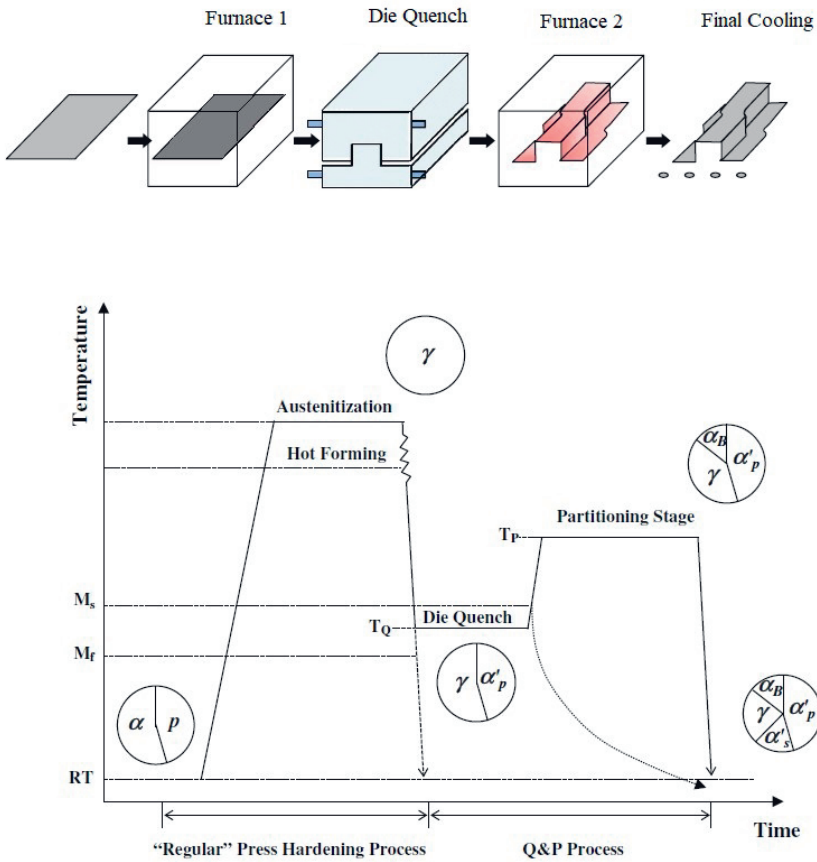


Figure 3-2 Application of Q&P process during Press Hardening[70]

3.2.2 Welding

Welding is also one critical process for which the microstructure and properties of the FZ and HAZ can be strongly affected. So, usually different kind of pre and/or post welding treatment is necessary to avoid the brittleness and failure from this region. Normally, this treatment takes several minutes, but the idea of using Q&P treatment in connection to welding gives the opportunity to accelerate the phase transformation rate, as well as providing comparable properties with the base metal to the weld zone. (See Figure 3-3)

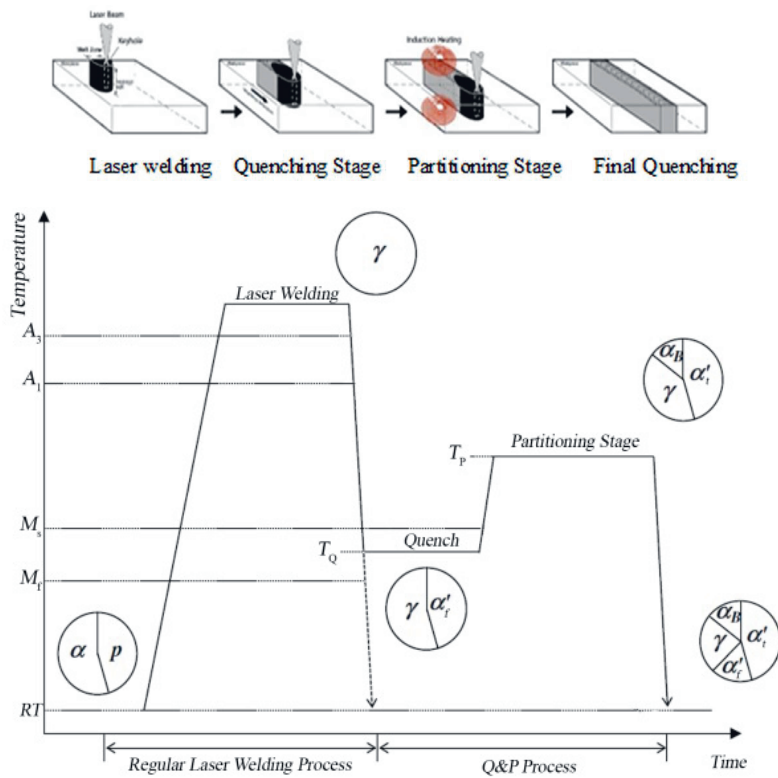


Figure 3-3 Application of Q&P process directly after laser welding [71].

However, there are questions regarding the application of Q&P after welding that are investigated in this work. For instance:

- How the Q&P treatment could be applied on the sample, just after the welding?
- How successful is this treatment to secure the weld zone from the risk of brittle martensite formation?
- How does this post-welding treatment affect the size of precipitates?
- What are the limitations and advantages of using this method in comparison with regular pre/post welding methods?

3.2.3 Bearing steels

Despite works on Quenching and Partitioning of low/medium carbon high silicon steels during the last 15 years, provides a wealth of information on the microstructure, mechanical properties, kinetics of transformation, etc. there is still a significant lack of information on using Q&P for high carbon ($C > 0.5$ wt%) steels. Since the main application of Q&P steels, up to now has been in automotive industry, relatively high elongation (over 15%) and good weldability have been necessary. Consequently, this attracts researchers to concentrate their work on carbon level of 0.15 to 0.35 wt%. But steels with higher carbon contents are also used in other applications such as rail steels, spring steels, wear resistant steels, forging grades, wire ropes, tire reinforcement, pre-stressed concrete, and high strength bars [72].

In this study, the feasibility of using Q&P treatment for steels with higher carbon contents, resulting in extremely high strength values have been investigated. The main question has been, if there is any chance to stabilize austenite and increase the elongation to the acceptable level. The benefit of such work is mainly the increase of phase transformation rate to shorten the process time to only a few minutes. Conventional heat treatment for low alloy high carbon steels is quenching and tempering for a few hours, such as traditional 100Cr6 steel resulting in 2 GPa strength and 1-2 % elongation. In addition, CFB steels which showed higher elongation needs to be austempered for tens to hundreds of hours heating at low temperatures (125–350 °C).

3.3 Objectives

Multiphase microstructures in steel have been extensively studied in the past two decades but combining non-equilibrium phases still offers great potential for further development of these steel grades. Presence of strong microconstituents as martensite or bainite beside the softer austenite will result in an improved combination of mechanical properties. Specifically, microstructure on the basis of carbon-depleted martensite and retained austenite which could transform into martensite during the mechanical loading, gives a great opportunity to shorten the process as described at the beginning of section 3-1.

The objectives of this work has been to investigate the following main topics:

- Shortening the ordinary processing time for advanced high strength steels without losing their excellent properties
- Development of the Q&P processing routes in service to industry, i.e. welding.
- Understanding the effect of different variants of thermal treatment on the microstructure and mechanical properties.
- Investigation of benefits and limitations of application of the suggested novel processes in practice.

4 Materials and Methods

4.1 Materials

Two different AHSS have been used in this study. The first one is “Domex 960” from SSAB, Sweden, which is a low carbon low silicon steel for investigation of Q&P post-welding treatment and the second one is “06CV” produced by Ascometal, France which is high carbon high silicon steel. Their chemical compositions are listed in Table 4-1.

Table 4-1 The chemical composition of Domex 960 and 06CV steels.

	C%	Si%	Mn%	Ti%	Mo%	Cr%	Ni%	V%	N%
Domex 960	0.082	0.23	1.79	0.184	0.503	0.064	0.296	0.012	0.004
06CV	0.6	1.6	1.25	-	0.15	1.75	-	0.12	-

The phase diagram of Domex 960 and 06CV sheets of steel are simulated by ThermoCalc® with the thermodynamic database TCFE8 and mobility

database of MOBFE3 [73]. Results are shown in Figure 4-1 and Figure 4-2, respectively.

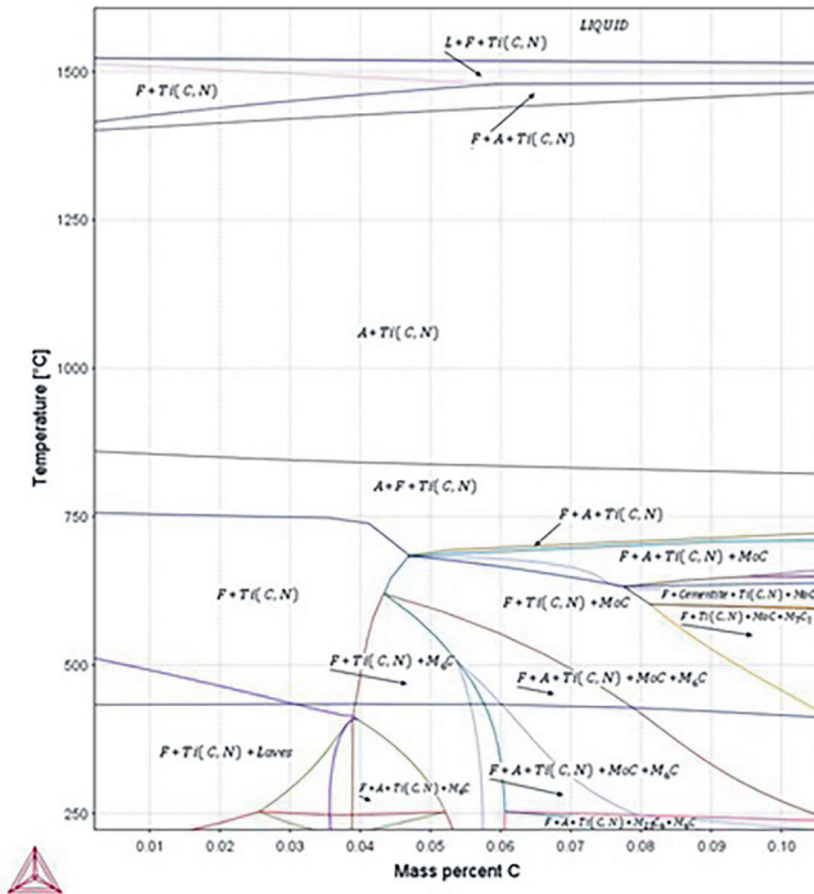


Figure 4-1 Phase diagram based on the chemical composition of Domex 960 vs carbon simulated by ThermoCalc.

It can be seen in Figure 4-1 that the only phase in addition to carbides for this level of carbon is ferrite.

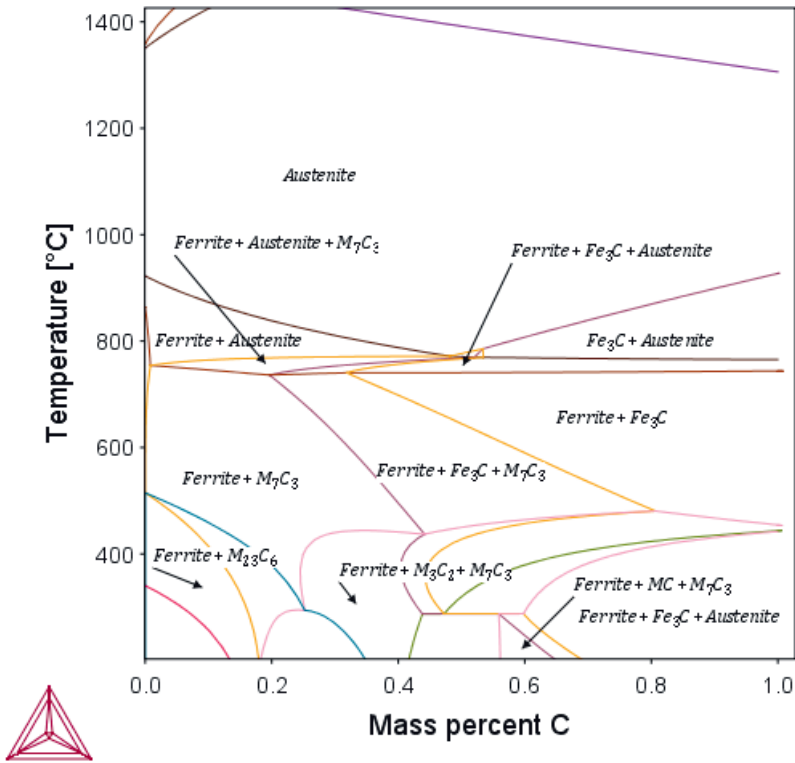


Figure 4-2 Phase diagram based on the chemical composition of 06CV vs carbon simulated by Thermocalc.

Figure 4-2 implies that mainly because of having high Silicon content, the eutectoid carbon composition is shifted to the left. In addition, LOM pictures and microhardness results ($HV_{0.5} = 346 \pm 7.6$), confirms a fully pearlitic microstructure of the as-received material.

4.2 Heat Treatment

The heat treatments that have been performed for both steels are mentioned in the corresponding papers. The selection of the austenitizing temperatures, quenching temperatures and partitioning temperatures and times were based on the critical temperature of each steel.

Austenitizing was performed above the A_3 temperature. The quenching rate and temperatures were selected, based on the CCT diagrams of the steels. In order to select the QT, the M_s is calculated according to the empirical equations mentioned in Table 2-1 and/or related brochures from the companies or previous studies on these steels. Based on these information, 3 different QT were selected to have a different amount of initial martensite calculated by using Eq. 2-1. Following the first quench, the partitioning conditions were selected using the CCT diagrams to limit the diffusive transformations.

4.2.1 Q&P treatment of Domex 960

The selected heat treatment conditions are schematically shown in Figure 4-3. Totally 27 different samples were heat treated by using Gleeble. After that, the same heat treatment was repeated by using an induction heater immediately after laser welding as shown in Figure 4-4.

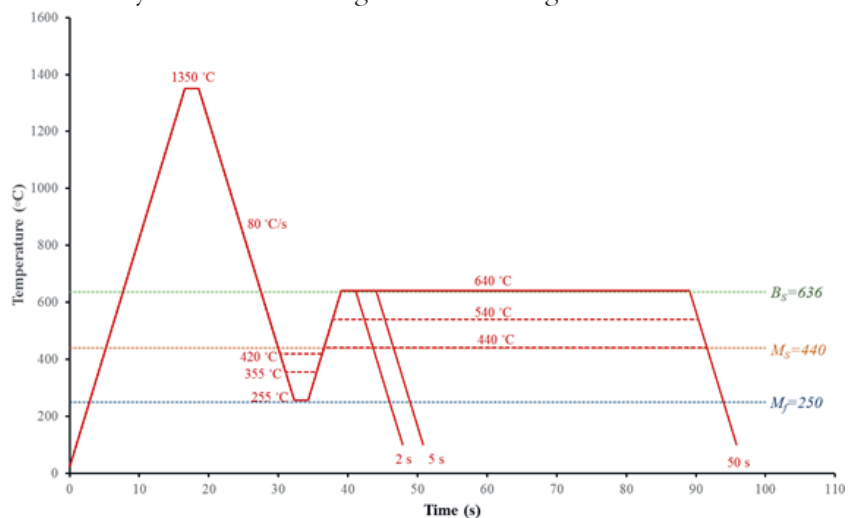


Figure 4-3 Schematic of heat treatment for Domex 960 used in paper 1 to 3.

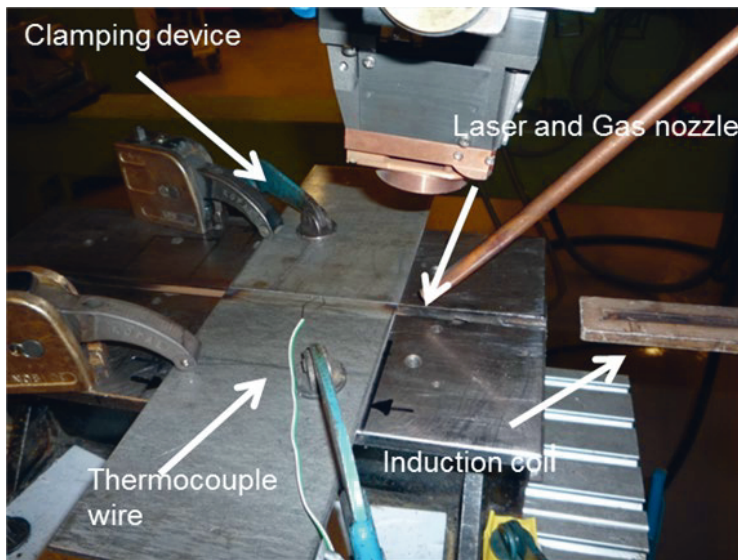


Figure 4-4 The configuration of the equipment used for laser welding and Q&P treatment.

Ytterbium fiber laser with 5kW power, the travel speed of 1.1m/min, argon as a shielding gas with a flow rate of 20litre/min were used for laser welding of the 5.5 mm sheet of Domex 960. Thermocouples were welded 1.5 mm far from Fusion Zone (FZ) to monitor the temperature. As can be seen in Figure 4-4, the induction heater was used to control the quenching temperature and for applying the partitioning condition directly after the welding.

4.2.2 Q&P treatment of 06CV

The Q&P conditions, which have been used for the 06CV steel, are shown in Figure 4-5.

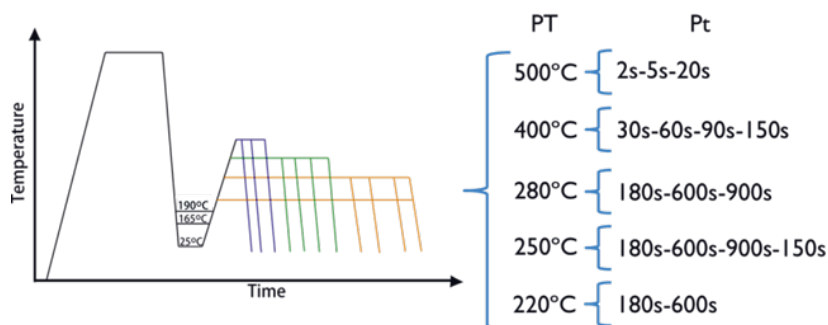


Figure 4-5 Schematic illustration of the Q&P conditions evaluated. PT and Pt refer to partitioning temperature and partitioning time respectively.

The austenitization temperature of the sample treated by Gleeble was carried out at 910°C for 5 minutes. But the austenitization of the samples which were heat treated by using Nabertherm N11/H batch furnace, was carried out at 890°C for 1h. The quenching stage was performed in either Therm Concept salt bath (for QT190 and QT165) or oil (for samples quenched until room temperature). Samples quenched until 190°C or 165°C were held in the salt bath for 1 minute, in order to stabilize the temperature of the salt bath and subsequently they were partitioned at the selected temperature in a second salt bath. The batch furnace and the salt bath can be seen in Figure 4-6. It should be noted that, for samples quenched until room temperature, the oil was removed before they were partitioned in the salt bath. All samples were cooled to room temperature in air after the partitioning.

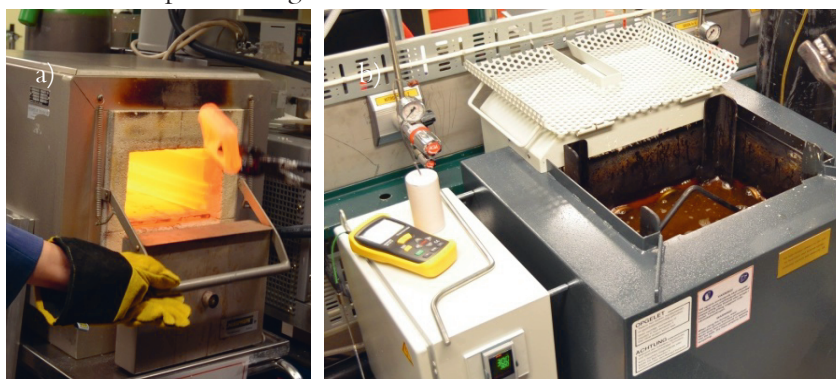


Figure 4-6 a) the batch furnace and b) the salt bath furnace, which were used for heat treatments.

In order to analyze the actual thermal profile achieved in the samples, the K-type thermocouples were welded on the samples.

Samples of 10x10x75mm were heat treated and the cross section used to evaluate the microstructure, hardness and impact toughness, while tensile test samples were machined, and heat treated in a second round using same parameters and same equipment.

It should be mention that the austenitization was performed in air atmosphere, so decarburization of the surface could occur. In order to remove the decarburized layer accurately, the hardness along the distance from the surface was measured in advance. The hardness profile as shown in Figure 4-7, demonstrated that grinding of approximately 250 μm is necessary after the heat treatment of tensile test samples, which is shown in Figure 4-8.

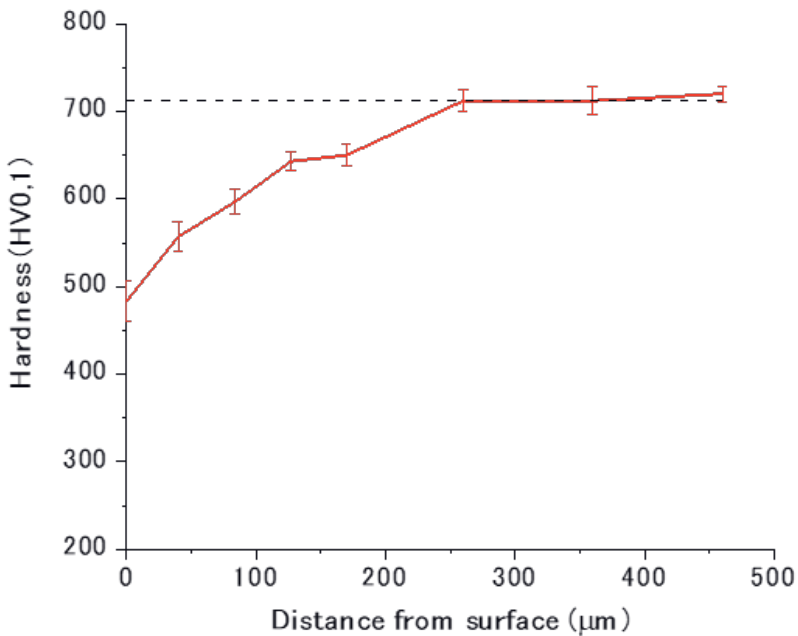


Figure 4-7 The Hardness (HV0.1) profile along the cross-section of the heat treated tensile test samples. Decreasing the hardness close to the surface is associated with decarburization during the heat treatment.

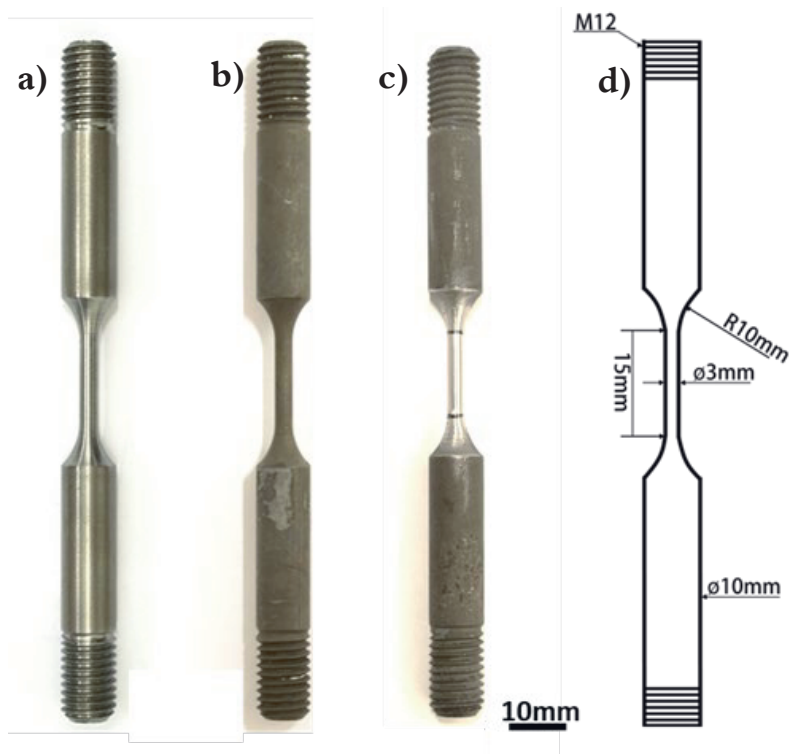


Figure 4-8 Shape and layout of tensile test samples a) As-machined b) After heat treatment c) After grinding d) Layout of specimens.

4.3 Material characterization techniques

Sample preparation for microstructure studies including light optical microscopy (LOM), micro-hardness measurement, scanning electron microscopy (SEM), Electron backscatter diffraction (EBSD), and X-ray diffraction studies were performed by conventional manual grinding and polishing. The specimens were ground using Buehler MetaServ 250 (P220- P600- P1200- P2500) and polished ($6\ \mu\text{m}$ - $3\ \mu\text{m}$ - $1\ \mu\text{m}$ - $0.25\ \mu\text{m}$) step by step, followed by the last stage of Colloidal Silica ($0.06\ \mu\text{m}$).

4.3.1 Light Optical Microscopy

The optical microscopy (OM) analysis was carried out using Nikon Eclipse MA200. Nital and LePera color etching (Table 4-2) were utilized to reveal and distinguish the structure.

Table 4-2 Etching solutions that have been used in this study.

Etching Solution	Effect on microstructure	Observations
LePera Equal portions of solutions: (a) 1% Na ₂ S ₂ O ₅ in aqueous dilution (b) 4% picric acid in ethanol	Ferrite yellow/blue; bainite brown, retained austenite and fresh martensite white	Austenite and fresh martensite not separately identifiable.
2%-Nital (a) 98ml ethanol 99% (b) 2ml nitric acid 65%	Reveals alpha grain boundaries and constituents.	Most common etchant for steels and casts iron. The 2 or 4% solution is commonly used. Use by immersion of sample for up to 60 s.

4.3.2 Microhardness

A Matsuzawa MXT microhardness tester was utilized to study the Vickers Hardness (HV) variations of the samples. The applied load is selected based on the purpose of the study. Normally, a load of 500g (HV_{0.5}) was used in order to obtain an indentation size with a diagonal larger than 20 μm, that could include all the phases present in the microstructure. The specified load in each case is mentioned in the corresponding article.

4.3.3 SEM, EDX, and EBSD

A JEOL JSM-IT300LV microscope, equipped with Oxford X-Max energy dispersive spectroscopy (EDS) was used when necessary for SEM-EDS analysis. Samples were etched with 2%-Nital as mentioned in table 4-2, before SEM studies.

In addition, FE-SEM Helios Nanolab 600 (FEI company) have been used for SEM and especially high-resolution EBSD. The samples for EBSD were polished very carefully to avoid mechanical transformation of RA to M and then the EBSD was performed on polished samples.

4.3.4 XRD Analysis

A transversal cutting was performed by Struers Secotom-10 using a feed speed of 0.05 mm/s aiming to introduce the lowest amount of plastic deformation. A final cutting parallel to the first cut surface was performed in order to obtain samples of 10x10x5 mm size. Subsequently, the samples were ground and polished as mentioned earlier.

Panalytical Empyrean diffractometer was operated to obtain XRD patterns, collecting (2θ) data from 40° to 100° with a step size of 0.0131303° , and a scan speed of $0.026796^\circ/\text{s}$.

HighScore Plus v4.7.1 software was utilized to perform Rietveld analysis and determine the phase fractions and their lattice parameters.

4.3.5 Charpy-V impact toughness

The Charpy-V Impact Tests were carried out according to ASTM Standard E 23- “Standard Test Methods for Notched Bar Impact” and the energy absorbed during the test is reported in joule (J). The dimensions of the samples are shown in Figure 4-9.

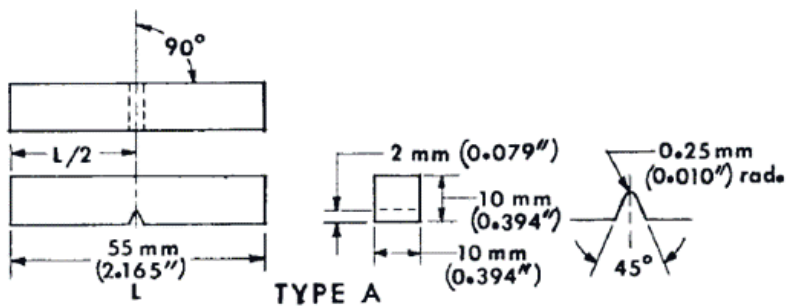


Figure 4-9 Charpy V-Notched dimensions according to ASTM Standard E 23- “Standard Test Methods for Notched Bar Impact Testing of Metallic Materials”.

4.3.6 Tensile Testing

Tensile test specimens of Domex 960 were cut from different welded sheets which were Q&P treated based on different conditions, in advance. The size of the samples was normal A-50 according to the standard EN ISO 6892-1:2009. It should be noticed that the FZ was located in the center of the specimens, but the place of fracture is different based on the

properties of the samples as can be seen in Figure 4-10. Samples were tested by using Instron 250 kN.



Figure 4-10 Examples of laser welded +Q&P treated tensile test samples.

The dimensions of the tensile test specimens of 06CV are specified in Figure 4-8. It should be noted that the gage length is 15mm with a diameter of 3 mm ($L/D=5$). The tensile tests were carried out at room temperature in Gleeble 3800, with a longitudinal glass extensometer (HZT extensometer), which is designed to operate at high temperatures. The arrangement of the specimen in Gleeble 3800 before the test is shown in Figure. 4-11.

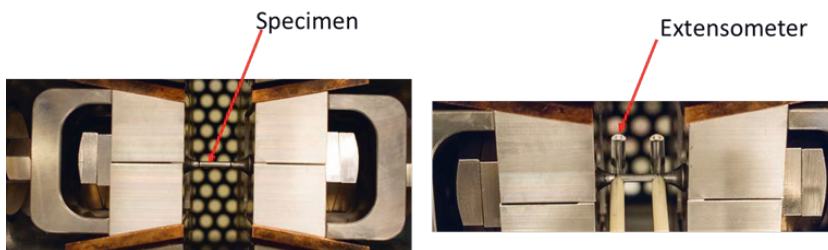


Figure 4-11 The outlook of the tensile test specimen and extensometer in Gleeble 3800.

Chapter 5

5 Results and discussion:

Based on the results presented in papers I to V, the following three sections give a summary, of these by describing the thermal treatments performed, the microstructures created, and the mechanical properties achieved. The goal for chapter 5 is to give additional information and more details and comparisons to what is presented in the articles and not to repeat the results presented in the different articles.

5.1 Thermal Treatments:

The thermal treatment that has been used for Domex 960 mentioned in papers I, II and III is the same as in the Q&P process but since this steel has not high enough carbon and silicon content for stabilization of retained austenite by carbon enrichment during “second heating” was improbable. So, because of the similarity between the thermal processes, it was named as Q&P but the goal of using this process was not only to

produce a martensitic microstructure with retained austenite but also to take the advantage of pre-existing martensite to accelerate the bainite transformation, in addition to tempering of the primary martensite and results in a non-brittle multiphase microstructure.

The thermal treatment for 06CV that has been discussed in paper IV and V is identical with Q&P. The best results were observed by quenching to room temperature in which the initial fraction of martensite is around 80%. So, this case is the same as quenching and tempering but for a higher temperature and shorter times than traditional tempering conditions to design the properties by controlling the microstructural evolution.

5.2 Microstructure

Results from LOM, SEM, EDX, EBSD, and XRD are presented in this section.

5.2.1 The microstructure of Domex 960

Microstructural observations revealed the presence of tempered martensite with fine carbonitrides inside them, bulky fresh martensite, bainite laths and Ti(C, N) precipitates. The base material was thermo-mechanically treated, so it had a very fine microstructure as shown in Figure 5-1.

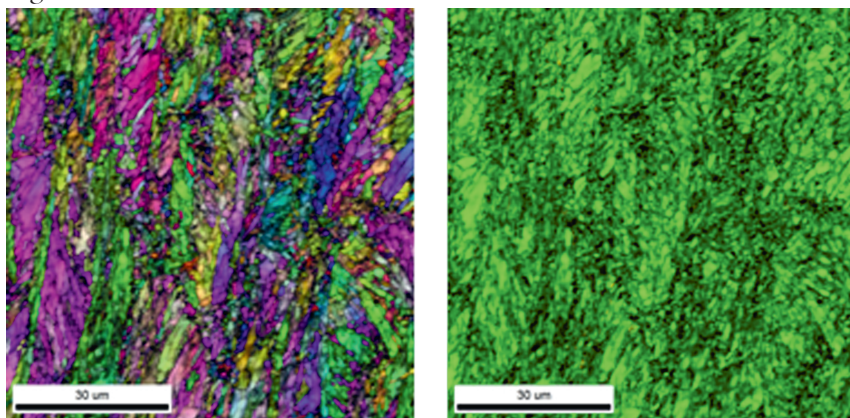


Figure 5-1 EBSD of the as-received (a) IPF+IQ (b) Phase map+ IQ.

The amount of each microconstituent depends on the Q&P treatment history. Besides, two sizes of precipitates have been observed; i) coarse

Ti(C, N) precipitates from casting which were not dissolved during the Q&P process (shown in Figure 5-2) and ii) secondary precipitates which are very fine and are distributed all over the microstructure which can grow during the Q&P process (see Figure 5-3) (more details are mentioned in paper III).

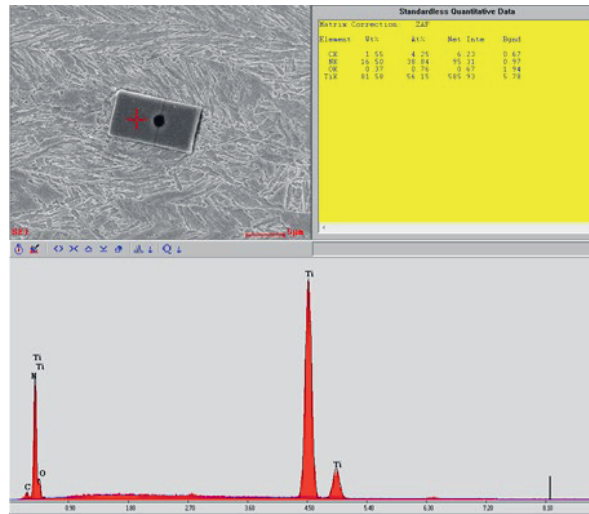


Figure 5-2 very large Ti(C, N) precipitates in the base material which is formed during the casting which h are sparsely distributed.

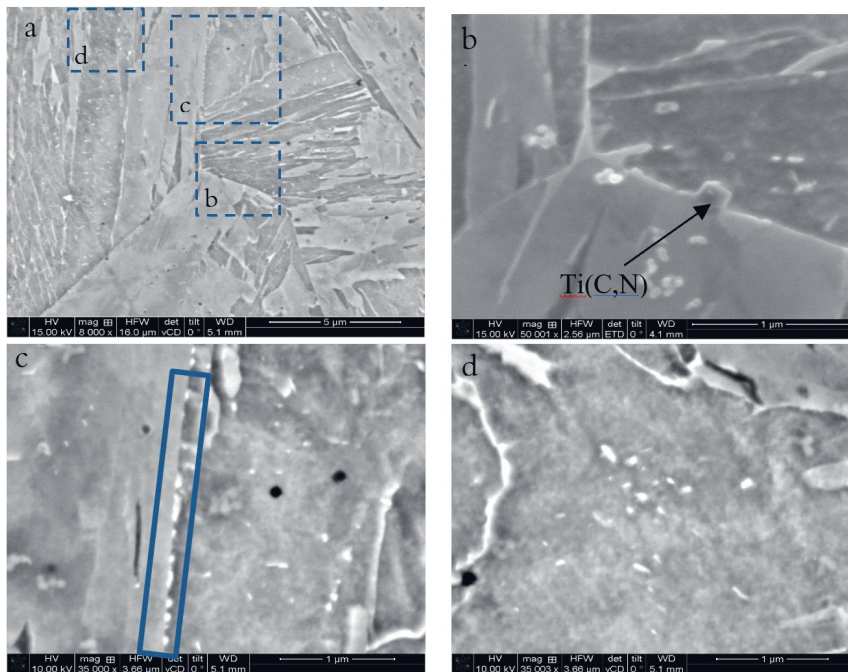


Figure 5-3 SEM pictures of different shapes of precipitates in the post-weld heat treated sample at $QT=355^{\circ}C$ and $PT=640^{\circ}C$ for 50sec. (mentioned in paper III)

5.2.2 The microstructure of 06CV

In general, the main microconstituents of Q&P treated samples are fresh and tempered martensites, which could have both lath and plain morphology, bainite and retained austenite. To quantify the amount of different phases, 3 different methods have been used, color etching, EBSD, and XRD.

For all samples, LePera color etching method have been used. Therefore, the fraction of phases were measured by using the image analysis software “Image J”. Figure 5-4 shows the result of this tint etching for a 06CV sample which is quenched to $165^{\circ}C$ and partitioned at $280^{\circ}C$ for 5 minutes in 2 magnifications. As can be seen, preliminary martensite is clearly dark blue, bainite is brown and the white parts are retained austenite or fresh martensite.

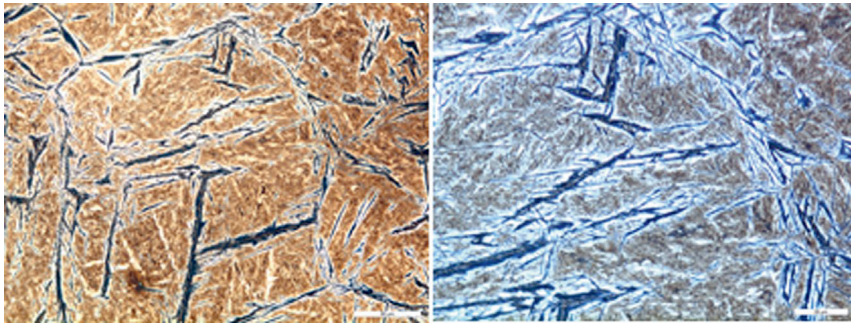


Figure 5-4 The microstructure of a Q&P treated 06CV steel sample in which Blue: Tempered Martensite, Brown: Bainite, White: Retained austenite or fresh martensite.

EBSD is also used to confirm the phases corresponding to different colors of the above-mentioned tint etching. For example, Figure 5.5 shows that the white colour around the tempered martensite is austenite, as expected. More information about this figure can be found in paper V.

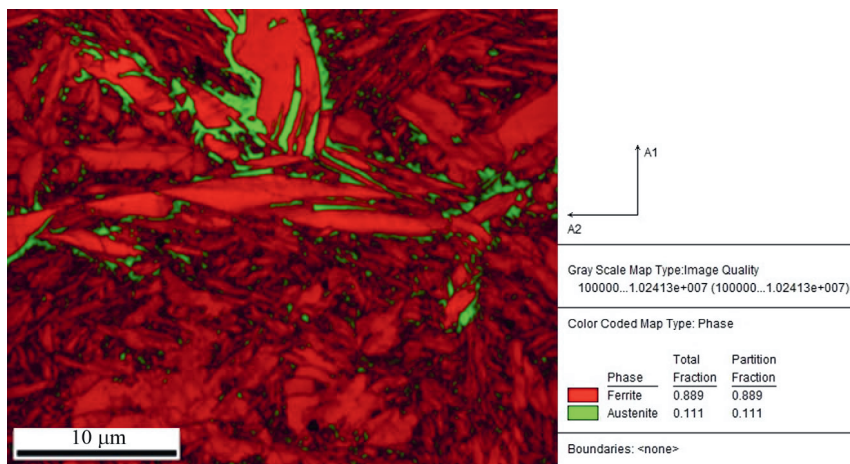


Figure 5-5 Superimposed image quality map and color-coded phase map of sample QT165-PT500-Pt5. Austenite appears green. Regions of all BCC structured phases (i.e. tempered or fresh martensite/bainite) appear red. The brighter regions are likely tempered martensite while darker grayscale indicates regions are likely martensite/bainite.

In addition, based on the tetragonality information of the phases and by using PDF4 database, and Retvield analysis the amount of fresh martensite could be extracted from XRD patterns in addition to retained austenite and the other ferritic structures with lower tetragonality. The method is shown in Figure 5-6.

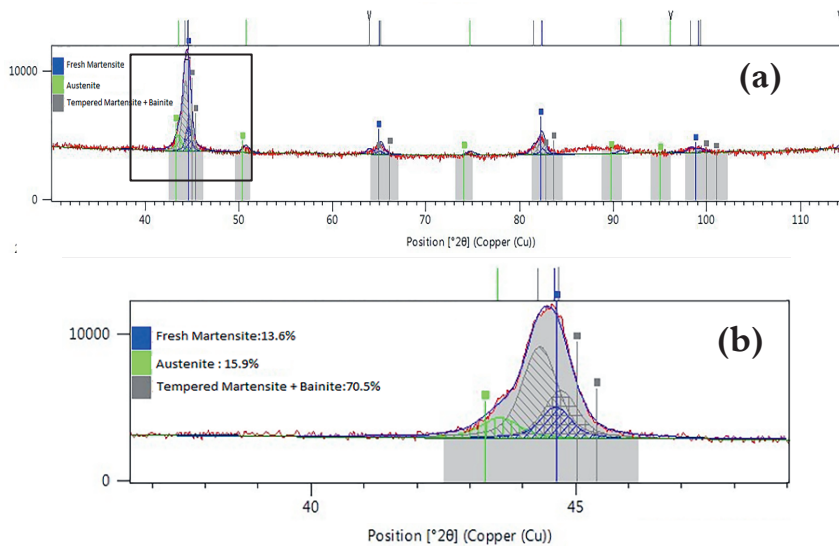


Figure 5-6(a) XRD pattern of sample QT165-PT280 -pt600 (b) Large zoom of the first peak in (a) to show how the peaks of tempered and fresh martensite were differentiated.

5.3 Mechanical properties

The mechanical properties studied in the papers I to V were hardness, Charpy impact toughness, tensile strength and elongation values.

5.3.1 Mechanical properties of Domex 960

Since the coarse-grained zone of HAZ has the highest risk for failure in a welded material, all Q&P conditions have been tested by using Gleeble on samples with the size of normal Charpy impact test pieces. Hardness and Charpy values were measured in advance. The results of this part are reported in Paper I. Subsequently, the laser welding and Q&P treatment were performed on sheets of 5.5 mm thickness and tensile testing was also carried out. Results showed that all samples have higher strength than the base metal and in optimized conditions also higher ductility and toughness. Paper II and III gives detailed information about the results and especially in paper III, the main reasons which could potentially influence the toughness in different Q&P conditions are studied and discussed in detail.

5.3.1 Mechanical properties of 06CV

The mechanical properties, including hardness, impact toughness and tensile test results, of steel 06CV are extensively described by different process control maps in paper V. The reason was to get an overview of the properties as a function of different Q&P processing parameters. In a few Q&P conditions, hardness of over 800 HV but a very brittle structure is observed. For some other cases both good toughness and hardness were achieved. Samples with satisfactory ductility and over 2 GPa tensile strength showed over 700 HV in hardness. All these properties could be used in different applications with specific demands. In addition, other tests including fatigue and wear (rolling- sliding) test are ongoing or planned for continued investigation of this steel.

6 Summary of appended papers

Paper I

Title: Microstructure Analysis and Mechanical Properties of Low Alloy High Strength Quenched and Partitioned Steel

Authors: F. Forouzan; S. Gunasekaran; A. Hedayati, E. Vuorinen; F. Mücklich

Summary: In **paper I**, the effect of different Q&P conditions on microstructure and mechanical properties of Domex 960 steel have been investigated. Three different quenching temperatures, three partitioning temperatures and three partitioning times have been selected to process the 27 specimens by Gleeble® 1500 at Oulu University.

Microstructure characterization has been performed by optical microscopy, scanning electron microscopy (SEM), Energy Dispersive X-

Ray (EDX) and X-ray diffraction and the mechanical properties that were studied are hardness and impact toughness. The SEM analyses revealed the presence of tempered martensite with precipitates (Ti(C,N)) inside them, bainite laths and bulky retained austenite and/or untempered martensite for all samples. The amount and size of each micro-constituent depend on the Q&P conditions.

The hardness increases as the quenching temperature is decreased, however, at the highest partitioning temperature (640°C) the hardness increases sharply due to extensive precipitate formation. Results showed that although Domex960 has very low carbon content (0.08wt%) and small amounts of Si to slow down the diffusional transformations, the properties of the final structure can be improved by selecting proper Q&P conditions.

Author's contribution: The author performed the experimental work with help of Suresh Gunasekaran (second author), analyzed the data, wrote the paper and presented this work at 8th International Conference on Materials Structure & Micromechanics of Fracture, Brno, Czech Republic, June 27–29, 2016.

Paper II

Title: Post weld-treatment of laser welded AHSS by application of quenching and partitioning technique

Authors: E. Forouzan, E. Vuorinen, F. Mücklich

Due to the very high cooling rate of laser welding usually brittle martensite form in the HAZ. So, in this study the effect of Q&P treatment on the HAZ just after welding is simulated by using Gleeble thermomechanical simulator and thereafter tested (which more detailed in paper I). In this paper, the same cycles tested in Gleeble were repeated after laser welding by using an induction heater close to the weld zone. The microstructures were analyzed using LOM, SEM, EBSD, EDX, and XRD and mechanical properties were studied by micro-hardness measurements across the weld, tensile and impact toughness tests. Microstructural observations revealed the presence of tempered martensite with precipitates, bulky fresh martensite, bainite laths, and precipitates. EBSD analysis of the samples showed that short isothermal heating times of 2 or 5 s were long enough for tempering the primary martensite formed after quenching. Although higher temperature increases diffusion rate, phase transformation to ferrite is more pronounced in samples tempered at 540°C in comparison with 640°C since increasing temperature from 540°C to 640°C will increase the carbon solubility in ferrite and decrease the stress concentrations in the structure. Tensile test results of the welded samples showed that all the heat treated samples have higher strength than the minimum defined strength of the material. Samples with more than 60% martensite created during the first quench which are then tempered properly, showed up to 80% increase of the elongation at failure (A_5) value in comparison with the reference weld, saving the strength limit of base metal. However, the impact toughness of samples tempered at 640 °C was surprisingly low. So, in **paper III** different factors which can cause this low toughness were investigated in detail.

Author's contribution: First author has performed most of the experiments, analyzes, and writing of the article, which is published in **Materials Science and Engineering: A**.vol.698, 174-182, 2017.

Paper III

Title: Effect of Carbon Partitioning, Carbide Precipitation, and Grain Size on Brittle Fracture of Ultra-High-Strength, Low-Carbon Steel after welding by a Quenching and Partitioning Process

Authors: F. Forouzan, A. Guitar, E. Vuorinen, F. Mücklich,

Paper III has been focused on the possible main causes of the very low impact toughness results of a group of samples mentioned in **paper II** which have very good strength and ductility. In this regard; i) The carbon content and amount of retained austenite; ii) Precipitate size and distribution, and; iii) Martensite/bainite packet size, were investigated. Results show that there is no retained austenite in these low toughness samples. In addition, although the number density of the precipitates in these samples are 1.5 times higher than for the tough samples, their average size is the same or even smaller. But the packet sizes of martensite and/or bainite lathes are significantly larger after partitioning at 640°C. Therefore, it could be concluded that the increase of the number density of small precipitates in the sample partitioned at 640 °C compensates the effect of the increase of crystallographic packets size. The strength and ductility values are kept at a high level, but the impact toughness will decrease considerably.

Author's contribution: First author has done most of the experiments and some of the experiments was performed together with the second author. In addition, simulations, analyze of the data, and writing of the article was accomplished by the first author.

Published in **Metals**, vol. 8, 747, **2018**.

Paper IV

Title: Optimization of Quenching Temperature to Minimize the Micro Segregation Induced Banding Phenomena in Quenching and Partitioning (Q&P) Steels

Authors: F. Forouzan, L. Borasi, E. Vuorinen, and F. Mücklich

In this paper has an issue that can occur in Q&P steels been treated. Mn and Cr are favorable elements for Q&P steels but because they will increase the risk of microsegregation, this paper is focused on this problem and how that can affect the microstructure and properties of a Q&P treated steel. In addition, the question of how it is possible to minimize the effect of segregation in Q&P steels by selection of quenching temperature is discussed.

Author's contribution: First author has performed most of the experimental work, while the second author has performed some of the experiments. In addition, analyze of the data, and writing of the article was accomplished by the first author.

Published in **Steel Research Int.**, 90 (1), Article ID 1800281, 2019.

Paper V

Title: Process Control Maps to Design an Ultra-High Strength-Ductile Steel

Authors: F. Forouzan, L. Borasi, E. Vuorinen, F. Mücklich

Paper V is about the Q&P process of a high carbon high silicon steel (0.6 wt% C, 1.5 wt%Si) and the resulting microstructure and mechanical properties. In this work, the effect of Q&P conditions on the amount retained austenite and its carbon content, hardness, Charpy impact toughness, tensile strength, and elongation are demonstrated by several color-contour process maps. This work has shown also very promising results; tensile strength of 2.4-2.5 GPa and elongation at fracture up to 4.8-5.7 %, by quenching to room temperature and partitioning at 400 °C for 30 seconds. This result is better than several hours tempering of traditional Q&T steels and on the same level as maraging steels with a high amount of expensive alloying element or CFB steels which needs several hours of austempering treatment.

Author's contribution: First author has done most of the experimental work, while some of the experiments was performed with the help of the second author. In addition, analyze of the data, and writing the article is accomplished mainly by the first author.

Submitted to Materials Science and Technology, Jan 2019.

7 Conclusions and Future work

The work presented in this thesis has shown that the application of quenching and partitioning technique in order to increase the phase transformation rate as post welding heat treatment and for producing well stabilized austenite for bearing steels in comparison with traditional techniques have promising results. These kinds of approaches to utilize Q&P have not been reported earlier and it can be seen as novel knowledge which could be used in other technical applications as well.

7.1 Important conclusions

- Application of Q&P after laser welding not only gives a quick industrial processing method for post welding treatments but also

improves the microstructure and mechanical properties of the HAZ.

- Application of Q&P process for low silicon steel to increase the phase transformation rate needs more attention to the competing mechanisms like carbide precipitation, bainite transformation, and grain growth.
- Growing of martensite packet size was observed after the partitioning stage. This phenomenon is very important because the martensite packet size influences the toughness significantly by changing the DBTT.
- An ultra-high strength steel with 0.6 wt% carbon and high silicon content is produced by Q&P process. The best results were observed after quenching to room temperature and tempering at a higher temperature (400 °C) than normal tempering temperatures for a few seconds. The tensile strength of 2.4-2.5 GPa and elongation of 4-6 %, with the hardness over 700 HV is achieved.
- Using the above-mentioned treatment can reduce the cost to around 1/50 compared with maraging steels and the time at least to 1/15 of the advanced methods of CFB steels with similar properties.
- Micro-segregation is a common issue in especially high Mn steels that can affect the properties after Q&P treatment. Generally, by increasing the under cooling ($QT-M_s$) inhomogeneity in the segregated bands after Q&P has less effect in forming different micro constituents. But there is an optimum point far below the M_s which gives the minimum difference between the bands and by increasing the undercooling after that the difference in hardness and inhomogeneity will increase again.

7.2 Future work

With regard to the objective of this work; increasing the phase transformation rate and shortening the whole heat treatment time by partial transformation of austenite to martensite, this is the main task which could be investigated more in detail and be tested on other applications. The following topics are of interest:

- Study the kinetics of other transformations (i.e. bainite transformation, stabilization of austenite) in presence of pre-existing martensite by using in-situ XRD.
- Optimization of Q&P for higher carbon steels (i.e. 1%C steel) in order to reach an acceptable ductility.
- Further modification of Q&P to reach over 10% ductility for high carbon steels. For instance, by grain refinement and/or additional tempering after the final quenching or modifications in chemical composition.
- Comprehensive comparison of mechanical properties, wear and fatigue of Q&P steels with ausferritic (CFB) steels for a wide range of chemical compositions.
- Investigation of the effect of tempering conditions on growth of martensite packets.
- Application of Q&P after MIG/MAG welding by developing; proper filler metal, high enough cooling rate after welding and the practical methodology of second heating for partitioning stage.
- Application of Q&P for spot welding and hot forming processes.

8 References

[1] J.R. Fekete, J.N. Hall, 1 - Design of auto body: Materials perspective, in: R. Rana, , S.B. Singh (Eds.), Automotive Steels, Woodhead Publishing, 2017, pp. 1-18.

[2] C. Lesch, N. Kwiaton, F.B. Klose, Advanced High Strength Steels (AHSS) for Automotive Applications – Tailored Properties by Smart Microstructural Adjustments, steel research int. 88 (2017) 1700210.

[3] D.K. Matlock, J.G. Speer, E. De Moor, P.J. Gibbs, Recent developments in advanced high strength sheet steels for automotive applications: an overview,.

[4] R.A. Kot and B.L. Bramfitt, eds. :, *Fundamentals of Dual-Phase Steels*; TMS AIME, Warrendale, PA. (1981).

[5] M.S. Rashid, B.V.N. Rao, Tempering characteristics of a vanadium containing dual phase steel, *Metallurgical Transactions A*. 13 (1982) 1679-1686.

[6] Marder, A.R., ;*Factors Affecting the Ductility of “Dual-Phase” Alloys* ; *Formable HSLA and Dual-Phase Steels*, A.T. Davenport, TMS AIME, Warrendale, PA, 1979, pp. 98.

[7] J.G. Speer, E. De Moor, K.O. Findley, D.K. Matlock, B.C. De Cooman, D.V. Edmonds, *Analysis of Microstructure Evolution in Quenching and Partitioning Automotive Sheet Steel*, *Metallurgical and Materials Transactions A*. 42 (2011) 3591.

[8] E. Billur, T. Altan, Three generations of advanced high-strength steels for automotive applications, Part III, *Stamp J*. (2014).

[9] H. Dong, X. Sun, Deformation induced ferrite transformation in low carbon steels, *Current Opinion in Solid State and Materials Science*. 9 (2005) 269-276.

[10] J. Choi, D. Seo, J. Lee, K. Um, W. Choo, Formation of Ultrafine Ferrite by Strain-induced Dynamic Transformation in Plain Low Carbon Steel, *ISIJ Int*. 43 (2003) 746-754.

[11] M. Delincé, Y. Bréchet, J.D. Embury, M.G.D. Geers, P.J. Jacques, T. Pardoen, Structure–property optimization of ultrafine-grained dual-phase steels using a microstructure-based strain hardening model, *Acta Materialia*. 55 (2007) 2337-2350.

[12] Y. Okitsu, T. Naito, N. Takaki, T. Sugiura, N. Tsuji, Mechanical Properties and Crash Worthiness of Ultrafine Grained Multi-Phase Steel Sheets for Automotive Body Applications, *SAE Int. J. Mater. Manuf*. 3 (2010) 237-245.

[13] V.F. Zackay, E.R. Parker, D. Fahr, R. Busch, The enhancement of ductility in high-strength steels, *Transactions of the ASM*. 60 (1967) 252-257.

- [14] F. Perrard, C. Scott, Vanadium Precipitation During Intercritical Annealing in Cold Rolled TRIP Steels, *ISIJ Int.* 47 (2007) 1168-1177.
- [15] A.Z. Hanzaki, P.D. Hodgson, S. Yue, Hot Deformation Characteristics of Si-Mn TRIP Steels with and without Nb Microalloy Additions, *ISIJ Int.* 35 (1995) 324-331.
- [16] E. De Moor, P.J. Gibbs, J.G. Speer, D.K. Matlock, J.G. Schroth, Strategies for third-generation advanced high-strength steel development, *Iron and Steel Technology.* 7 (2010) 133-144.
- [17] F.G. Caballero, 12 - Carbide-free bainite in steels, in: E. Pereloma, D.V. Edmonds (Eds.), *Phase Transformations in Steels*, Woodhead Publishing, 2012, pp. 436-467.
- [18] F.G. Caballero, C. García-Mateo, J. Cornide, S. Allain, J. Puerta, M. Crouvizier, T. Mastrotillo, L. Jantzen, E. Vuorinen, L.E. Lindgren, K. Eriksson, G. Berglund, A. Hirvi, V. Lang, T.T. Nyo, P. Suikkanen, A.J. Ristola, New advanced ultra high strength bainitic steels: ductility and formability (DUCTAFORM), 25977 (2013).
- [19] T. Sourmail, V. Smanio, C. Ziegler, V. Heuer, M. Kuntz, F. Caballero, C. Garcia-Mateo, J. Cornide, R. Elvira, A. Leiro, E. Vuorinen, T. Teeri, Novel Nanostructured Bainitic Steel Grades to Answer the Need for High-Performance Steel Components (Nanobain), 2013.
- [20] C. GARCIA-MATEO, F.G. CABALLERO, Ultra-high-strength Bainitic Steels, *ISIJ Int.* 45 (2005) 1736-1740.
- [21] F.G. Caballero, Bhadeshia, H. K. D. H., Very strong bainite, *Current Opinion in Solid State and Materials Science.* 8 (2004) 251-257.
- [22] C. Garcia-Mateo, F.G. Caballero, Bhadeshia, H. K. D. H., Acceleration of low-temperature bainite, *ISIJ Int.* 43 (2003) 1821-1825.
- [23] J. Schmitt, T. Iung, New developments of advanced high-strength steels for automotive applications, *Comptes Rendus Physique.* (2018).

[24] B. Kim, J. Sietsma, M.J. Santofimia, The role of silicon in carbon partitioning processes in martensite/austenite microstructures, *Materials & Design*. 127 (2017) 336-345.

[25] J.G. Speer, F.C. Rizzo, D.K. Matlock, D.V. Edmonds, The "Quenching and Partitioning Process": Background and Recent Progress. *Materials Research*. 8 (2005) 417-423.

[26] M.J. Santofimia, L. Zhao, J. Sietsma, Overview of Mechanisms Involved During the Quenching and Partitioning Process in Steels, *Metallurgical and Materials Transactions A*. 42 (2011) 3620-3626.

[27] E. De Moor, S. Lacroix, A.J. Clarke, J. Penning, J.G. Speer, Effect of retained austenite stabilized via quench and partitioning on the strain hardening of martensitic steels, *Metallurgical and Materials Transactions A*. 39 (2008) 2586.

[28] Y. Toji, H. Matsuda, D. Raabe, Effect of Si on the acceleration of bainite transformation by pre-existing martensite, *Acta Materialia*. 116 (2016) 250-262.

[29] D.V. Edmonds, K. He, F.C. Rizzo, B.C. De Cooman, D.K. Matlock, J.G. Speer, Quenching and partitioning martensite—A novel steel heat treatment, *Materials Science and Engineering: A*. 438-440 (2006) 25-34.

[30] D. Kim, J. Speer, H. Kim, B. De Cooman, Observation of an Isothermal Transformation during Quenching and Partitioning Processing, *Metallurgical and Materials Transactions A*. 40 (2009) 2048-2060.

[31] F. HajyAkbar, J. Sietsma, R.H. Petrov, G. Miyamoto, T. Furuhashi, M.J. Santofimia, A quantitative investigation of the effect of Mn segregation on microstructural properties of quenching and partitioning steels, *Scripta Materialia*. 137 (2017) 27-30.

[32] D.T. Pierce, D.R. Coughlin, K.D. Clarke, E. De Moor, J. Poplawsky, D.L. Williamson, B. Mazumder, J.G. Speer, A. Hood, A.J. Clarke, Microstructural evolution during quenching and partitioning of 0.2C-1.5Mn-1.3Si steels with Cr or Ni additions, *Acta Materialia*. 151 (2018) 454-469.

- [33] M.C. Somani, D.A. Porter, L.P. Karjalainen, R.D.K. Misra, On Various Aspects of Decomposition of Austenite in a High-Silicon Steel During Quenching and Partitioning, *Metallurgical and Materials Transactions A*. 45 (2014) 1247-1257.
- [34] Y. Toji, G. Miyamoto, D. Raabe, Carbon partitioning during quenching and partitioning heat treatment accompanied by carbide precipitation, *Acta Materialia*. 86 (2015) 137-147.
- [35] Y.S. Allain, G. Geandier, J. Hell, M. Soler, F. Danoix, M. Gouné, Effects of Q&P Processing Conditions on Austenite Carbon Enrichment Studied by In Situ High-Energy X-ray Diffraction Experiments, *Metals*. 7 (2017).
- [36] A.S. Nishikawa, M.J. Santofimia, J. Sietsma, H. Goldenstein, Influence of bainite reaction on the kinetics of carbon redistribution during the Quenching and Partitioning process, *Acta Materialia*. 142 (2018) 142-151.
- [37] F. HajyAkbar, J. Sietsma, G. Miyamoto, T. Furuhashi, M.J. Santofimia, Interaction of carbon partitioning, carbide precipitation and bainite formation during the Q&P process in a low C steel, *Acta Materialia*. 104 (2016) 72-83.
- [38] D.T. Pierce, D.R. Coughlin, K.D. Clarke, E. De Moor, J. Poplawsky, D.L. Williamson, B. Mazumder, J.G. Speer, A. Hood, A.J. Clarke, Microstructural evolution during quenching and partitioning of 0.2C-1.5Mn-1.3Si steels with Cr or Ni additions, *Acta Materialia*. 151 (2018) 454-469.
- [39] X.D. Wang, Z.H. Guo, Y.H. Rong, Mechanism exploration of an ultrahigh strength steel by quenching-partitioning-tempering process, *Materials Science and Engineering: A*. 529 (2011) 35-40.
- [40] D. De Knijf, R. Petrov, C. Föjler, L.A.I. Kestens, Effect of fresh martensite on the stability of retained austenite in quenching and partitioning steel, *Mater. Sci. Eng. A*. 615 (2014) 107-115.
- [41] M.J. Santofimia, R.H. Petrov, L. Zhao, J. Sietsma, Microstructural analysis of martensite constituents in quenching and partitioning steels, *Mater Charact*. 92 (2014) 91-95.

- [42] M.-. Wang, J.-. Hell, C.C. Tasan, Martensite size effects on damage in quenching and partitioning steels, *Scripta Materialia*. 138 (2017) 1-5.
- [43] B. Hutchinson, J. Hagström, O. Karlsson, D. Lindell, M. Tornberg, F. Lindberg, M. Thuvander, Microstructures and hardness of as-quenched martensites (0.1–0.5% C), *Acta Materialia*. 59 (2011) 5845-5858.
- [44] Bhadeshia, H K D H, S.R. Honeycombe, 5 - Formation of Martensite, in: Bhadeshia, H K D H, S.R. Honeycombe (Eds.), *Steels* (Third Edition), Butterworth-Heinemann, Oxford, 2006, pp. 95-128.
- [45] P. Payson, C.H. Savage, Martensite reactions in alloy steels, *Trans.ASM*. 33 (1944) 261-280.
- [46] R.A. Grange, H.M. Stewart, The temperature range of martensite formation, *Trans.AIME*. 167 (1946) 467-501.
- [47] A.E. Nehrenberg, Contribution to Discussion on Grange and Stewart, *Trans.Amer.Inst.Min.Met.Engrs*. 167 (1946) 494-498.
- [48] A.G. Haynes, W. Steven, The temperature of formation of martensite and bainite in low-alloy steel, *J.Iron Steel Inst*. 183 (1956) 349-359.
- [49] K.W. Andrews, Empirical formulae for the calculation of some transformation temperatures, *J.Iron Steel Inst*. 203 (1965) 721-727.
- [50] S. Van Bohemen, Bainite and martensite start temperature calculated with exponential carbon dependence, *Materials Science and Technology*. 28 (2012) 487-495.
- [51] A. Stormvinter, G. Miyamoto, T. Furuhashi, P. Hedström, A. Borgenstam, Effect of carbon content on variant pairing of martensite in Fe-C alloys, *Acta Materialia*. 60 (2012) 7265-7274.
- [52] P. Zhang, Y. Chen, W. Xiao, D. Ping, X. Zhao, Twin structure of the lath martensite in low carbon steel, *Progress in Natural Science: Materials International*. 26 (2016) 169-172.

[53] S. Morito, H. Tanaka, R. Konishi, T. Furuhashi, T. Maki, The morphology and crystallography of lath martensite in Fe-C alloys, *Acta Materialia*. 51 (2003) 1789-1799.

[54] N.H. van Dijk, A.M. Butt, L. Zhao, J. Sietsma, S.E. Offerman, J.P. Wright, S. van der Zwaag, Thermal stability of retained austenite in TRIP steels studied by synchrotron X-ray diffraction during cooling, *Acta Materialia*. 53 (2005) 5439-5447.

[55] C. Garcia-Mateo, F.G. Caballero, J. Chao, C. Capdevila, d.A. Garcia, Mechanical stability of retained austenite during plastic deformation of super high strength carbide free bainitic steels, *J. Mater. Sci.* 44 (2009) 4617-4624.

[56] X.C. Xiong, B. Chen, M.X. Huang, J.F. Wang, L. Wang, The effect of morphology on the stability of retained austenite in a quenched and partitioned steel, *Scripta Materialia*. 68 (2013) 321-324.

[57] A.J. Clarke, J.G. Speer, D.K. Matlock, F.C. Rizzo, D.V. Edmonds, M.J. Santofimia, Influence of carbon partitioning kinetics on final austenite fraction during quenching and partitioning, *Scr. Mater.* 61 (2009) 149-152.

[58] D.P. Koistinen, R.E. Marburger, A general equation prescribing the extent of the austenite-martensite transformation in pure iron-carbon alloys and plain carbon steels, *Acta Metallurgica*. 7 (1959) 59-60.

[59] F.G. Caballero, C. Garcia-Mateo, 9 - Phase transformations in advanced bainitic steels, in: E. Pereloma, , D.V. Edmonds (Eds.), *Phase Transformations in Steels*, Woodhead Publishing, 2012, pp. 271-294.

[60] T. Sourmail, F.G. Caballero, F. Moudian, D. De Castro, M. Benito, *High Hardness and Retained Austenite Stability in Si-Bearing Hypereutectoid Steel through New Heat Treatment Design Principles*, 2018.

[61] T. Ko, S.A. Cottrell, The formation of bainite, *Journal of the Iron and Steel Institute*. 172 (1952) 8.

- [62] V. Smanio, T. Sourmail, Effect of partial martensite transformation on bainite reaction kinetics in different 1%C steels, *Diffus Def Data Pt B.* 172-174 (2011).
- [63] I.A. Yakubtsov, G.R. Purdy, Analyses of Transformation Kinetics of Carbide-Free Bainite Above and Below the Athermal Martensite-Start Temperature, *Metallurgical and Materials Transactions A.* 43 (2012) 437-446.
- [64] M.J. Santofimia, van Bohemen, S. M. C., J. Sietsma, Combining bainite and martensite in steel microstructures for light weight applications, *Journal of the Southern African Institute of Mining and Metallurgy.* 113 (2013) 143-148.
- [65] T. Sourmail, F.G. Caballero, F. Moudian, D. De Castro, M. Benito, High hardness and retained austenite stability in Si-bearing hypereutectoid steel through new heat treatment design principles, *Materials & Design.* 142 (2018) 279-287.
- [66] E. Vuorinen, Structure and properties of advanced fine grained steels produced using novel thermal treatments, Doctoral thesis / Luleå University of Technology 1 jan 1997 → (2012) 43.
- [67] E. Vuorinen, Time diffusivity estimations in press hardening and welding processes with quenching and partitioning heat treatments, *EEIGM International Conference on Advanced materials research :* 21/03/2013 - 22/03/2013. (2013) 1.
- [68] X. Han, Y. Zhong, K. Yang, Z. Cui, J. Chen, Application of Hot Stamping Process by Integrating Quenching & Partitioning Heat Treatment to Improve Mechanical Properties, *Procedia Engineering.* 81 (2014) 1737-1743.
- [69] X. Han, Y. Zhong, S. Tan, Y. Ding, J. Chen, Microstructure and performance evaluations on Q&P hot stamping parts of several UHSS sheet metals, *Science China Technological Sciences.* (2017).
- [70] E.J. Seo, L. Cho, B.C. De Cooman, Application of Quenching and Partitioning (Q&P) Processing to Press Hardening Steel, *Metallurgical and Materials Transactions A.* 45 (2014) 4022-4037.

[71] F. Forouzan, E. Vuorinen, F. Mücklich, Post weld-treatment of laser welded AHSS by application of quenching and partitioning technique, *Materials Science and Engineering: A*. 698 (2017) 174-182.

[72] E. Vuorinen, N. Ojala, V. Heino, C. Rau, C. Gahm, Erosive and abrasive wear performance of carbide free bainitic steels – comparison of field and laboratory experiments, *Tribology International*. 98 (2016) 108-115.

[73] A.B. Thermo-Calc Software, MOBFE3: TCS Steels/Fe-Alloys Mobility Database,.

Paper I

Microstructure Analysis and Mechanical Properties of Low Alloy High Strength Quenched and Partitioned Steel

Farnoosh Forouzan^{1,a}, Suresh Gunasekaran^{1,b}, Ali Hedayati^{1,c},
Esa Vuorinen^{1,d} and Frank Mücklich^{2,e}

¹ Department of Engineering Sciences and Mathematics, Luleå University of Technology, SE-97187 Luleå, Sweden

² Department for Materials Science, Functional Materials, Saarland University, D-66041 Saarbrücken, Germany

^afarnoosh.forouzan@ltu.se, ^bsuresh.gunasekaran@icloud.com, ^cali.hedayati@ltu.se, ^desa.vuorinen@ltu.se, ^emuecke@matsci.uni-sb.de

Keywords: AHSS, Gleeble, Quenching and partitioning (Q&P), X-ray, mechanical properties

Abstract. Gleeble study of the quenching and partitioning (Q&P) process has been performed on Domex 960 steel (Fe, 0.08 %C, 1.79 %Mn, 0.23 %Si, 0.184 %Ti, and 0.038 %Al). The effect of different Q&P conditions on microstructure and mechanical properties were investigated. The aim of the process is to produce a fine grained microstructure for better ductility and controlled amounts of different micro-constituents to increase the strength and toughness simultaneously. Three different quenching temperatures, three partitioning temperatures and three partitioning times have been selected to process the 27 specimens by Gleeble® 1500. The specimens were characterized by means of OM, SEM, XRD, hardness and impact tests. It was found that, fine lath martensite with retained austenite is achievable without high amount of Si or Al in the composition although lack of these elements may cause the formation of carbides and decrease the available amount of carbon for partitioning into the austenite. The hardness increases as the quenching temperature is decreased, however, at highest partitioning temperature (640°C) the hardness increases sharply due to extensive precipitate formation.

Introduction

Significant research efforts have been directed towards the development of advanced high-strength steels (AHSS). The main objective has been to obtain a good combination of strength and ductility. AHSS steels are usually multiphase and, thus the combination of different phases (ferrite, martensite, retained austenite (RA), etc.) leads to unique mechanical properties. The martensite and bainite constituents contribute to an increase of strength, whereas RA provides an improvement of ductility [1]. The microstructural heterogeneity results also in significant stress and strain partitioning among the micro-constituents during plastic deformation. The thermal processing route, “quenching and partitioning” (Q&P), has been used for production of martensitic microstructures containing enhanced levels of retained austenite caused by carbon diffusion from martensite into austenite. Elements such as Si or Al hinder the carbide formation in steels. [2]. The mechanical behaviour depends on morphology, distribution and mechanical properties of the individual phases [3]. The Q&P processing technique can also give a higher transformation rate in different manufacturing processes like press hardening, welding, etc. [4]. Initial studies on welding of a spring steel showed that it is possible to control the hardness in the fusion zone (FZ) and the part of the heat affected zone (HAZ) which is subjected to a risk of martensite formation at the end of the welding process. The results showed that a quenching process producing 50 % martensite followed by partitioning during 90 seconds could restore the same hardness in the FZ and HAZ as conventional pre- and post-heat treatments lasting 30 + 30 minutes [5]. The aim of this study has been to investigate the effects of using different Q&P variables during welding of modern thermo-mechanically produced steel by simulating the process with Gleeble test and study the amount of retained austenite, microstructure and mechanical properties achieved after these treatments.

Experimental procedure

Table 1 shows the chemical composition of the AHSS, Domex 960, produced by SSAB Company.

Table 1. Chemical composition of Domex 960.

C%	Si%	Mn%	P%	S%	Al%	Ti%	Mo%	Cr%	Ni%	Cu%	V%	N%	Fe
0.082	0.23	1.79	0.008	0.001	0.038	0.184	0.503	0.064	0.296	0.016	0.012	0.004	Balance

Specimens (75×5.5 mm) were cut from 6 mm thick plates and subjected to Q&P heat treatment cycles in the Gleeble® 1500 simulator. The process started with heating to above the A_3 temperature (1350 °C for 2 sec) and was followed by quenching to one of 3 (255, 355 and 420 °C) temperatures. Then the samples were reheated with a heating rate of 80 °C/s, kept isothermally at 440 °C (close to Ms), 540 °C (between Ms and Bs) or 640 °C (above Bs) for 2, 5 or 50 seconds for partitioning and finally quenched with a rate of 80 °C/s to room temperature.

After regular grinding and polishing steps until 0.05 µm, samples were etched by Nital 3% and scanning electron microscopy (SEM) was done by JSM 6460 LV, with accelerating voltage of 15kV. X-ray diffraction (XRD) analysis was performed using monochromatic Cu-K α radiation at 40 KV and 45 mA to scan the angular 2 θ range of 35° to 100°. Data was analysed using High Score Plus software (vers.3.0.1). Micro Vickers hardness measurements were performed on the specimens using the load of 0.5 kg. Impact tests were carried out according to the standard EN ISO 6892-1:2009.

Results

The microstructural investigation of the samples show bulky micro-constituents which are most likely tempered martensite with titanium nitride precipitates inside martensite and retained austenite in flat dark areas with fine bainitic ferrite laths. Comparison of microstructures of the samples quenched at same temperature in Fig. 1 implies that since the amounts of martensite in all conditions are approximately the same, the longer the partitioning time and higher the temperature, the higher the number and size of precipitates and thicker the bainitic laths are. However, the particles cannot be seen in Fig. 1(i) which is heated at 640 °C for 50s probably because larger precipitates can be formed at the grain boundaries and be hidden there. In addition, the amount of stabilized retained austenite at room temperature after the heat treatment cycle increases as the temperature or time increase in samples partitioned at 440 °C or 540 °C but for the samples partitioned at 640 °C the retained austenite transforms to other phases.

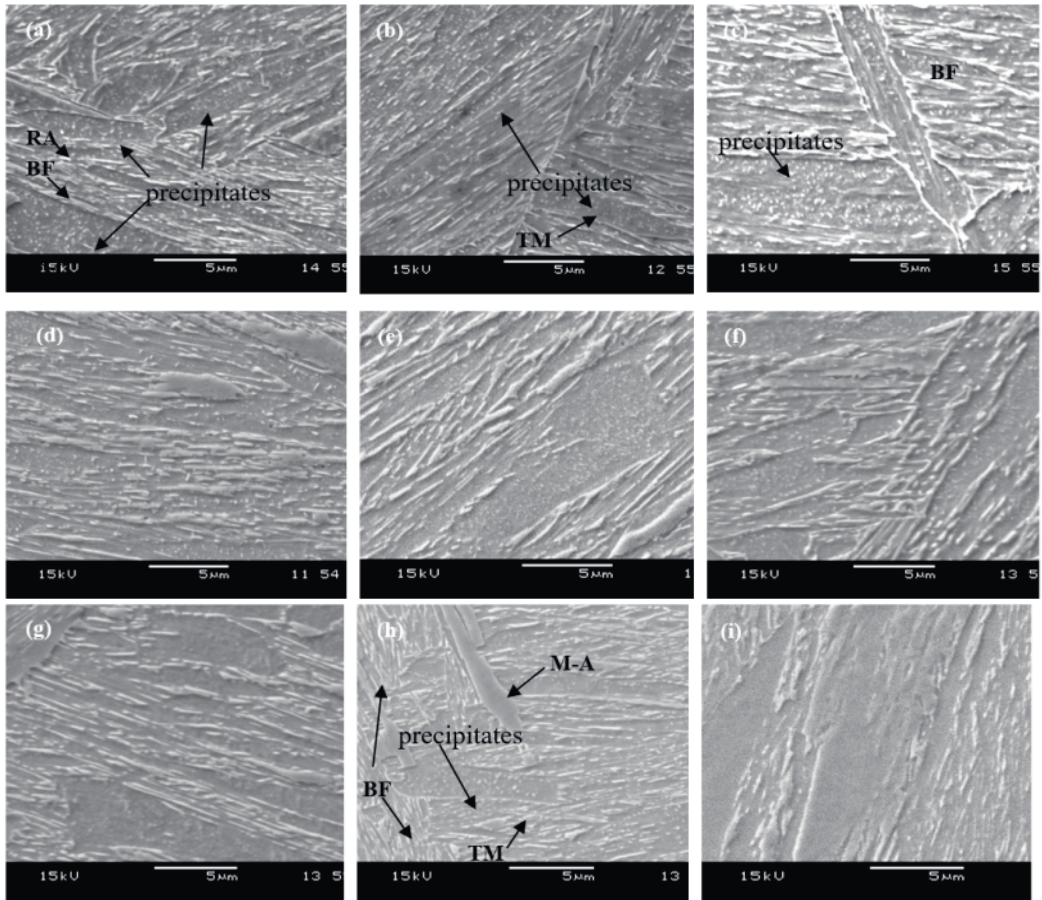


Figure 1. The XRD analyze of one of the softest samples shows around 6% austenite, . In Fig. 2(a) the first two peaks around 40° and 42° shows one type of titanium nitride and all other peaks are related to retained austenite (γ) and ferrite/martensite (α). It is hard to distinguish martensite from ferrite with XRD since their peaks are expected to be found at the same angles or very close to each other.

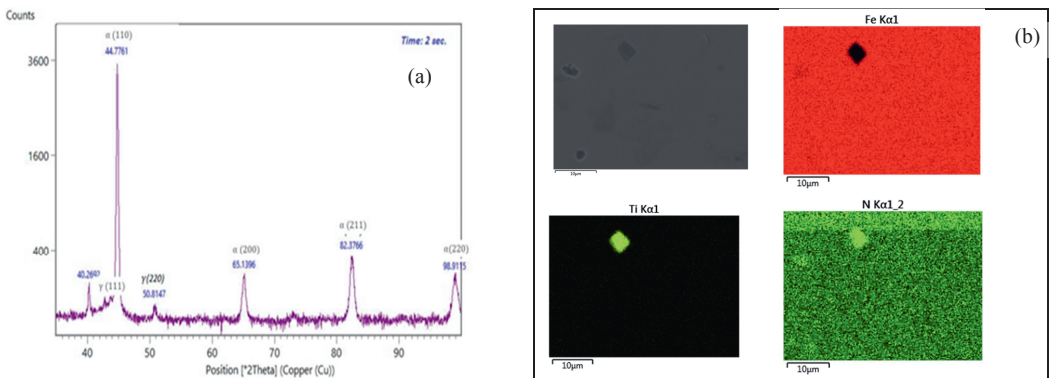


Figure 2. (a) XRD pattern of the sample quenched at 355°C and heated at 540°C for 2 seconds (b) EDS result of sample quenched at 355°C and partitioned at 640°C for 50 seconds.

Only the martensite diffraction peaks for the (002) and (112) planes around $2\theta = 60^\circ$ and 78° respectively, can distinctly be separated from the austenite and ferrite peaks but these peaks are weak and cannot be seen in these samples. It means that most of the martensite in the structure is tempered and during the last quench no or very small amount of retained austenite is transformed to martensite which is not detectable in XRD pattern. Also characterization of the precipitates with EDS in Fig 2(b), confirms the formation of titanium nitrides during partitioning.

Fig 3(a) shows the hardness values of the samples. The hardness is higher for all treated samples in comparison with the received material ($320 \text{ HV}_{0.5}$). Typically, increasing the partitioning time or temperature will decrease the hardness value as a result of martensite tempering and partitioning of the adequate carbon to retained austenite and stabilize that. But, samples which are partitioned at 640°C for 50 s have significantly higher hardness since this condition provides enough time for the hardening by precipitation to counteract the tempering effect. The energy absorbed during Charpy impact test, shows that samples partitioned at 640°C have the lowest results while the samples isothermally heated at 540°C show the best results, see Fig. 3(b).

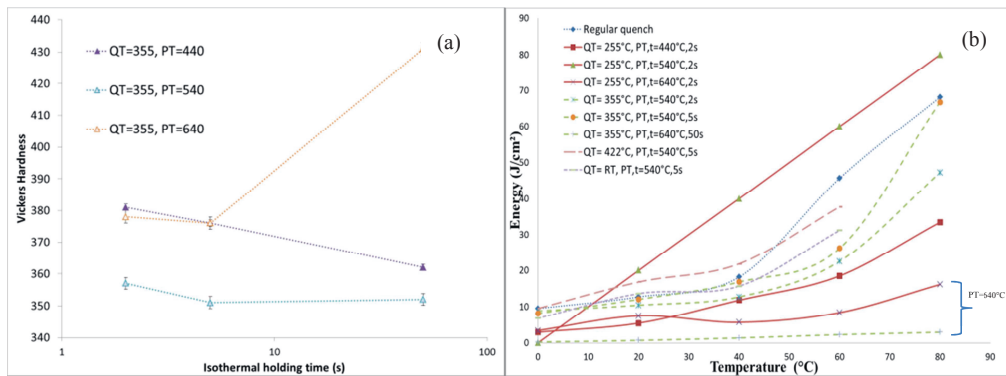


Figure 3. (a) Hardness results and (b) Impact toughness test results of different samples.

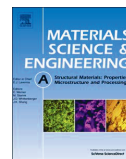
Conclusions:

- 1) The SEM analyse reveals the presence of tempered martensite with precipitates (titanium nitride) inside, bainite laths and bulky retained austenite and/or untempered martensite for all samples. The amount and size of each micro-constituent depends on the Q&P conditions.
- 2) The hardness values of all treated samples were higher than the base material due to the formation of martensite and precipitates in all cases. The specimens which were partitioned at 640°C for 50s have noticeably higher hardness than the other samples because of the increasing amount of precipitates in the structure at that temperature.
- 3) Although there are just small amounts of Si and Al which can slow down the carbide formation, the austenite can be stabilised by selecting proper Q&P conditions.
- 4) Impact toughness results show more brittle behaviour for samples partitioned at 640°C even for a very short partitioning time of 2 seconds but the values for samples in which the partitioning temperature is below the B_s temperature are much better.

References

- [1] Speer JG, De Moor E, Clarke AJ. Critical Assessment 7: Quenching and partitioning. *Materials Science and Technology* 2015 Jan 2015;31(1):3-9.
- [2] de Diego-Calderón I, De Knijf D, Monclús MA, Molina-Aldareguia JM, Sabirov I, Föjer C, et al. Global and local deformation behavior and mechanical properties of individual phases in a quenched and partitioned steel. *Materials Science and Engineering: A* 2015 4/10;630(0):27-35.
- [3] Chen JH, Kikuta Y, Araki T, Yoneda M, Matsuda Y. Micro-fracture behaviour induced by M-A constituent (Island Martensite) in simulated welding heat affected zone of HT80 high strength low alloyed steel. *Acta Metallurgica* 1984 10;32(10):1779-1788.
- [4] Seo E, Cho L, De Cooman B. Application of Quenching and Partitioning (Q&P) Processing to Press Hardening Steel. *Metallurgical and Materials Transactions A* 2014;45(9):4022-4037.
- [5] Vuorinen E, Bax B, Navara E. Weldability of hardenable silicon alloyed spring steel. Conference proceedings of Acta Metallurgica Slovaca Conference, No 14, 2010, 247-254.

Paper II



Post weld-treatment of laser welded AHSS by application of quenching and partitioning technique



Farnoosh Forouzan^{a,b,*}, Esa Vuorinen^a, Frank Mücklich^b

^a Department of Engineering Sciences and Mathematics, Luleå University of Technology, SE-97187 Luleå, Sweden

^b Department for Materials Science, Functional Materials, Saarland University, D-66041 Saarbrücken, Germany

ARTICLE INFO

Keywords:

AHSS
Quenching and partitioning
Microstructure
Mechanical properties

ABSTRACT

Two-step quenching and partitioning (Q & P) treatment was applied on specimens of an advanced high strength steel (AHSS) after laser welding, for post welding treatment. In order to avoid formation of brittle martensite phase, which usually form due to very high cooling rate of laser welding. To simulate the effect of different Q & P parameters after welding in the most critical part of HAZ, several cycles were performed in Gleeble simulator and analyzed in advance. Subsequently some of the cycles were repeated after laser welding by using an induction heater close to the weld. Different techniques including SEM, EBSD and XRD were used to analyze the microconstituents of the structure and mechanical properties were investigated by micro-hardness measurements across the weld, tensile and impact toughness tests. The final structure consists of controlled amount of tempered martensite with precipitates, bainite laths and small amount of fresh martensite depending on the thermal cycles. In addition, samples heated at a temperature between Ms and Bs (in this case 540 °C) showed the best mechanical properties. Therefore, this technique not only improves the microstructure and mechanical properties of the fusion zone (FZ) and heat affected zone (HAZ) but gives also a quick industrial processing method for post welding treatments.

1. Introduction

The number of application in which advanced high strength steels (AHSS) are used, is growing due to their high toughness that can reduce the weight, fuel consumption and costs and last but not least, reduce the environmental impact. But processing of AHSS in which some kind of heat treatment is required to reach the desired mechanical properties, in order to be able to use them in different applications needs more caution [1].

One process method used by the industry is laser welding since it can increase the productivity, can be applied to variety of product geometries, thicknesses and materials without distortion; and it can reduce the weight of the component. There are two modes of laser welding, conduction limited welding and penetration keyhole welding. The resulting weld has wide heat affected zone (HAZ) in the former mode, while in the latter mode it acts as a line source of energy penetrating into the body of material producing narrower and deeper welds. The keyhole mode has higher power density than 10^6 (W/cm²) which vaporizes the material and forms a cavity hole, which will be filled by the surrounded molten metal as the laser beam moves along the weld. The conduction mode show welding results in depth to width

of about 3:1 compared to about 10:1 or higher for the keyhole mode. The cooling rate which is a function of the laser power and the interaction time between the beam and the substrate, is a key factor in defining the microstructure and mechanical properties of the welds [2]. The cooling rates estimated by different setting of laser welding parameters have been found to be much higher than the critical cooling rate for martensite formation. So, there is a risk of martensite transformation in the fusion zone (FZ) and HAZ [3]. In addition, grain growth in the HAZ can change the initial mechanical properties of the material. Thus, controlling the microstructure within the fusion zone and heat affected zone is a challenging topic that can be approached by different ways. Mostly, the idea is to control the micro-constituents by adjusting the welding parameters like speed or power of welding or by using different post-weld heat treatments [4].

Quenching and Partitioning (Q & P) is a heat treatment process in order to give fine grained microstructure by stabilizing the austenite in the steel. The whole procedure consists of three main parts, (i) fully or partially austenitization (ii) quenching the steel to a temperature between Ms and Mf to produce a specific volume fraction of martensite and subsequently (iii) heating to a temperature below or above the Ms temperature, partitioning temperature (PT), where the carbon can

* Corresponding author at: Department of Engineering Sciences and Mathematics, Luleå University of Technology, SE-97187 Luleå, Sweden.
E-mail addresses: farnoosh.forouzan@ltu.se (F. Forouzan), esa.vuorinen@ltu.se (E. Vuorinen), muecke@matsci.uni-sb.de (F. Mücklich).

diffuse from martensite to austenite during the partitioning stage [4]. Therefore, the microstructure consists of retained austenite and martensite (also ferrite, bainite and precipitates depending of the CCT diagram of the steel) [5–7]. Presence of Si and Mn in the chemical composition of the steel is useful to suppress the cementite formation and slow down the kinetic of transformations. However, carbide precipitation and decomposition of austenite to bainite are not completely suppressed. So, during the partitioning step of the samples, there are a few phenomenon competing; i) carbon partitioning from preliminary martensite to austenite ii) carbide precipitation and iii) decomposition of austenite to bainite. Therefore, understanding the prevailed transformation at each condition has an important influence on predicting the final microstructure. The carbon concentration is one effective factor which makes austenite to stabilize at room temperature. Very fine austenite grain size, less than 5 μm , decreases the martensite start temperature significantly [8,9]. In addition, Lee et al. [10] reported that with decreasing austenite grain size, both B_s and B_f decreased and overall bainitic transformation rate was accelerated.

The Q & P process can produce not only complex fine grained microstructure but also give a higher transformation rate in different manufacturing processes [11,12]. By applying the Q & P processing concept to laser welding (see Fig. 1), the toughness of FZ and HAZ are expected to be preserved or even improved in comparison with the Base Metal (BM). Also, since the production speed is the most important parameter in industry, this method can significantly decrease the typical post-welding heat treatment times.

Different pre- and post-weld and Q & P treatments respectively of a spring steel containing 0.55% C and 1.64% Si, in austempered condition were investigated in order to avoid martensite formation in the FZ and HAZ. Results show that application of the quenching and partitioning (Q & P) process enables the control of hardness and a structure similar to the original carbide free bainite instead of martensite was achieved [13].

In the present study, Q & P process was implemented just after welding. The Q & P heat treatment starts with air cooling of the weld area to a temperature between M_s and M_f . The process is continued by isothermal holding at the same or higher temperature as quenching and the final step was quenching to room temperature. This technique is a promising method to produce a good combination of controlled amount of martensite from the first and final quenching that guarantee high strength. Since, this steel doesn't contain high levels of Si or Al in its structure, austenite stabilizing at low temperatures is very difficult. So, partitioning stage in this work is actually like the tempering stage for martensite formed in the first step, providing opportunity for phase transformation of retained austenite to bainite and precipitation of carbides, nitrides and carbonitrides in the steel.

The steel used in this study, is an Advanced High Strength Steel (AHSS) with low carbon and silicon contents. The effect of using a post weld heat-treatment similar to Q & P methodology after laser welding has been investigated from microstructural and mechanical strength point of view.

2. Experimental methods and materials

The chemical composition of the steel sheet, Domex 960 from SSAB, used in the present study is shown in Table 1. The typical application of this AHSS is advanced lifting devices and lighter transport solutions and components: The 5.5 mm-thick sheets were received in the thermo-mechanically rolled, annealed and grain refined condition with the yield strength of 960 MPa and elongation (A_5) of approximately 8% and had a microstructure consisting of ferrite and martensite. The transformation start temperature to martensite (M_s) is 440 °C.

Primarily, to see the effect of Q & P, 27 experiments simulating the weld in controlled conditions in Gleeble 1500, were performed at the Material Engineering Laboratory, Oulu University, Finland. The dimension of Gleeble specimens was 75 mm \times 10 mm \times 5.5 mm. As shown in Fig. 2, all Gleeble specimens were fully austenitized at 1350 °C for 2 s which is selected to simulate the coarse grain part of HAZ, with the highest probability to get martensitic structure. Then samples quenched with the cooling rate of 80 °C/s to (M_s -185 °C), (M_s -85 °C) or (M_s -20 °C) and isothermally hold at (M_s), (M_s +100) or (M_s +200) for 2, 5 or 50 s partitioning time before final quenching to room temperature.

Laser welding was conducted on the 200 mm \times 100 mm sheets of 5.5 mm thickness. The sheets were prepared by cutting and after that machining to get flat surface for the laser welding. The keyhole penetration mode with the ytterbium Fiber Laser (YLR Laser-15000) was selected for the welding. Other welding parameters were adjusted to, 5 kW power, travel speed of 1.1 m/min, Argon was used as a shielding gas with flow rate of 20 l/min. The laser welded specimens were subjected to post-heat treatment directly after the laser welding with help of induction heater, placed above the specimen. The induction heating was steered by adjusting only the Voltage while the induction current was kept at max level. The thermocouple was spot welded 1.5 mm from the fusion zone (FZ) of the weld, and connected to data logger RS-232 to control the temperature during Q & P and to adjust the voltage in short time (less than 1 s). Different Q & P conditions of the investigated specimens are shown in Table 2. In addition, samples 16 and 17 are not post-weld heat-treated, and therefore denominated as "Ref. Weld".

2.1. Microstructural characterization

After grinding and polishing step by step until 0.05 μm , specimens were etched with 3% Nital for optical microscopy (OM) and scanning electron microscopy (SEM). The specimens were prepared for electron backscatter diffraction (EBSD) examination with a final polishing step of colloidal silica and after that were the samples electropolished by LectroPol-5, Struers, with A2 electrolyte at 30 V for 8 s. The analyses were done by orientation imaging microscopy (OIM) on a JSM-IT300 under the acceleration voltage of 20 kV; tilt angle 70; step size 200 nm. The orientation data were post-processed with the AZtech, oxford and Tango software. The same instrument was also used for Energy Dispersive Spectroscopy (EDS). Furthermore, volume fractions of retained austenite were determined by means of X-ray diffraction (XRD) analysis using a monochromatic Cu-K α radiation at 40 kV and 45 mA. Diffractometer was used to scan the angular 2θ range of 35° to

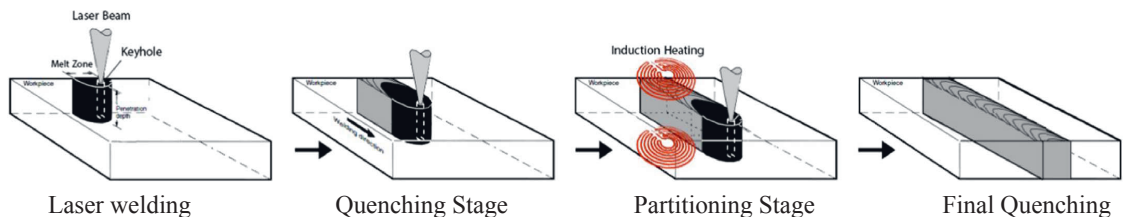


Fig. 1. Schematic of the keyhole fiber laser welding process with Q & P post weld heat treatment.

Table 1
Chemical composition of the steel.

C%	Si%	Mn%	P%	S%	Al%	Ti%	Mo%	Cr%	Ni%	Cu%	V%	N%	Fe
0.082	0.23	1.79	0.008	0.001	0.038	0.184	0.503	0.064	0.296	0.016	0.012	0.004	Balance

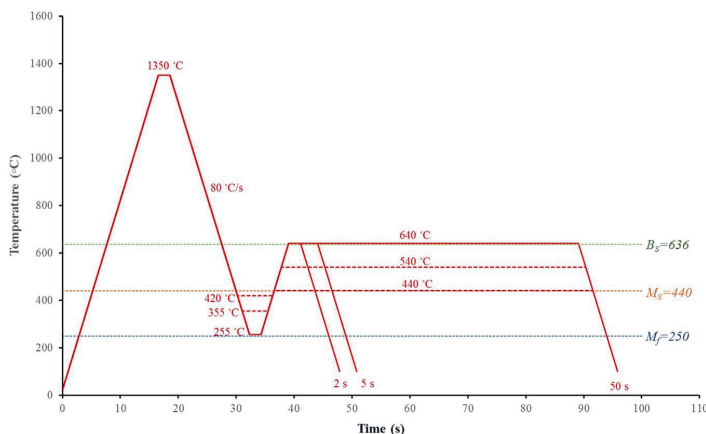


Fig. 2. Schematic of quench and partitioning process in Gleeble simulator.

Table 2
Post-heat treatment procedure for laser welded specimens.

Weld no.	Quenching temperature (QT)	Partitioning temperature (PT)	Holding time
1	255 °C	440 °C	2 s
2	255 °C	440 °C	5 s
3	255 °C	540 °C	2 s
4	255 °C	540 °C	5 s
5	255 °C	640 °C	2 s
6	255 °C	640 °C	5 s
7	355 °C	440 °C	2 s
8	355 °C	440 °C	5 s
9	355 °C	540 °C	2 s
10	355 °C	540 °C	5 s
11	355 °C	640 °C	5 s
12	355 °C	640 °C	50 s
13	422 °C	440 °C	5 s
14	422 °C	540 °C	2 s
15	422 °C	540 °C	5 s
16	Room temp.	540 °C	5 s
17	Room temp.	–	–

100°, the scanning time of every diffractogram was 10 min. The data was analyzed using High Score Plus software (vers.3.0.1).

2.2. Mechanical characterization

Micro Vickers hardness measurements were performed on the Gleeble specimens using the load of 0.5 kg. A load of 0.3 kg was used for the welded samples in which the hardness was determined at both surface and root positions each 0.3 mm across 32 mm of the weld. Tensile tests and impact tests were carried out according to the standard EN ISO 6892-1:2009.

3. Results and discussion

3.1. Gleeble simulation results

Fig. 3 shows OM and SEM micrographs of a few Gleeble samples in

different magnifications. The microstructures consist of martensite and bainite. Tempering of martensite, produced in quenching stage, during the second stage provides enough energy for carbon atoms to escape from martensite by diffusion to the retained austenite around, as well as nitride/carbide precipitation with highest enthalpy in this steel (Ti, V, Mo), by nucleation on the dislocations of the matrix, or at primary austenite grain boundaries and martensite lath boundaries.

Based on Koistinen–Marburger equation [14], the volume fraction of preliminary martensite after the first quenching and prior to tempering were predicted as shown in Table 3.

However, the amount of carbon that actually is transported from martensite to the austenite depends on the partitioning conditions. Theoretically the volume fraction of phases after heat treatment can be approximately predicted by the method developed by Clarke et al. [15]. Following that method, by using Santofimia et al. [16] calculations, the possible martensite austenite interface mobility imposed by the thermal stability of carbon-concentration gradient within the martensite and austenite grains before partitioning step can be included.

A comparison of samples with almost 60% preliminary martensite by OM (Fig. 3b–d), shows a decrease of the white blocks of un-etched fresh martensite by increasing the tempering time or temperature. The amount of bainite in the structure is increased instead. This shows that the amount of diffused carbon in retained austenite was not high enough to stabilize the retained austenite. Also, there are some large particles of Ti(C, N) in all samples. They are formed during the casting process and can be found in the as-received material. But a closer look shows a large number of fine precipitates (around 100 nm) in the tempered martensite matrix, Fig. 3(e) and (f). In Fig. 3(g), some precipitates can be distinguished but in Fig. 3(h) it is very difficult to find them because the increased tempering time at this high temperature of 640 °C, enhances the solubility of carbon in ferrite [17]. Hence, the amount of carbon accessible to form precipitates and escape from ferrite is low and carbon can be solved inside ferrite but can also contribute to coarsening of the Ti(C, N) precipitates created before the first quenching step or be formed during the partitioning at the expense of decreasing the number of small precipitates according to Ostwald ripening mechanism.

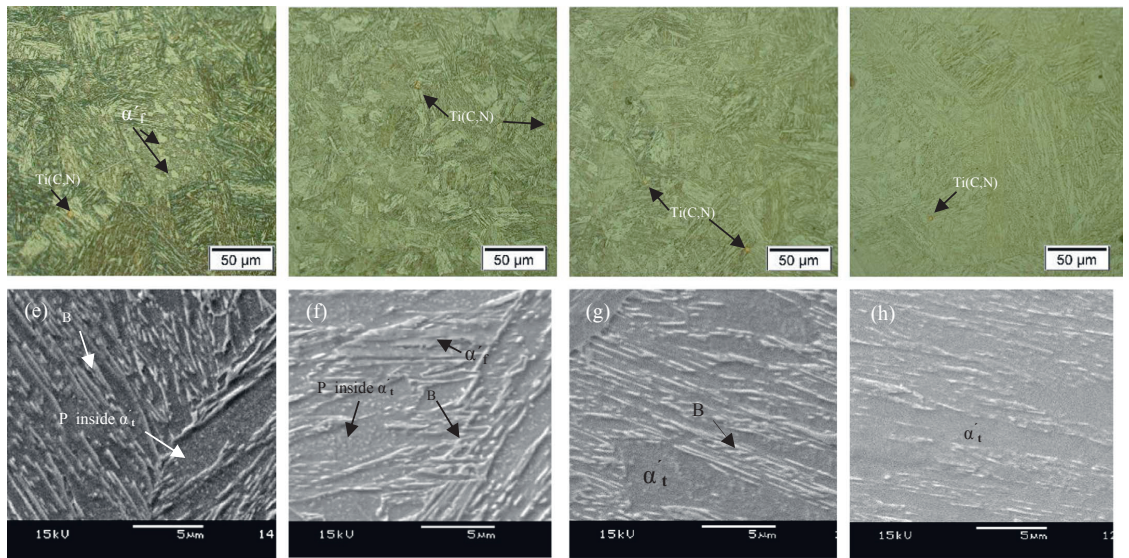


Fig. 3. Microstructure of the following Gleeble samples (a,e) QT=422 °C, PT=540 °C for 2 s (b,f) QT=355 °C, PT=540 °C for 50 s, (c,g) QT=355 °C, PT=640 °C for 2 s (d,h) QT=355 °C, PT=640 °C for 50 s. P: Precipitate, α_t : Tempered Martensite, α_f : Fresh Martensite, B: Bainite.

Table 3
Predicted martensite fraction of the specimens quenched to different temperatures, according to Koistinen-Marburger equation.

Quenching temperature (°C)	Martensite volume fraction (%)
422	17.9
355	60.7
255	86.9

Fig. 4 shows examples of the x-ray diffraction results of samples quenched just below the M_s (so, it has a small amount of martensite (according to Table 3:18%), from the first quench just below M_s and subsequently heated to 640 °C and hold for different times (2, 5, 50 s). Generally, it can be seen that the longer holding time, the lower amount of retained austenite is formed in the structure. However, since there is not enough Si to retard the carbide formation and enough of C to enrich the retained austenite and stabilize it, the fraction of retained austenite based on Rietveld refinement [18] method shows 1.6, 2 and 0.2 wt% retained austenite respectively, see Fig. 4(a)–(c). These low amounts cannot have a significant effect on the mechanical properties of the steel.

As expected, Figs. 5 and 6 confirms that increasing of the partitioning time at tempering temperatures much lower than the B_s tempera-

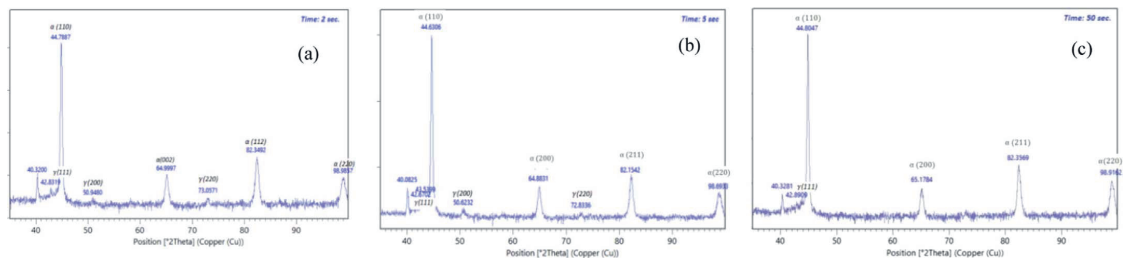


Fig. 4. X-Ray Diffraction spectrum of Domex 960 showing bainitic ferrite (110) and retained austenite in (111). Austenitizing at 1350 °C, cooling to 422 °C, heating at 640 °C for 2 (a), 5 (b) and 50 (c) seconds respectively.

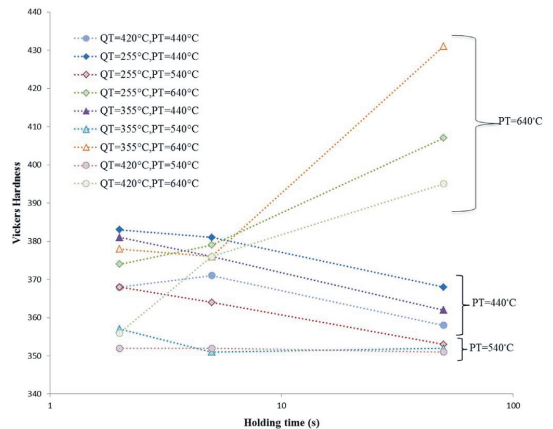


Fig. 5. Effect of different Q & P conditions on hardness of Gleeble samples.

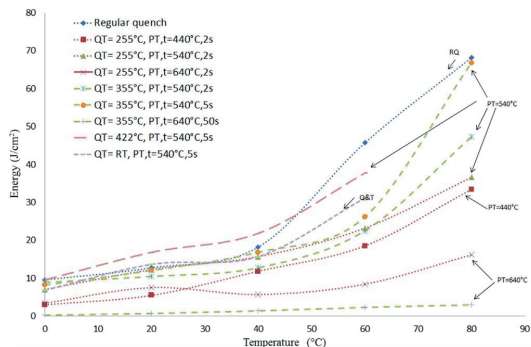


Fig. 6. Charpy V notch impact energies of Gleeble treated samples after Q&P in comparison with quenched and Q & T samples.

ture decreases the hardness. This is due to increasing the tempering of primary martensite and carbon enrichment and stabilizing of the austenite when sufficient level of carbon is reached or that better conditions for transformation of austenite to lower bainite which is much softer than untempered martensite is provided, whereas precipitates are still very fine. On the other hand, tempering at B_s (640 °C) has inverse effect on hardness and shows high increase of hardness for all samples heated for 50 s. No significant effect was caused by the different quenching temperatures. It was shown that even 2 s at 640 °C is enough to transform all the retained austenite in this low carbon low alloy steel while increasing the holding time will promote the precipitate formation and growth. As a consequence, the structure will be more brittle and harder.

3.2. Laser welding results

The microstructural investigation of the laser welded samples shows almost the same microstructure as Gleeble samples. Blocks of tempered martensite with small carbides are apparent in the samples tempered at 540 °C as shown in Fig. 7(a) while samples tempered at 640 °C Fig. 7(b) have fewer precipitates inside tempered martensite. EDS analysis (Fig. 8) confirmed that the fine precipitates are mainly made of the same elements, titanium and nitrogen as the large precipitates, since these elements have the highest attraction to precipitate during phase transformation in this steel [19].

It was desirable to understand the mechanisms and to confirm phase interpretations during tempering stage specially to distinguish fresh martensite from tempered martensite and bainitic ferrite as well as the presence of austenite. Therefore, two samples with the same quenching temperature of 350 °C and different mechanical properties were studied

with electron backscatter diffraction (EBSD) technique. One sample, post weld heat treated at 540 °C for 2 s and another one at 640 °C for 50 s. Phase map analysis of both samples showed that around 99% of both samples have BCC structure. So, discrimination of martensite (body centered tetragonal) from ferrite (body centered cubic) structure which is not easy due to their very similar crystallographic structure, and even more difficult in low carbon steels having low tetragonality distortion is the main question to clarify, if possible by EBSD. Some previous studies [20,21] did clarify that it is possible to distinguish martensite from ferrite by the fact that martensite has high dislocation density and carbon content, in comparison with ferrite and that this will decrease the quality of patterns and image quality (IQ). Knijf et al. [22] also compared the image quality map with the Kernel average mis-orientation map and showed that the dark regions associated with fresh martensite, has a higher Kernel average mis-orientation than the rest of the microstructure.

Fig. 9(a) and (d) show the quality map of the mentioned samples. In this study, darker area can refer to fresh martensite and/or bainite while brighter shows tempered martensite. During austenite (fcc) to bainite (bcc) transformation, structure is expanded, so this volume change is accumulated in the structure. It is important to consider that all low quality patterns are not those two, it could be also because of grain boundaries, volume surrounding precipitates, etc. On the other hand, Fig. 9(b) and (e) shows local mis-orientation map indicating degree of deformation while (c) and (f) show areas with high internal stress/deformation (high dislocation density) in red and stress-free structured areas in yellow while the recrystallized grains are blue. So that in the first sample (Fig. 9c) there are 51.9%, 41% and 7.05% red, yellow and blue areas while these values are 59.5%, 37.5% and 3% respectively in the second sample (Fig. 9f). As can be seen, the brighter areas in (a) and (d) are blue colored areas in (b) and (e) respectively. The maximum deformation/internal stress can be seen as red dots in the local mis-orientation pictures which are mostly located on the grain boundaries between green and blue areas. These dots are probably representing large precipitates. More interestingly, comparing Fig. 9(b) and (c) or (e) and (f) shows that despite that the blue areas in mis-orientation map are yellow in the recrystallization map, there are some stresses caused by the formation of precipitates and existence of extra carbon in the center of the structured areas (tempered martensite). Recrystallization of the grains on the boundaries of deformed and structured areas, is in accordance with tempering stages which starts with precipitation of transition carbides, then decomposition of retained austenite to bainite, consequently precipitation of cementite and on the fourth stage recrystallization and precipitation (in this case Ti (C,N)). So, the best area to start recrystallization is on the grain boundaries with the highest energy through the deformed areas. However, there is still an unanswered question. Why the recrystallized and structured areas in the sample which is tempered at 540 °C for 2 s are larger than those in the sample which is tempered at 640 °C for

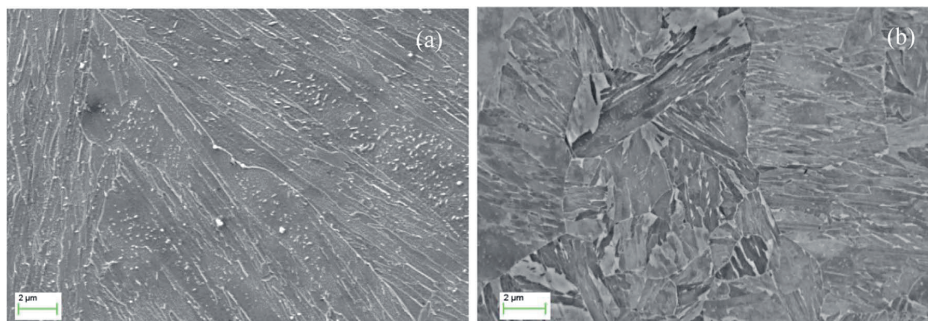


Fig. 7. SEM micrographs of the specimens obtained by quenching to 255 °C and then isothermally heated with the following conditions: (a) 540 °C for 2 s, (b) 640 °C for 50 s.

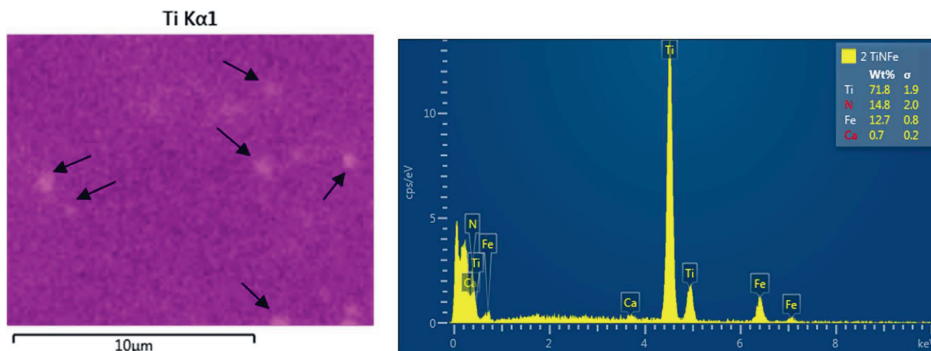


Fig. 8. EDS result of the sample tempered at 440 °C for 2 s shows that precipitates in the structure consist of Titanium nitride.

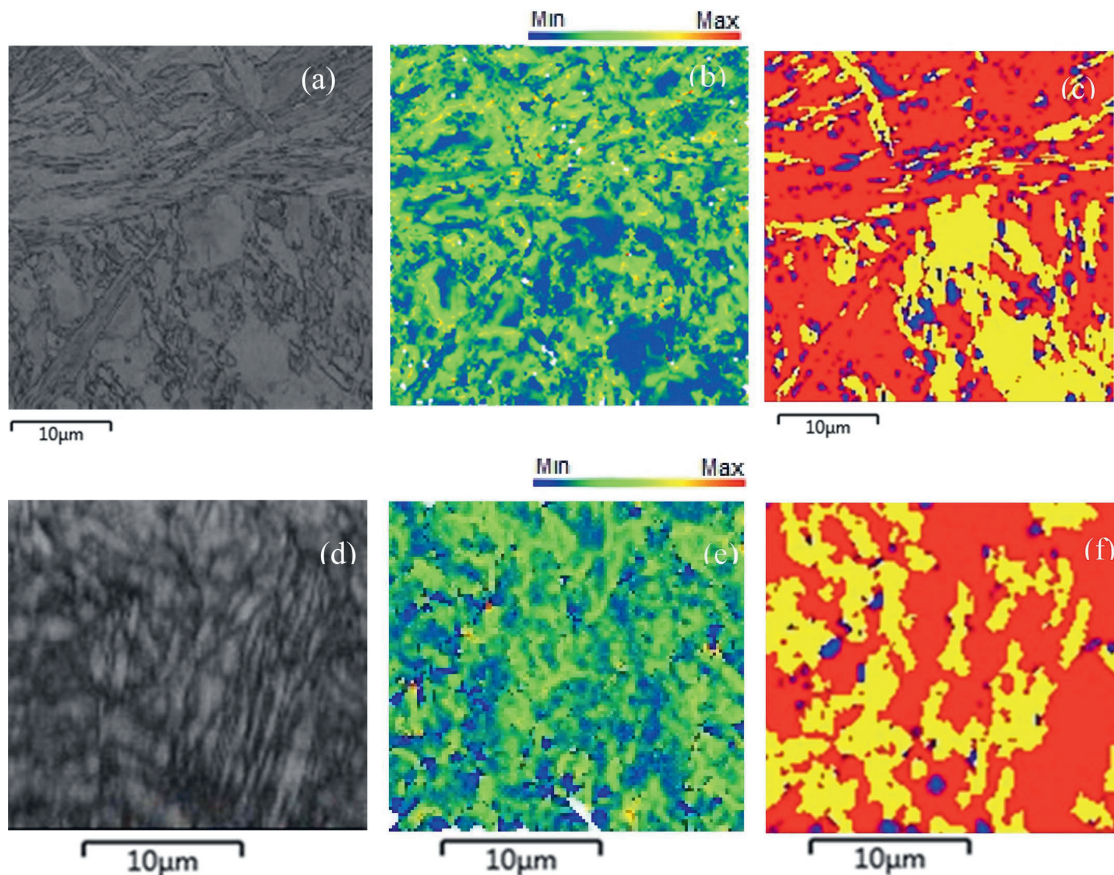


Fig. 9. EBSD analysis of (a, d) the band contrast, (b, e) local mis-orientation map showing deformation degree between Min (0) to Max (5), (c, f) recrystallization analysis (recrystallized=blue, structured=yellow, deformed=red) for two samples both quenched to 355 °C then heat treated at (a,b,c) 540 °C for 2 s and at (d,e,f) 640 °C for 50 s. (For interpretation of the references to color in this figure legend, the reader is referred to the web version of this article).

50 s?

As can be seen in SEM pictures (Fig. 7), the sample which is partitioned at 540 °C for 2 s is full of very fine (50–250 nm) precipitates in the tempered martensite. These particles increase the resistance against dislocation movement and causes some internal stress in the

martensite during tempering at 540 °C. So, the tendency of primary martensite to recrystallize will increase. But at higher temperature (like 640 °C) the solubility of carbon in ferrite will increase -especially since this steel (Domex 960) has a very low amount of carbon- therefore, fewer precipitates which are large Ti(C, N) particles can be found in the

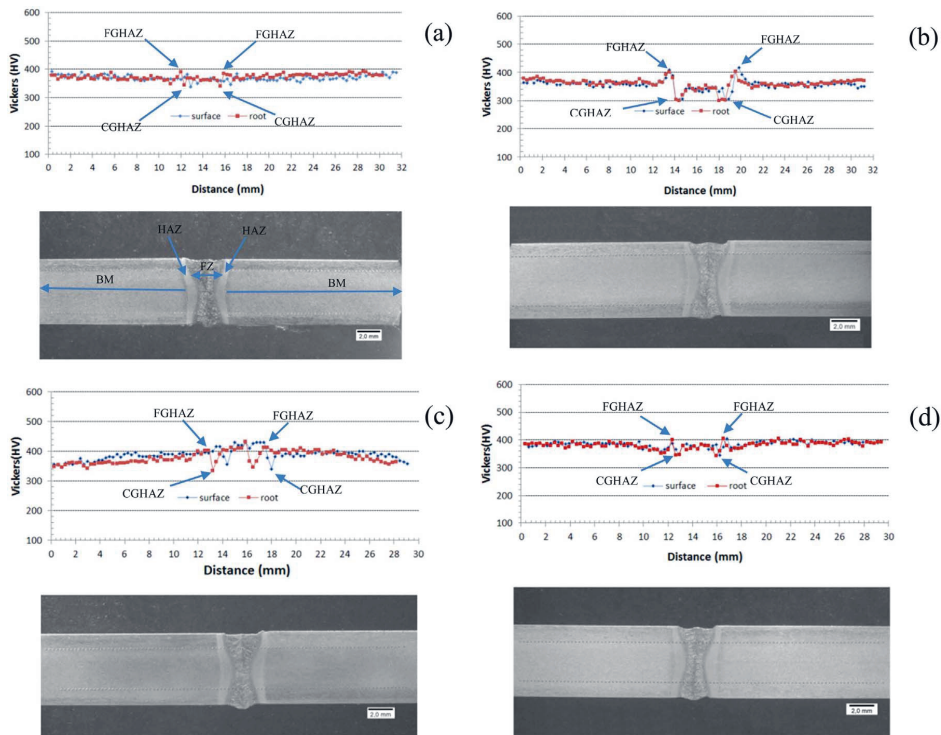


Fig. 10. Vickers hardness profile of laser welded samples and subsequently (a) Quenched to 255 °C and tempered at 440 °C for 2 s (b) Quenched to 355 °C and tempered at 640 °C for 2 s (c) Quenched to 355 °C and tempered at 640 °C for 50 s (d) Quenched to room temperature. FZ: Fusion Zone, HAZ: Heat Affected Zone, FGHAZ: Fine Grain HAZ, CGHAZ: Coarse Grain HAZ, BM: Base metal.

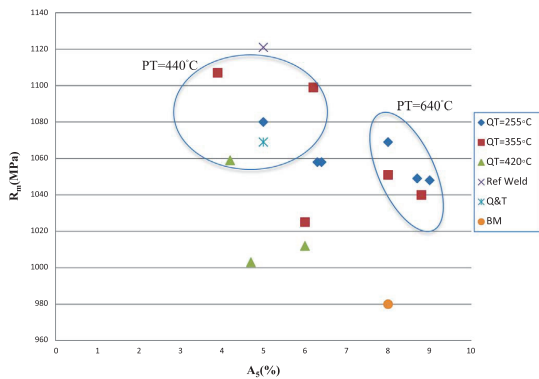


Fig. 11. Tensile test results of different samples.

structure. Zajac et al. [17], by using a thermo-calc modeling showed that the solubility of carbon in ferrite in equilibrium with cementite is approximately 5 times higher at 640 °C than at 540 °C.

3.2.1. Mechanical properties

Typically, micro-hardness profile of AHSS across the weld shows a slight increase when entering the HAZ area from base metal and subsequently sharp drop before the FZ. Since during the welding, both FZ and the inner HAZ are fully austenitized, the high temperature in the inner HAZ lead to coarse grains which have higher tendency for

hardening and the next zone of HAZ heated to lower temperature recrystallizes to austenite but does not have the possibility for grain growth and this part of HAZ results in fine grains with better mechanical properties [23]. The softer zone (CGHAZ) results from local tempering of the martensite phase through welding as well as the normal cause for hardness drop in FZ which is the increased size of grains. The normal increase of hardness in HAZ is caused by the grain refined zone (FGHAZ) [24] (Fig. 10).

Investigating the strength and elongation of the samples verify the hardness results. Table 3, shows that the yield strength of all the samples is higher than the base metal (980 MPa) and elongation in a few cases is almost equal or higher than the reference value of this AHSS. It means that in spite of mostly martensitic structure in the weld created during the first quench, the tempering stage even for 2 s has a great effect on stress and carbon release of the martensite and could help softening the structure and generate secondary hardening by creating titanium carbonitrides form martensite, simultaneously. Tensile test results of the welded samples which were quenched to 255 °C (almost 90% martensite from first quench) show that tempering at 440 °C for a few seconds is not enough to temper martensite and provide enough energy for nucleation and growth of bainite and they also exhibit limited ductility. But ductility of the samples which were tempered at 540 °C or 640 °C increased up to 2 times higher than reference weld without losing the limit of strength (see sample No. 5 and 7 in Fig. 11). Samples which were quenched to 355 °C, with almost 60% martensite, shows almost the same trend when tempered at 440 °C, but for tempering temperatures 540 °C and 640 °C, an increase with 20% and 76% in ductility can be seen. It seems that although heating at 440 °C for 5 s can lead to good results, for tempering of the

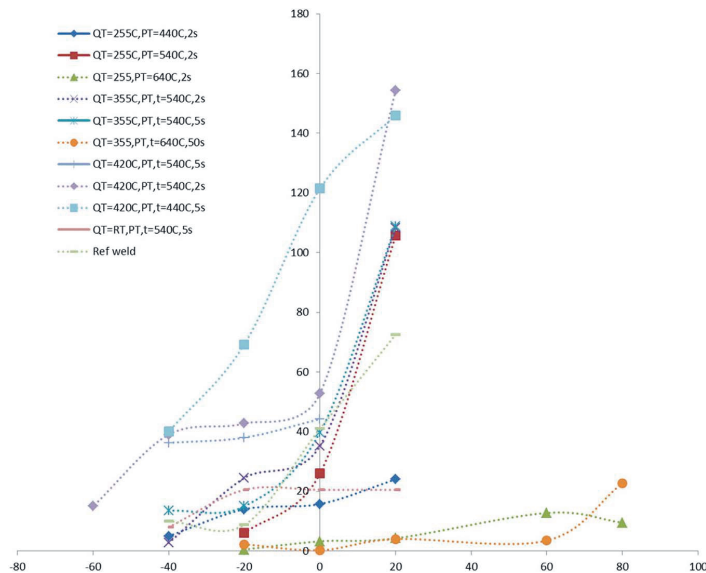


Fig. 12. Impact toughness test results of different samples in fusion zone.

first quenched martensite, this is not enough to complete the bainitic transformation in this sample with low amount of nucleation sites. So, the rest of the retained austenite is transformed to martensite in the second quench, while samples which were quenched to 440 °C are not affected by the first quenched martensite, why their properties are approximately the same as for the Ref. weld.

Selecting the best conditions for quenching and tempering is becoming more interesting when impact Charpy test results of the best tensile test samples are investigated. For example, despite very good elongation and strength of sample number 18 (QT:355 °C, PT:640 °C), the Charpy energy absorbed before failure by these samples are the lowest ones. Fig. 12 shows the results of impact toughness tests performed on the FZ of the welds.

It has been shown that contrary to acceptable mechanical properties due to bainitic structure, nucleation of microcracks in Ti microalloyed bainitic steels takes place in brittle Ti (C, N) particles and not in carbides. So, when the structure contains coarse Ti (C, N) particles (regularly larger than 0.5 μm), they will act as a dominant microstructural feature to promote cleavage fracture [25,26]. Therefore, samples quenched to 422 °C followed by partitioning at 540 °C for 2 and 5 s and at 440 °C for 5 s leads to the best mechanical properties.

4. Conclusions

In order to find a method for quick transformation of austenite to non-brittle, fine grained but strong and ductile structure, after laser beam welding process, in the FZ and HAZ, a type of quenching and tempering treatment directly after welding has been implemented for low carbon AHSS. The results show that:

- Microstructural observations revealed the presence of tempered martensite with precipitates, bulky fresh martensite, bainite laths and Ti(C, N) precipitates. The amount of each micro-constituent depends on the quenching and tempering conditions. For instance, there are some islands of fresh martensite in samples kept at low temperature for short time while the amount of large Ti(C, N) precipitates, found in samples tempered at 640 °C are higher.
- EBSD analysis of the samples showed that short isothermal heating

times of 2 or 5 s were long enough for tempering the primary martensite formed after quenching. Although higher temperature increases diffusion rate, phase transformation to ferrite is more pronounced in samples tempered at 540 °C in comparison with 640 °C since increasing temperature from 540 °C to 640 °C will increase the carbon solubility in ferrite and decrease the stress concentrations in the structure.

- Tensile test results of the welded samples showed that all the heat treated samples have higher strength than minimum defined strength of the material. Samples with more than 60% martensite created during first quench which are then tempered properly, showed up to 80% increase of the elongation at failure (A_5) value in comparison with the reference weld, with saving the limit of base metal strength. In addition, increasing the partitioning temperature and time leads to increase of the ductility and decrease of the strength.
- However, the impact toughness of samples tempered at 640 °C was surprisingly low. This could be a result of initiation of microcracks from coarse Ti(C, N) particles in this structure.

References

- [1] E. De Moor, P.J. Gibbs, J.G. Speer, D.K. Matlock, J.G. Schroth, Strategies for third-generation advanced high-strength steel development, *Iron Steel Technol.* 7 (2010) 133–144.
- [2] A. De, C.A. Walsh, S.K. Maiti, H.K.D.H. Bhadeshia, Prediction of cooling rate and microstructure in laser spot welds, *Sci. Technol. Weld. Join.* 8 (2003) 391–399.
- [3] J. Gould, S. Khurana, T. Li, Predictions of microstructures when welding automotive advanced high-strength steels, *Weld. J.* 85 (2006) 111.
- [4] J.G. Speer, D.V. Edmonds, F.C. Rizzo, D.K. Matlock, Partitioning of carbon from supersaturated plates of ferrite, with application to steel processing and fundamentals of the bainite transformation, *Curr. Opin. Solid State Mater. Sci.* 8 (2004) 219–237.
- [5] E. Paravicini Bagliani, M.J. Santofimia, L. Zhao, J. Sietsma, E. Anelli, Microstructure, tensile and toughness properties after quenching and partitioning treatments of a medium-carbon steel, *Mater. Sci. Eng.: A* 559 (2013) 486–495.
- [6] J.G. Speer, E. De Moor, A.J. Clarke, Critical assessment 7: quenching and partitioning, *Mater. Sci. Technol.* 31 (2015) 3–9.
- [7] M.J. Santofimia, L. Zhao, J. Sietsma, Overview of mechanisms involved During the quenching and partitioning process in steels, *Metall. Mater. Trans. A* 42 (2011) 3620–3626.
- [8] A. García-Junceda, C. Capdevila, F.G. Caballero, C.G. de Andrés, Dependence of martensite start temperature on fine austenite grain size, *Scr. Mater.* 58 (2008)

- 134–137.
- [9] H. Yang, H.K.D.H. Bhadeshia, Austenite grain size and the martensite-start temperature, *Scr. Mater.* 60 (2009) 493–495.
- [10] S. Lee, J. Park, Y. Lee, Effect of austenite grain size on the transformation kinetics of upper and lower bainite in a low-alloy steel, *Scr. Mater.* 59 (2008) 87–90.
- [11] E. Seo, L. Cho, B. De Cooman, Application of quenching and partitioning (Q & P) processing to press hardening steel, *Metall. Mater. Trans. A* 45 (2014) 4022–4037.
- [12] J. Sun, H. Yu, Microstructure development and mechanical properties of quenching and partitioning (Q & P) steel and an incorporation of hot-dipping galvanization during Q & P process, *Mater. Sci. Eng.: A* 586 (2013) 100–107.
- [13] E. Vuorinen, B. Bax, E. Navara, Weldability of hardenable silicon alloyed spring steel, *Conf. Proc. Acta Metall. Slov. Conf.* 14 (2010) 247–254.
- [14] D.P. Koistinen, R.E. Marburger, A general equation prescribing the extent of the austenite-martensite transformation in pure iron-carbon alloys and plain carbon steels, *Acta Metall.* 7 (1959) 59–60.
- [15] A.J. Clarke, J.G. Speer, D.K. Matlock, F.C. Rizzo, D.V. Edmonds, M.J. Santofimia, Influence of carbon partitioning kinetics on final austenite fraction during quenching and partitioning, *Scr. Mater.* 61 (2009) 149–152.
- [16] M.J. Santofimia, J.G. Speer, A.J. Clarke, L. Zhao, J. Sietsma, Influence of interface mobility on the evolution of austenite–martensite grain assemblies during annealing, *Acta Mater.* 57 (2009) 4548–4557.
- [17] W.B. Hutchinson, S. Zajac, R. Lagneborg, T. Siwecki, The Role of Carbon in Enhancing Precipitation Strengthening of V-Microalloyed Steels, 284, 1998, pp. 295–302.
- [18] H.M. Rietveld, *J. Appl. Crystallogr.* 2 (1969) 65–71.
- [19] H. Bhadeshia, R. Honeycombe, *Steels: Microstructure and Properties: Microstructure and Properties*, Butterworth-Heinemann, Elsevier, Oxford, UK, 2011 ISBN: 9780750680844.
- [20] G. Thomas, J. Speer, D. Matlock, J. Michael, Application of electron backscatter diffraction techniques to quenched and partitioned steels, *Microsc. Microanal.* 17 (2011) 368–373.
- [21] M.J. Santofimia, R.H. Petrov, L. Zhao, J. Sietsma, Microstructural analysis of martensite constituents in quenching and partitioning steels, *Mater. Charact.* 92 (2014) 91–95.
- [22] D. De Knijf, R. Petrov, C. Föjler, L.A.I. Kestens, Effect of fresh martensite on the stability of retained austenite in quenching and partitioning steel, *Mater. Sci. Eng. A* 615 (2014) 107–115.
- [23] X. Wang, C. Chen, H. Wang, S. Zhang, M. Zhang, X. Luo, Microstructure formation and precipitation in laser welding of microalloyed C–Mn steel, *J. Mater. Process. Technol.* 226 (2015) 106–114.
- [24] N. Sreenivasan, M. Xia, S. Lawson, Y. Zhou, Effect of laser welding on formability of DP980 steel, *J. Eng. Mater. Technol.* 130 (2008) (041004-041004).
- [25] A. Echeverria, M.A. Linaza, J.M. Rodriguez-Ibabe, Cleavage Fracture Micromechanisms in Ti, Ti-V and C-Mn-B Microalloyed Bainitic Steels, 284, 1998, pp. 351–360.
- [26] D.P. Fairchild, D.G. Howden, W.A.T. Clark, The mechanism of brittle fracture in a microalloyed steel: Part II. Mechanistic modeling, *Metall. Mater. Trans. A* 31 (2000) 653–667.

Paper III

Article

Effect of Carbon Partitioning, Carbide Precipitation, and Grain Size on Brittle Fracture of Ultra-High-Strength, Low-Carbon Steel after Welding by a Quenching and Partitioning Process

Farnoosh Forouzan ^{1,2,*}, M. Agustina Guitar ², Esa Vuorinen ¹ and Frank Mücklich ²

¹ Department of Engineering Sciences and Mathematics, Luleå University of Technology, SE-97187 Luleå, Sweden; esa.vuorinen@ltu.se

² Department of Materials Science, Functional Materials, Saarland University, D-66041 Saarbrücken, Germany; a.guitar@mx.uni-saarland.de (M.A.G.), muecke@matsci.uni-sb.de (F.M.)

* Correspondence: famoosh.forouzan@ltu.se; Tel.: +46-920-493-217

Received: 16 August 2018; Accepted: 18 September 2018; Published: 23 September 2018



Abstract: To improve the weld zone properties of Advanced High Strength Steel (AHSS), quenching and partitioning (Q&P) has been used immediately after laser welding of a low-carbon steel. However, the mechanical properties can be affected for several reasons: (i) The carbon content and amount of retained austenite, bainite, and fresh martensite; (ii) Precipitate size and distribution; (iii) Grain size. In this work, carbon movements during the partitioning stage and prediction of Ti (C, N), and MoC precipitation at different partitioning temperatures have been simulated by using Thermocalc, Dictra, and TC-PRISMA. Verification and comparison of the experimental results were performed by optical microscopy, X-ray diffraction (XRD), Scanning Electron Microscopy (SEM), and Scanning Transmission Electron Microscopy (STEM), and Energy Dispersive Spectroscopy (EDS) and Electron Backscatter Scanning Diffraction (EBSD) analysis were used to investigate the effect of martensitic/bainitic packet size. Results show that the increase in the number density of small precipitates in the sample partitioned at 640 °C compensates for the increase in crystallographic packets size. The strength and ductility values are kept at a high level, but the impact toughness will decrease considerably.

Keywords: low-carbon AHSS; Q&P; toughness; modelling; precipitation; martensite packet

1. Introduction

The automotive industry focuses on increasing the use of advanced high-strength steels (AHSS) in order to satisfy the current demand for decreasing the fuel consumption by reduced weight and increasing vehicle safety by using these steels in different energy-absorbing components [1]. Usually, these AHSS are produced by thermomechanical processes, which control the microstructure and grain size as well as the precipitation hardening of micro-alloyed steels.

During welding of AHSS, the weld area will be completely changed and the excellent properties (i.e., tensile strength, toughness) will be lost. This means that the welded area could be the best area for crack propagation [2]. Therefore, pre-and/or post-welding treatment is necessary to improve the properties of this zone. Laser welding is a popular method in the industry because it is fast, creates narrow and deep welds, and can be used for different materials and shapes. So, in this work, a quenching and partitioning [3] method has been applied for post-welding treatment in order to control the microstructure [4]. The final structure will contain tempered martensite (which increases the yield strength) with retained austenite (which improves the ductility), and, depending on the

Q&P conditions and chemical composition of the steel, some bainite and fresh martensite can also be formed [3–5].

However, carbide/nitride precipitation during the partitioning step cannot be avoided, even in low-carbon [6] or in high-carbon, high-silicon steels [7]. Therefore, one of the critical aspects is to monitor the behavior of precipitates during the process. Although precipitates and/or particles are designed to strengthen the material by a precipitation hardening mechanism, they could act as cleavage initiation sites and deteriorate the toughness [8–10]. Fairchild et al. [11] showed that a strong inclusion-matrix bond is why TiN inclusions are potent cleavage initiators in steels even with modest Ti contents. Another study by Di Schino et al. [12] on the effect of Nb microalloying on the heat-affected zone (HAZ) showed that a small difference in Nb content is able to influence the size of the bainitic packet, which results in both toughness and hardness.

Several works have been done on the mechanism of Q&P up to now [4,13–17], while only a few papers have investigated the fracture mechanisms and toughness of Q&P steels [18,19]. Fracture causes could mainly be related to: (i) Kinetics of carbon partitioning and stabilization of retained austenite (RA) in the structure, because it has been shown that increasing volume fraction of RA due to the TRIP effect delays the crack propagation [20]; (ii) Kinetics, size, number density and shape of secondary precipitates; and (iii) Microstructural refinement can be very effective for improving the toughness. Wang et al. [21] found that, when the cleavage crack encounters another packet of martensite, it may be arrested and then largely changes its propagation direction.

Previous studies by the authors [4,22] on the effect of Q&P after laser welding of a low-carbon steel showed that samples partitioned at a higher temperature had the best tensile properties but very low Charpy V impact toughness results. In the present work, in order to investigate the origins of such contradictory results, the abovementioned main issues are studied. Carbon diffusion from α' to retained austenite was modeled by a diffusion-controlled transformation tool (DICTRA) [23] during quenching and partitioning. The type, size, and distribution of the precipitates were evaluated using a scanning transmission electron microscope (STEM) in order to verify the precipitation prediction modeling by TC-PRISMA. Finally, the effect of the packet size of martensite/bainite laths on crack propagation has been investigated by electron backscatter diffraction (EBSD).

2. Materials and Methods

Laser welding was conducted on 5.5 mm thick sheets of ‘Domex 960’ advanced high strength steel from SSAB (Stockholm, Sweden). This steel is thermomechanically processed (TMP) and was received in TMP condition with a yield strength of 960 MPa and elongation (A5) of approximately 8%. The chemical composition of the steel is given in Table 1, but for Thermocalc simulations, a simplified composition of Fe–0.08 wt % C–1.78 wt % Mn–0.5 wt % Mo–0.187 wt % Ti–0.004 wt % N is assumed. All calculations were carried out with the thermodynamic database TCFe8 [24] and mobility database of MOBFE3 [25].

Table 1. The chemical composition of the steel used in the experiments (wt %).

C	Si	Mn	P	S	Al	Ti	Mo	Cr	Ni	Cu	V	N	Fe
0.082	0.23	1.79	0.008	0.001	0.038	0.184	0.503	0.064	0.296	0.016	0.012	0.004	Balance

For the welding, process the keyhole penetration mode, with ytterbium Fiber Laser (YLR Laser–15000, IPG Photonics, Oxford, MA, USA), 5 kW power, travel speed of 1.1 m/min, and Argon shielding gas with a flow rate of 20 L/min, was used. The welded specimens were subjected to post heat treatment immediately after the laser welding. For that, an induction heater was placed above the specimen. The temperature was monitored during the whole procedure of welding and Q&P, by using welded thermocouples located 1.5 mm from the fusion zone (FZ). For the same quenching temperature (QT) of 355 °C (approx. equal to 60% initial martensite), three partitioning temperatures (PT) of 440 °C

(20 °C above M_s), 540 °C (half between M_s and B_s), and 640 °C (B_s) and three partitioning times (Pt) were tested.

Tensile testing was performed on cross weld specimens; the tensile axis was kept perpendicular to the rolling direction of the steel sheet, while the weld zone is located exactly in the middle of the dog-bone-shaped A50 samples. Charpy V notch samples were prepared according to the standard EN ISO 6892-1:2009 and testing was conducted on transverse specimens with a notch in the center of FZ. Results showed that all the samples that were partitioned at 640 °C had very low impact toughness.

In order to investigate the reasons, the samples that showed the best and the worst toughness were selected for comparison, see Table 2.

Table 2. Mechanical properties of samples Q&P treated immediately after laser welding. (Energy = Absorbed energy during Charpy V test at 20 °C.)

Sample Code	QT (°C)	PT (°C)	Pt (s)	A ₈₀ (%)	A ₅ (%)	R _{p0.2} (MPa)	R _m (MPa)	Energy (J/cm ²)
S(540, 5)	355	540	5	4	6	1005	1025	109
S(640, 50)	355	640	50	6	8	1034	1051	4

The precipitate characterization was determined from C-replicas taken from weld area (FZ) and HAZ with a FE-SEM Helios Nanolab 600 (FEI, Hillsboro, OR, USA) working with an acceleration voltage of 30 kV and a 1.4 nA beam current. The precipitate sizes were determined by image analysis (I-A) of STEM micrographs using the software A4i© (Aqinto AG, Berlin, Germany). The carbide chemistry was identified in transmission using energy-dispersive X-rays (EDX) (Jeol Ltd., Tokyo, Japan) at 30 kV accelerating voltage. Electron Backscatter Diffraction (EBSD) was carried out on HAZ using an accelerating voltage of 20 kV, a beam current of 11 nA, and a step size of 150 nm and 100 nm for Q&P and base metal (BM) samples, respectively. The raw data were filtered by confidence index (CI) of CI > 0.09 after a CI cleanup and grain dilation (grain tolerance angle 5° and minimum grain size 2). The grains were defined as at least two adjacent points with similar orientation within a range of 15° misorientation.

3. Results and Discussion

3.1. Fracture Results

Figure 1 shows dimple and cleavage mix-mode fracture in all fractographies, but the average radius of dimples in S(540, 5) (Figure 1a) is smaller than the other samples including the reference weld without any heat treatment (Figure 1c), and S(640, 50) (Figure 1b).

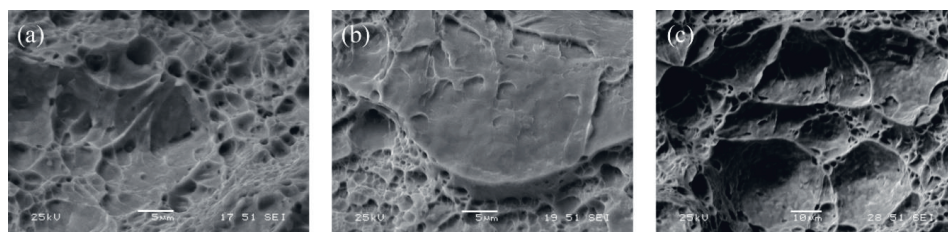


Figure 1. Fracture surface after tensile test of following samples; (a) S(540, 5), shows ductile fracture of HAZ (b) S(640, 50), shows brittle fracture of HAZ and (c) reference weld.

3.2. Thermodynamic Modeling

In order to understand the critical temperatures of phase transformation and formation of stable precipitates in an equilibrium condition of Domex 960, the amount of phases at different temperatures was calculated with ThermoCalc [23]. Although the temperatures and amount of phases could be far

from the real conditions during Q&P, this calculation could give a good overview of the most stable microconstituents. Figure 2 shows that Ti(C, N) has the highest tendency to form the first carbonitrides in this system. It will start when there is still some liquid in the system and the precipitation will continue until it reaches room temperature. After that, two other carbides (M_7C_3) and cementite will nucleate around 700 °C, but they are not stable and will disappear very soon around 600 °C, while their amount is also very small (e.g., 0.001 mol). The next important precipitate in this system in the critical temperature range of 440 °C to 640 °C, is MoC, as expected from its enthalpy for carbide formation in comparison with other alloying elements in this steel [26]. The kinetics of nucleation and growth of these elements modeled by the TC-Prisma [23] module are illustrated in Figure 3.

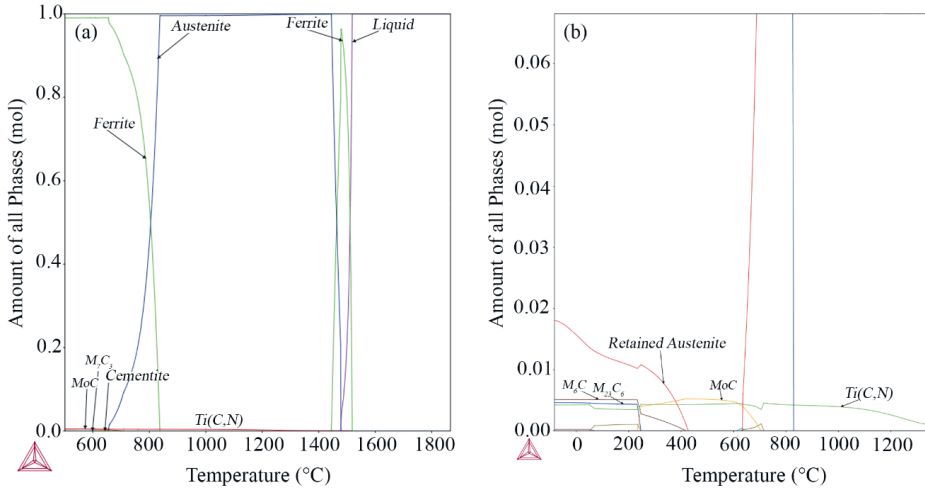


Figure 2. Amount of all phases calculated with ThermoCalc: (a) full range of phases; (b) focus on carbides.

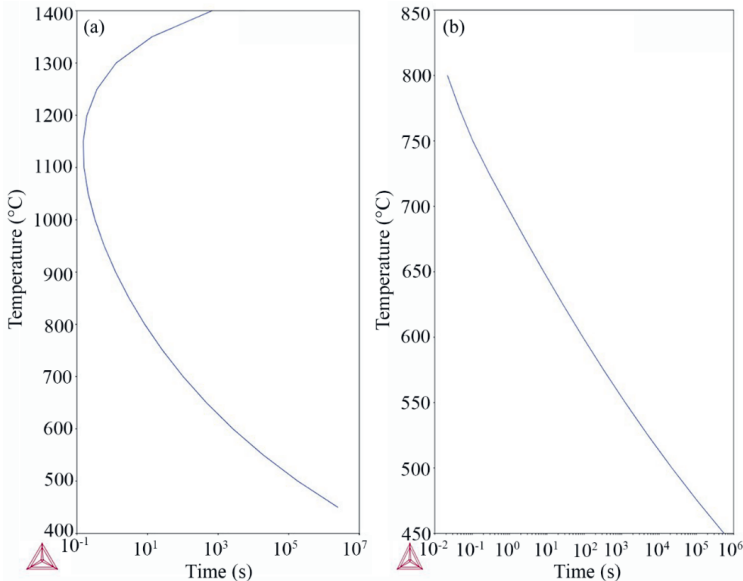


Figure 3. Time-temperature-precipitation (TTP) diagrams of (a) Ti(C, N); (b) MoC.

According to Figure 3a, Ti(C, N) nucleates at very high temperature, with a maximum rate at ca. 1150 °C, at which it takes only 0.2 s. At lower temperatures up to 800 °C, the nucleation takes under 10 s. The time for nucleation grows exponentially with decreasing temperature and nucleation takes a longer time than the longest partitioning time used in this work (maximum 50 s). On the other hand, Figure 3b shows that, although nucleation of this carbide (MoC) is very fast, 600 °C is a critical temperature for this Q&P, because below this temperature nucleation takes more than 100 s, which means that nucleation of MoC cannot occur during this heat treatment. In summary, Ti(C, N) precipitation could be an issue during welding and previous Ti(C, N) particles from casting could still remain in the structure, but MoC precipitation occurs during the partitioning stage at 640 °C.

3.3. Carbon Partitioning

Understanding the carbon movement during the partitioning stage at different temperatures with regard to the first quenched martensite and retained austenite grain boundaries has an important role in the prediction of the phase transformations. Comparison between the diffusion coefficient of carbon in austenite (D_c^γ) and ferrite (D_c^α) in Table 3 shows that for the temperature range of $\gamma + \alpha$ (440–640 °C in this case) the equilibrium 'D' is more than 100 times higher in ferrite than austenite. This means that carbon can partition out of martensite rapidly but will then pile up behind the α'/γ grain boundary.

Table 3. Carbon diffusion coefficient in austenite (D_c^γ) and ferrite (D_c^α) and at different temperatures.

Carbon Diffusion Coefficient	440 °C	540 °C	640 °C
D_c^γ	3.30×10^{-16}	7.12×10^{-14}	2.82×10^{-21}
D_c^α	8.54×10^{-13}	4.49×10^{-17}	1.22×10^{-18}

In other words, this velocity is critical for the determination of the area of retained austenite around tempered martensite plates, especially for low-carbon steels, in order to design the structural and mechanical properties of the material, since three different phenomena could occur during the partitioning stage: (i) The amount of austenite's carbon enrichment to stabilize it after the final quench; (ii) Nucleation and growth of third phases (e.g., bainitic ferrite); and (iii) Carbide precipitation. Nishikawa et al. [27] modeled the influence of the bainite reaction on the kinetics of carbon redistribution during the Q&P process. Simulations indicate that the kinetics of carbon partitioning from martensite to austenite is controlled by carbon diffusion in austenite and is affected only to a small extent by the decomposition of austenite into bainitic ferrite.

Based on microscopy pictures of the samples, a model with 3 μm space for austenite until the next lath of martensite and a 2 μm space for ferrite, which represents martensite in this simulation, in a rectangular linear model with 50 nodes for calculations that are more frequent close to the interface, is assumed (see Figure 4).

Figure 5 shows the simulation results of carbon partitioning at 640 °C and 540 °C. Regarding the fact that Mn drops the chemical potential of carbon in austenite, it is expected that regions with high Mn concentration attract more carbon [13]. Therefore, adding 1.78 wt % Mn to the system makes carbon atoms pile up at the border of γ/α and causes a constant increase of the carbon content of austenite until 0.15 wt % after 50 s at 640 °C. If the partitioning process stops after 2 or 5 s, a small distance of approximately 0.5 μm could be enriched with up to 0.3 wt % C (Figure 5a). As can be seen in Figure 5b, diffusion at 540 °C is much slower and makes the boundary full of carbon up to 1.6 wt %.

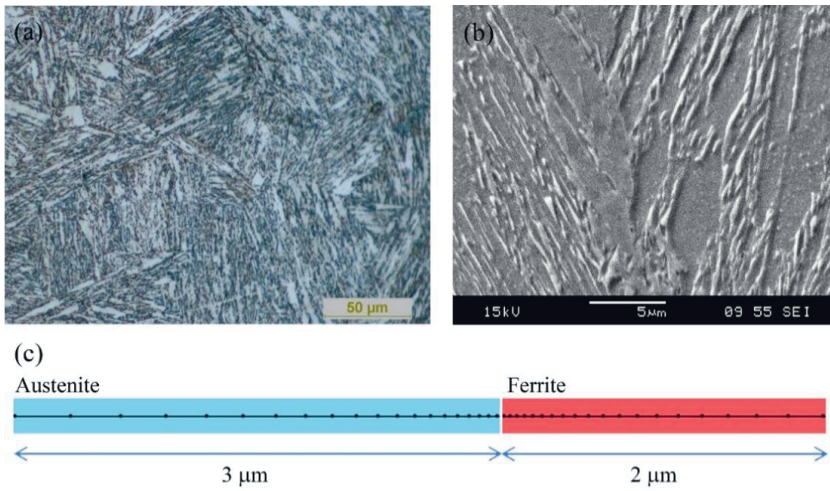


Figure 4. (a) Optical microscopy (OM) and (b) SEM pictures of samples quenched to 350 °C; (c) rectangular model with linear mesh assumed for 3 μm austenite and 2 μm martensite.

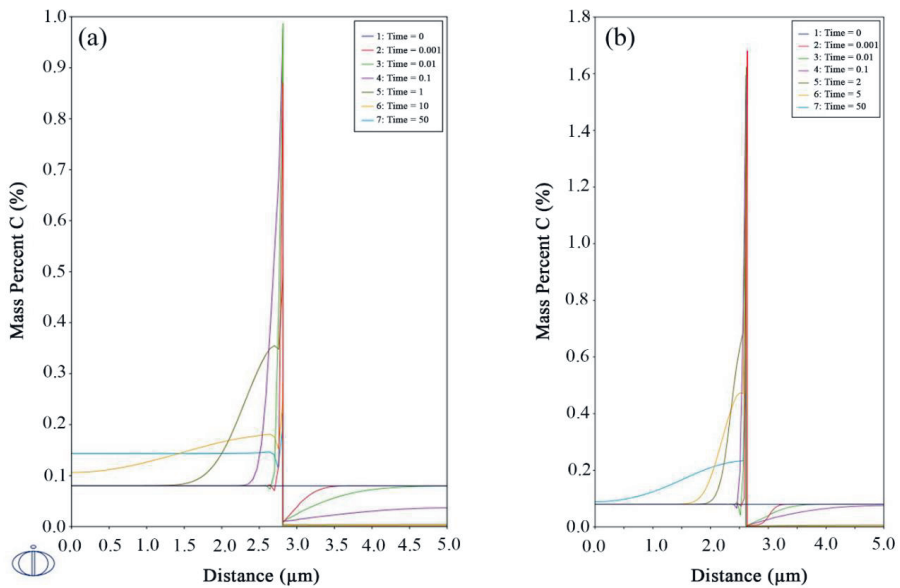


Figure 5. Carbon content of (a) Fe–0.08 wt % C–1.78 wt % Mn system at 640 °C; (b) Fe–0.08 wt % C–1.78 wt % Mn system at 540 °C.

In order to find the reason for the very low impact toughness results of samples partitioned at 640 °C while they have very good tensile properties, simulations were focused on S(640, 50) and S(540, 5) for comparison. The effect of temperature is shown in Figure 6a. Figure 6b shows the carbon movement inside austenite close to the martensite interface for these two samples, and the existence of retained austenite after the final quench after partitioning can be predicted.

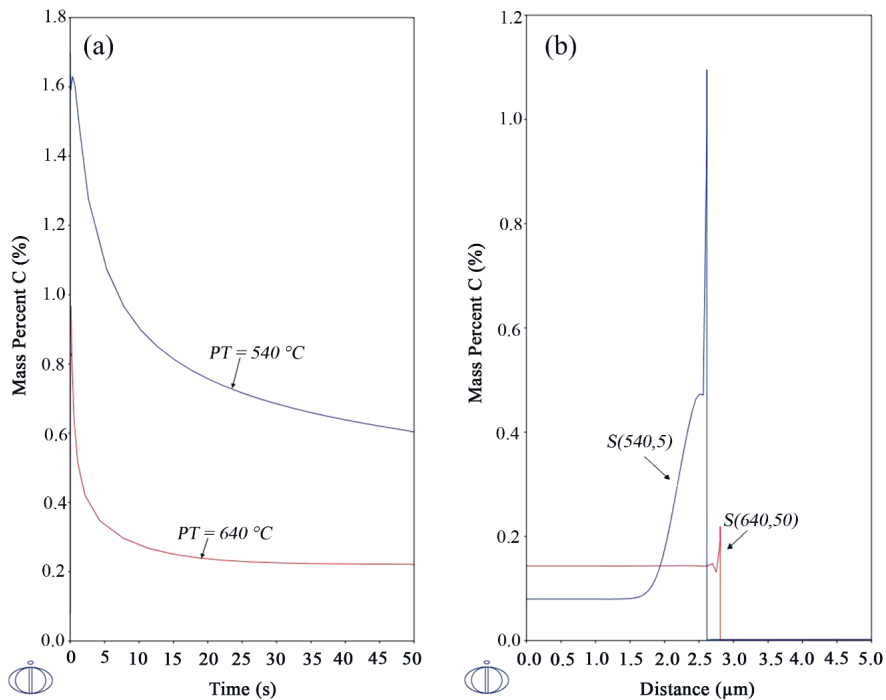


Figure 6. Comparison of samples partitioned at 540 °C, 5 s (blue) and 640 °C, 50 s (red), calculated using DICTRA. (a) The composition of the interface as a function of the time; (b) carbon content vs. location γ/α interface is at 3 μm distance).

Minimum estimated amount of C to stabilize austenite, based on different equations [28–33] for this steel is 0.9 to 1.2 wt % C at ambient temperature. So, comparing with Figure 6b implies that there is no chance for stabilizing the retained austenite in S(640, 50), but there is some possibility in samples treated at 540 °C or less. This is also confirmed by XRD measurements of these two samples S(540, 5) and S(640, 50).

Wu et al. [34] investigated the effect of austenite on fracture resistance of Q&P and showed that the energy absorption by transformation from austenite to martensite postponed the crack propagation and enhanced the fracture resistance of Q&P steels. Even a small amount of retained austenite at room temperature could have a significant effect on energy absorption during crack propagation.

3.4. Kinetics of Precipitation

In Figure 3 it was shown that precipitation of Ti(C, N) can start from the liquid. So, it is difficult to control the size and distribution of the Ti(C, N) particles in the structure. However, SEM pictures of the Q&P-treated sample shows small precipitates as well (Figure 7). EDS study of the particles confirmed the Ti content of these large and sharp-edged particles.

Beside these very large precipitates form during casting, there are some other particles that can nucleate, grow, or coarsen during welding and Q&P treatment. For example, in Figure 7 different particle types can be seen in the HAZ. For example, in region (b) a Ti(C, N) particle nucleated and coarsened during welding and Q&P; region (c) shows accumulation of nucleated carbides at the grain boundary and (d) shows transition carbides that are created during tempering of martensite laths in the partitioning stage.

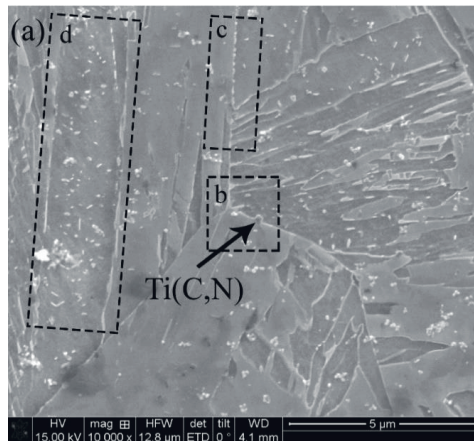


Figure 7. SEM pictures of S(640, 50) displays secondary precipitates at different size and shapes.

As reported by Gustafson [35], there are two sizes of TiC particles, one with sparsely distributed particles of micrometer size and a second with densely distributed particles with sizes of a few tens or hundreds of nanometers. In this work, precipitates with the smaller size were studied, under the assumption that the large primary particles are so sparsely distributed that they will not affect the coarsening of the secondary ones, since the coarsening of the large particles is expected to follow a much slower process and has no important influence on the mechanical properties.

Since the precipitates (especially the small ones) from casting will melt in FZ during welding, the most critical area will be HAZ. In order to model the nucleation and growth of precipitation using TC-Prisma, isothermal heating at 1350 °C for 5 s is considered. Figure 8, shows that the equivalent average diameter of Ti(C, N) particles is around 150 nm.

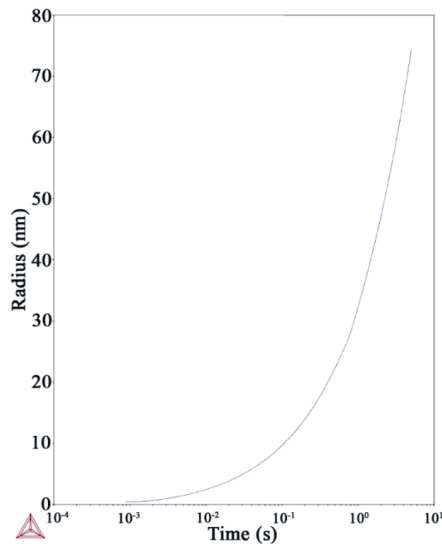


Figure 8. Prediction of precipitate size in HAZ considering isothermal heating at 1350 °C for 5 s, resulting in a particle size of around 150 nm.

Comparison of the precipitate coarsening rates in corresponding matrix phases using the ThermoCalc database shows that increasing the temperature from 540 °C to 640 °C will increase the coarsening rate of Ti(C, N) 1000 times to $1.27 \times 10^{-35} \text{ m}^3/\text{s}$ and of MoC 100 times to $3.875 \times 10^{-31} \text{ m}^3/\text{s}$.

Quantification of the precipitate size distribution in base material (BM) and in those partitioned at 540 °C and 640 °C was carried out by STEM from carbon replicas of the samples.

Figure 9 shows the particle size distribution for both partitioned samples (at 540 °C and 640 °C) and for the BM. The average particle size was calculated to be $0.263 \pm 0.108 \text{ }\mu\text{m}$, $0.207 \pm 0.089 \text{ }\mu\text{m}$, and $0.07 \pm 0.11 \text{ }\mu\text{m}$ for S(540, 5), S(640, 50), and BM, respectively. The precipitates quantification in the BM became more complicated since it presents particles over a large range of sizes. SEM analysis of precipitates show a few large particles (between 0.2 and 0.65 μm) at relatively low magnification (20,000 \times). However, at higher magnifications (e.g., 80,000 \times), a large quantity of small particles (<0.2 μm) can be distinguished. For this reason, the analysis of the precipitates in this sample was performed at two different magnifications.

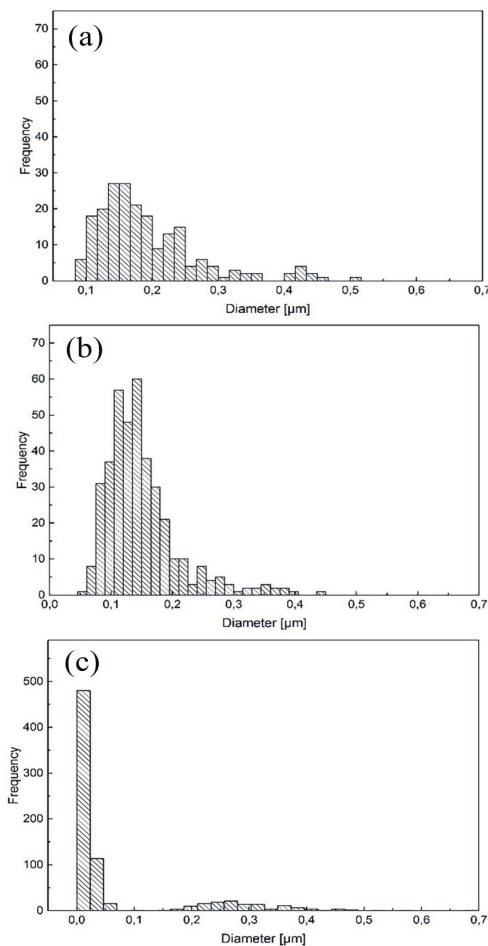


Figure 9. Measured size distribution of precipitates vs. number of particles for post-welding heat-treated samples (a) at QT = 355 °C and PT = 540 °C for 5 s; (b) at QT = 355 °C and PT = 640 °C for 50 s; (c) base metal.

Figure 10 shows STEM images from C replicas corresponding to the samples. An apparently larger particle density can be observed in the sample partitioned at 640 °C, when comparing the same area of both samples (Figure 10a,b). However, the particle density has not been systematically analyzed in this case. Two hundred six and 388 particles were considered for S(540, 5) and S(640, 50), respectively, and this was compared with the base metal (see Figure 9).

Results indicate that the approximate average size of particles in treated samples are $0.263 \pm 0.108 \mu\text{m}$ for the sample partitioned at 540 °C and $0.207 \pm 0.089 \mu\text{m}$ for the one partitioned at 640 °C, while the number density of particles after partitioning at 640 °C is around 1.5 times higher than for 540 °C. This can be seen when comparing Figure 10a,b.

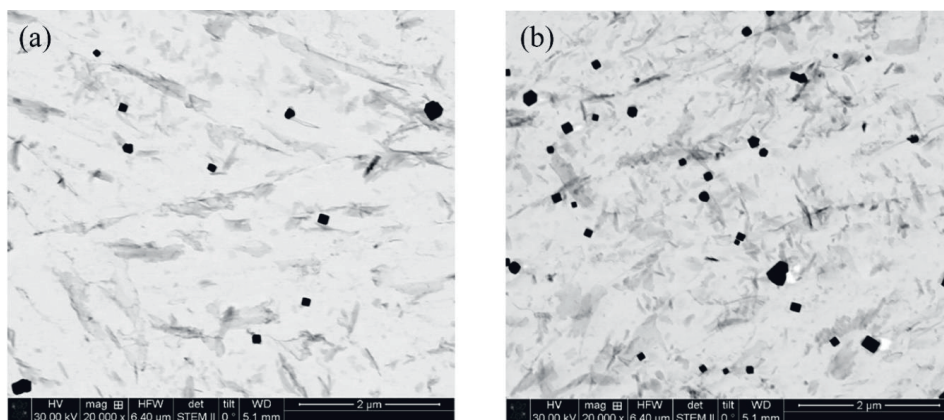


Figure 10. Comparison between distribution, number density, and shape of the particles in carbon replicas made from the sample: (a) S(540, 5) and (b) S(640, 50).

From EDS measurements, it was determined that the particles in samples partitioned at 540 °C and 640 °C are principally MoC (round shaped particles) and Ti(C, N) (rectangular shaped particles).

3.5. Grain Size Effect

As mentioned before, the structure is made of tempered and fresh martensite lathes from the first and second quench and bainite from the partitioning stage. So, the toughness of such structure is increased by a high density of the high angle boundaries created, because this kind of boundary acts as an obstacle for cleavage propagation, forcing the cleavage crack to change its microscopic plane of propagation in order to accommodate the new local crystallography [22,36,37]. In addition, the presence of coarse martensite laths leads to early strain localization, especially when they are in the vicinity of untempered martensite islands [38]. However, the complexity of the lath martensitic/bainitic structure makes the grain size measurement very difficult. For this reason, the region of martensite/bainite lathes with a determined crystallographic orientation is defined as a block [39]. Clusters of blocks form a packet when they share the same $(111)_{\gamma}$, to which the corresponding $(001)_{\alpha}$ is almost parallel [40]. Since the blocks and packages present high angle grain boundaries ($>11^{\circ}$), the toughness of the material might be influenced by their size [41]. In this study, the effective grain size of the martensite/bainite was determined from EBSD measurements, considering grain boundary misorientation $\geq 15^{\circ}$. Figure 11 shows the inverse pole figure (IPF) superimposed on the image quality map (IQ) for the treated samples. Results shows that partitioning at a lower temperature (540 °C) leads to a refinement of the effective grain size (block packages), as can be noticed by the change in the color orientation. Kawata et al. [42] showed that the bainite block is coarsened by ausforming, especially for a higher temperature, by formation of preferred variants in a packet. In contrast, the same ausforming treatments refine the lath martensite block. In fact, packet size will

influence the ductile–brittle transition temperature (DBTT). As mentioned in Equation (1), DBTT (T) is inversely proportional to the root square of the distance between high-angle grain boundaries (d), where K is a constant [36]:

$$T = T_0 - Kd^{-2}. \quad (1)$$

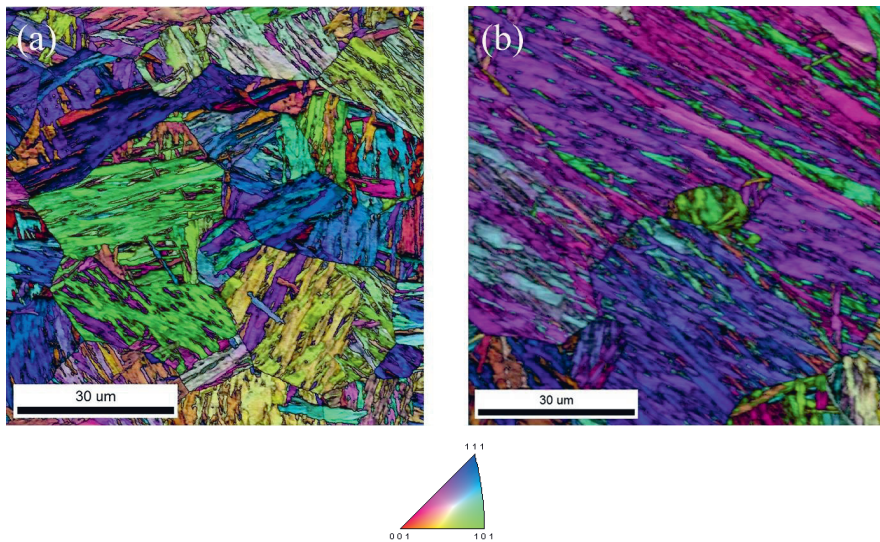


Figure 11. IPF + IQ picture from EBSD analysis of samples: (a) S(540, 5); (b) S(640, 50).

4. Conclusions

The aim of this work was to investigate the reason for brittle fracture of the samples from a low-carbon, low-Si AHSS, which were post-weld heat-treated by the Q&P method around B_s temperature (640 °C). Their strength and ductility were the best in comparison with other samples partitioned at lower temperatures, i.e., 540 °C and 440 °C. Results show that since $D_c^{\alpha'}$ is much higher than D_c^{γ} carbon diffuses out from martensite and piles up behind the border of α'/γ . The partitioning temperature controls the rate of carbon diffusion, but this amount at the α'/γ border cannot reach the level necessary to stabilize austenite at 640 °C, while it can occur for a small area next to the border at 540 °C. Subsequently, this RA contributes to eliminating the brittle fracture due to the TRIP effect and increasing the impact toughness.

STEM results of carbon replicas revealed that there are many more very small precipitates (<0.1 μm) in the sample partitioned at 640 °C; this can increase the strength of the material via precipitation strengthening mechanism. On the other hand, EBSD results showed much larger crystallographic packets in this sample, which can result in a lowering of the material strength. The increase of strength by precipitation strengthening and the decrease of the strength due to larger packet size will counteract each other so that the tensile test results of the samples partitioned at 640 °C are still good.

Author Contributions: Concept and design of experiments: F.F. and E.V.; Experiments, simulations, analysis of data and writing the original draft: F.F.; Experiments and revising the paper: M.A.G.; Supervision: E.V. and F.M.

Funding: This research was funded by Erasmus+: Erasmus Mundus Joint Doctorate (EMJD)-Advanced Materials Engineering-DOCMASE, grant number “2011-0020”.

Acknowledgments: The support of the EUSMAT (European School of Materials) via the Ph.D. program ‘DOCMASE’ and Flavio Soldera is gratefully acknowledged by the authors.

Conflicts of Interest: The authors declare no conflict of interest.

References

1. Opbroek, E. *UltraLight Steel: A Global Consortium Changes the Future of Automotive Steel*; Xlibris: Bloomington, IN, USA, 2013; ISBN 1479773441.
2. Shome, M.; Tumuluru, M. *Welding and Joining of Advanced High Strength Steels (AHSS)*, 1st ed.; Woodhead Publishing: Cambridge, UK, 2015; ISBN 9780857098580.
3. Speer, J.; Matlock, D.K.; De Cooman, B.C.; Schroth, J.G. Carbon partitioning into austenite after martensite transformation. *Acta Mater.* **2003**, *51*, 2611–2622. [[CrossRef](#)]
4. Forouzan, F.; Vuorinen, E.; Mücklich, F. Post weld–treatment of laser welded AHSS by application of quenching and partitioning technique. *Mater. Sci. Eng. A* **2017**, *698*, 174–182. [[CrossRef](#)]
5. Clarke, A.J.; Speer, J.G.; Miller, M.K.; Hackenberg, R.E.; Edmonds, D.V.; Matlock, D.K.; Rizzo, F.C.; Clarke, K.D.; De Moor, E. Carbon partitioning to austenite from martensite or bainite during the quench and partition (Q&P) process: A critical assessment. *Acta Mater.* **2008**, *56*, 16–22. [[CrossRef](#)]
6. Santofimia, M.J.; Zhao, L.; Sietsma, J. Microstructural Evolution of a Low–Carbon Steel during Application of Quenching and Partitioning Heat Treatments after Partial Austenitization. *Metall. Mater. Trans. A* **2009**, *40*, 46–57. [[CrossRef](#)]
7. Toji, Y.; Miyamoto, G.; Raabe, D. Carbon partitioning during quenching and partitioning heat treatment accompanied by carbide precipitation. *Acta Mater.* **2015**, *86*, 137–147. [[CrossRef](#)]
8. Charleux, M.; Poole, W.J.; Militzer, M.; Deschamps, A. Precipitation behavior and its effect on strengthening of an HSLA–Nb/Ti steel. *Metall. Mater. Trans. A* **2001**, *32*, 1635–1647. [[CrossRef](#)]
9. Soto, R.; Saikaly, W.; Bano, X.; Issartel, C.; Rigaut, G.; Charai, A. Statistical and theoretical analysis of precipitates in dual–phase steels microalloyed with titanium and their effect on mechanical properties. *Acta Mater.* **1999**, *47*, 3475–3481. [[CrossRef](#)]
10. Toji, Y.; Matsuda, H.; Herbig, M.; Choi, P.; Raabe, D. Atomic–scale analysis of carbon partitioning between martensite and austenite by atom probe tomography and correlative transmission electron microscopy. *Acta Mater.* **2014**, *65*, 215–228. [[CrossRef](#)]
11. Fairchild, D.P.; Howden, D.G.; Clark, W.A.T. The mechanism of brittle fracture in a microalloyed steel: Part I. Inclusion–induced cleavage. *Metall. Mater. Trans. A* **2000**, *31*, 641–652. [[CrossRef](#)]
12. Di Schino, A.; Di Nunzio, P.E. Effect of Nb microalloying on the heat affected zone microstructure of girth welded joints. *Mater. Lett.* **2017**, *186*, 86–89. [[CrossRef](#)]
13. HajyAkbar, F.; Sietsma, J.; Miyamoto, G.; Furuha, T.; Santofimia, M.J. Interaction of carbon partitioning, carbide precipitation and bainite formation during the Q&P process in a low C steel. *Acta Mater.* **2016**, *104*, 72–83. [[CrossRef](#)]
14. Clarke, A.J.; Speer, J.G.; Matlock, D.K.; Rizzo, F.C.; Edmonds, D.V.; Santofimia, M.J. Influence of carbon partitioning kinetics on final austenite fraction during quenching and partitioning. *Scr. Mater.* **2009**, *61*, 149–152. [[CrossRef](#)]
15. Somani, M.C.; Porter, D.A.; Karjalainen, L.P.; Misra, R.D.K. On Various Aspects of Decomposition of Austenite in a High–Silicon Steel During Quenching and Partitioning. *Metall. Mater. Trans. A* **2014**, *45*, 1247–1257. [[CrossRef](#)]
16. Santofimia, M.J.; Zhao, L.; Sietsma, J. Overview of Mechanisms Involved During the Quenching and Partitioning Process in Steels. *Metall. Mater. Trans. A* **2011**, *42*, 3620–3626. [[CrossRef](#)]
17. Thomas, G.A.; Speer, J.G. Interface migration during partitioning of Q&P Steel. *Mater. Sci. Technol.* **2014**, *30*, 998–1007. [[CrossRef](#)]
18. De Knijf, D.; Petrov, R.; Föjer, C.; Kestens, L.A. Effect of fresh martensite on the stability of retained austenite in quenching and partitioning steel. *Mater. Sci. Eng. A* **2014**, *615*, 107–115. [[CrossRef](#)]
19. De Knijf, D.; Puype, A.; Föjer, C.; Petrov, R. The influence of ultra–fast annealing prior to quenching and partitioning on the microstructure and mechanical properties. *Mater. Sci. Eng. A* **2015**, *627*, 182–190. [[CrossRef](#)]
20. De Diego–Calderón, I.; Sabirov, I.; Molina–Aldareguia, J.M.; Föjer, C.; Thiessen, R.; Petrov, R.H. Microstructural design in quenched and partitioned (Q&P) steels to improve their fracture properties. *Mater. Sci. Eng. A* **2016**, *657*, 136–146. [[CrossRef](#)]
21. Wang, C.; Wang, M.; Shi, J.; Hui, W.; Dong, H. Effect of microstructural refinement on the toughness of low carbon martensitic steel. *Scr. Mater.* **2008**, *58*, 492–495. [[CrossRef](#)]

22. Forouzan, F.; Gunasekaran, S.; Hedayati, A.; Vuorinen, E.; Mucklich, F. Microstructure analysis and mechanical properties of Low alloy High strength Quenched and Partitioned Steel. *DiVA* **2016**, *258*, 574–578. [CrossRef]
23. Andersson, J.O.; Helander, T.; Höglund, L.; Shi, P.F.; Sundman, B. Thermo-Calc & DICTRA, Computational tools for materials science. *Calphad* **2002**, *26*, 273–312.
24. Thermo-Calc Software TCFe9 Steels/Fe-alloys Database. Available online: <https://www.thermocalc.com/products-services/databases/thermodynamic/> (accessed on 20 September 2018).
25. A.B. MOBFE3: TCS Steels/Fe–Alloys Mobility Database. Thermo–Calc Software. Available online: <https://www.thermocalc.com/products-services/databases/mobility/> (accessed on 20 September 2018).
26. Bhadeshia, H.; Honeycombe, R. Microstructure and properties. In *Steels: Microstructure and Properties*, 3rd ed.; Butterworth–Heinemann: Cambridge, UK, 2011; ISBN 0080462928, 9780080462929.
27. Nishikawa, A.S.; Santofimia, M.J.; Sietsma, J.; Goldenstein, H. Influence of bainite reaction on the kinetics of carbon redistribution during the Quenching and Partitioning process. *Acta Mater.* **2018**, *142*, 142–151. [CrossRef]
28. Payson, P.; Savage, C.H. Martensite reactions in alloy steels. *Trans. ASM* **1944**, *33*, 261–280.
29. Grange, R.A.; Stewart, H.M. The temperature range of martensite formation. *Trans. AIME* **1946**, *167*, 467–501.
30. Van Bohemen, S. Bainite and martensite start temperature calculated with exponential carbon dependence. *Mater. Sci. Technol.* **2012**, *28*, 487–495. [CrossRef]
31. Nehrenberg, A.E. Contribution to Discussion on Grange and Stewart. *Trans. Am. Inst. Min. Met. Eng.* **1946**, *167*, 494–498.
32. Haynes, A.G.; Steven, W. The temperature of formation of martensite and bainite in low–alloy steel. *J. Iron Steel Inst.* **1956**, *183*, 349–359.
33. Andrews, K.W. Empirical formulae for the calculation of some transformation temperatures. *J. Iron Steel Inst.* **1965**, *203*, 721–727.
34. Wu, R.; Li, J.; Li, W.; Wu, X.; Jin, X.; Zhou, S.; Wang, L. Effect of metastable austenite on fracture resistance of quenched and partitioned (Q&P) sheet steels. *Mater. Sci. Eng. A* **2016**, *657*, 57–63. [CrossRef]
35. Gustafson, Å. Coarsening of TiC in austenitic stainless steel-experiments and simulations in comparison. *Mater. Sci. Eng. A* **2000**, *287*, 52–58. [CrossRef]
36. Díaz–Fuentes, M.; Iza–Mendia, A.; Gutiérrez, I. Analysis of different acicular ferrite microstructures in low–carbon steels by electron backscattered diffraction. Study of their toughness behavior. *Metall. Mater. Trans. A* **2003**, *34*, 2505–2516. [CrossRef]
37. Rodriguez–Ibabe, J. The Role of Microstructure in Toughness Behaviour of Microalloyed Steels. *Mater. Sci. Forum.* **1998**, *284–286*, 51–62. [CrossRef]
38. Wang, M.; Hell, J.; Tasan, C.C. Martensite size effects on damage in quenching and partitioning steels. *Scr. Mater.* **2017**, *138*, 1–5. [CrossRef]
39. Verbeke, K.; Barbé, L.; Raabe, D. Evaluation of the crystallographic orientation relationships between FCC and BCC phases in TRIP steels. *ISIJ Int.* **2009**, *49*, 1601–1609. [CrossRef]
40. Morito, S.; Tanaka, H.; Konishi, R.; Furuhashi, T.; Maki, T. The morphology and crystallography of lath martensite in Fe–C alloys. *Acta Mater.* **2003**, *51*, 1789–1799. [CrossRef]
41. Bhadeshia, H.K.D.H. Bainite in Steels. In *Theory and Practice*, 3rd ed.; Maney Publishing: Cambridge, UK, 2015; ISBN 1909662747, 9781909662742.
42. Kawata, H.; Sakamoto, K.; Moritani, T.; Morito, S.; Furuhashi, T.; Maki, T. Crystallography of ausformed upper bainite structure in Fe–9Ni–C alloys. *Mater. Sci. Eng. A* **2006**, *438*, 140–144. [CrossRef]



Paper IV

Optimization of Quenching Temperature to Minimize the Micro Segregation Induced Banding Phenomena in Quenching and Partitioning (Q&P) Steels

Farnoosh Forouzan,* Luciano Borasi, Esa Vuorinen, and Frank Mücklich

Mn, Cr, and Si are favorable elements for designing the quenching and partitioning (Q&P) steels while the microsegregation of them is a common phenomenon in the steels. This segregation makes the bands of enriched and depleted Mn–Cr regions, which affects the M_s temperature of the bands and consequently influence the volume fraction of initial martensite, retained austenite, and secondary fresh martensite in different bands. This issue leads to non-homogeneity in the microstructure and mechanical properties. In this study, the optimization method to minimize the inhomogeneity by selection of the quenching temperature is demonstrated.

1. Introduction

The “quenching and partitioning” (Q&P) is a promising heat treatment which could be used to produce 3rd generation of advanced high strength steels (AHSS) by producing a fine controlled complex microstructure of mainly martensite and retained austenite.^[1,2] So, selection of the quenching temperature (QT), partitioning temperature (PT), and time (Pt) play a very important role in designing the volume fraction of phases and optimizing the strength and ductility.^[3,4] But due to the sluggish diffusion of substitutional atoms in steels, the interdendritic chemical segregation cannot be completely removed by hot work processing. On the contrary, interstitially dissolved carbon atoms in steel have a high diffusion coefficient that allows a homogenization of the carbon content in the steel. Nevertheless, as the presence of other elements can locally modify the carbon activity, the segregation of substitutional atoms can lead to carbon content variations.^[5] For example, Mn and Cr decrease the carbon activity, and thus areas enriched with these elements can also result in a

local increase of the carbon content. In contrast, Si, P, and Mo increase the carbon activity and thus reject it to other regions.^[6] During hot rolling, the micro-segregations are aligned into bands in the rolling direction generating non-homogenous areas in the normal direction. This issue could make some problem, for example, localized deformation, hot-working, and corrosion behavior in microstructure.^[7,8] It is typical for TRIP steels to have bands of ferrite bainite-martensite-austenite.^[9,10] Effect of banding on mechanical properties of ferritic/pearlitic bands has been widely studied.^[11–13] Typically, no or very small effect has been

observed on the anisotropy of tensile properties while a significant anisotropy of reduction in area for impact properties was found.

Normally, “Q&P steels” contain over 1.5 wt% silicon to inhibit carbide precipitation as well as Mn, Ni, and Cr to retard ferrite, pearlite, and bainite formation and to effectively stabilize austenite for longer times at higher partitioning temperatures.^[14] Although the role of alloying additions like Mn, Ni, Cr, Si, etc. on microstructural development in Q&P steels is of significant interest,^[15–17] there is a lack of research on the effect of segregation of these elements.

Recently, HajyAkbari et al.^[18] investigated the effect of Mn segregation on 0.3C–1.3Si–3.2Mn (wt%) steel. They compared the overall volume fractions of the phases in the specimens quenched at two quenching temperatures of 180 and 240 °C, based on the simulations and experimental measurements considering two regions of poor and rich Mn. Results showed that microstructural non-homogeneity is more pronounced in the specimen quenched to a higher temperature.


The aim of this work is to investigate the effect of banding induced by micro-segregation of medium carbon and Mn–Cr containing steel on the final microstructure and mechanical properties after quenching and partitioning process and to optimize the quenching temperature to minimize the in-homogeneity.

2. Experimental Section

Rectangular specimens of 10 × 10 × 55 mm from a steel bar with the nominal chemical composition of 0.6% C–1.6% Si–1.25% Mn–1.75% Cr–0.15% Mo–0.12% V (wt%) were machined and treated using Gleeble 3800. Heat treatment starts with austenitization at 890 °C for 60 min, followed by quenching to 190 °C (QT190), 165 °C (QT165), 100 °C (QT100), and 25 °C (QT25) while the

F. Forouzan, L. Borasi, Dr. E. Vuorinen
Department of Engineering Sciences and Mathematics
Luleå University of Technology
SE-97187 Luleå, Sweden
E-mail: farnoosh.forouzan@ltu.se

F. Forouzan, Prof. F. Mücklich
Department for Materials Science
Functional Materials
Saarland University
D-66041 Saarbrücken, Germany

 The ORCID identification number(s) for the author(s) of this article can be found under <https://doi.org/10.1002/srin.201800281>.

DOI: 10.1002/srin.201800281

nominal martensite's start temperature (M_s) is 223 °C. Subsequently, samples are partitioned at 280 °C for 900 s and quenched to room temperature. The specimens studied by optical microscopy, microhardness, SEM, EDX, and XRD measurements were cut and mounted, then grinded and polished until 0.05 μm . In order to color etch, "Le Pera"^[19] method, which contains equal portions of 1% aqueous sodium metabisulfite and 4% picral solutions for 30 s, was used. Before SEM and EDS analyses, samples were etched with Nital (3%) for 15 s. "JSM-IT300" scanning electron microscope equipped with Oxford X-Max energy dispersive spectroscopy detector has been used. The data was processed with the AZtec oxford software. Furthermore, volume fractions of retained austenite were determined by X-ray diffraction (XRD) analysis using a monochromatic Cu-K α Q 4 radiation at 40 kV and 45 mA and the data were collected from 40° to 100° 2 θ with a step size of 0.0131°. Results were analyzed through Rietveld simulation using High Score Plus software (vers.3.0.1).

3. Results

Figure 1 shows the SEM images of Nital etched samples quenched to different temperatures. The comparison shows more significant microstructural banding at higher quenching temperatures (QT190 and QT165).

A detailed examination of dark and light bands in Figure 2 shows the presence of higher amount of initial martensite (as

dark blue etched feature) in the darker regions, while the predominantly white regions are associated with an increase in the local fraction of either retained austenite or fresh martensite transformed during final cooling.

A line-scan by EDS in a transversal direction to the banding (see Figure 3a) displays the segregation of both chromium and manganese with the same tendency. None of the other alloying elements has shown considerable segregation. The content of Mn and Cr decreases constantly in the regions associated with higher amount of initial martensite, while the maximum peaks are located in the regions exhibiting the presence of fresh martensite.

The analysis reports a variation from 1% up to 1.75% in Mn and between 1.5% and 2.1% for Cr, while the nominal composition of the steel has a 1.25% and 1.75% for Mn and Cr, respectively. In addition, a carbon alteration is expected due to the effect of Mn and Cr in the carbon activity. However, the C concentration will adjust to constant C activity in different band due to high carbon diffusivity. Since it is not possible to obtain a reliable quantification of carbon concentration by using EDS, its diffusion during austenitization has been modelled by Thermo-calc-Dictra using TCEFE9 and MOBFE3 database. Results show that carbon content varies from 0.57% up to 0.615% from Mn depleted regions toward enriched regions, when equilibrium conditions are assumed within the bands.

The effect of substitutional alloying elements on theoretical martensite start temperature are modelled by Bohemen^[20] as modified Andrews' equation,^[20,21] in Equation (1) and (2).

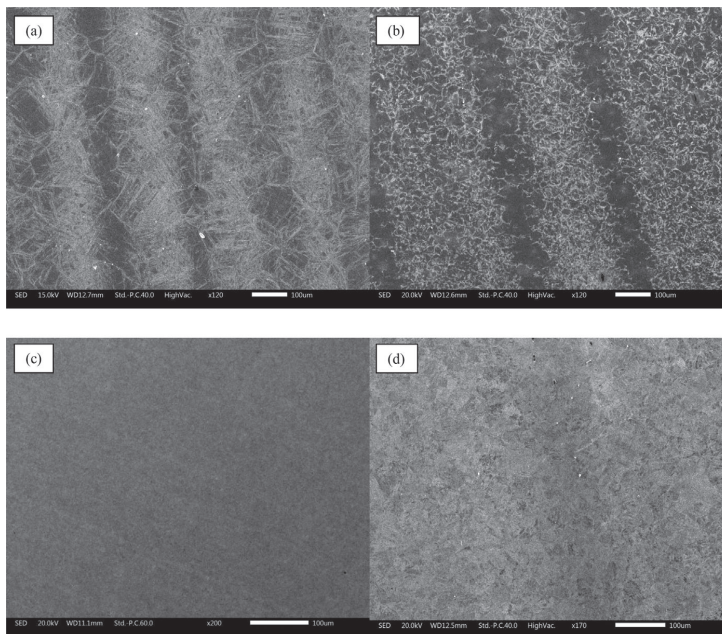


Figure 1. Comparison between the samples quenched to a) 190 °C, b) 165 °C, c) 100 °C, and d) 25 °C and thereafter partitioned at 280 °C for 900 s.

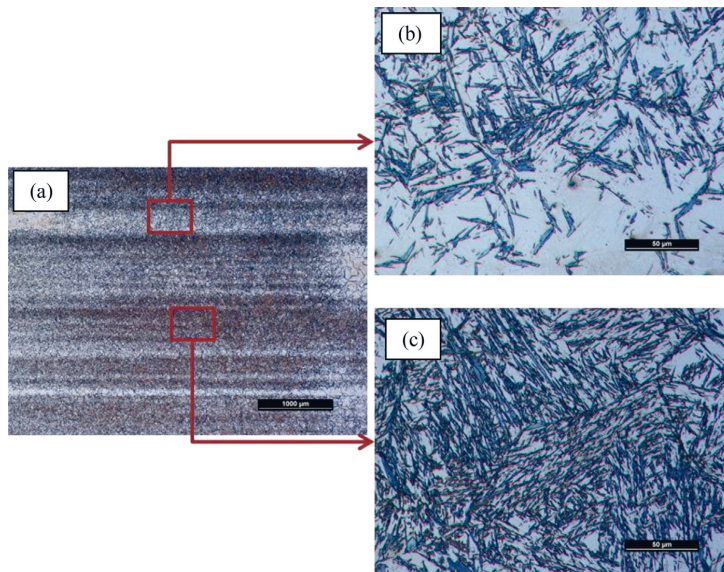


Figure 2. a) OM of QT190 sample, etched with LePera reagent shows initial (tempered) martensite as dark blue and retained austenite or fresh martensite as white (unetched). b) OM of bright band in higher magnification containing more retained austenite/fresh martensite. c) OM of darker band in higher magnification where dark regions of initial martensite predominate.

$$M_s(^{\circ}\text{C}) = 565 - \sum_{n=1}^i K_n x_n - 600(1 - e^{-0.96x_c}) \quad (1)$$

$$\sum_{n=1}^i K_n x_n (^{\circ}\text{C}) = -31x_{Mn} + 13x_{Si} + 10x_{Cr} + 18x_{Ni} + 12x_{Mo} \quad (2)$$

As these elements of alloy decrease the martensite start temperature (Equation (2)), a calculation of M_s was performed

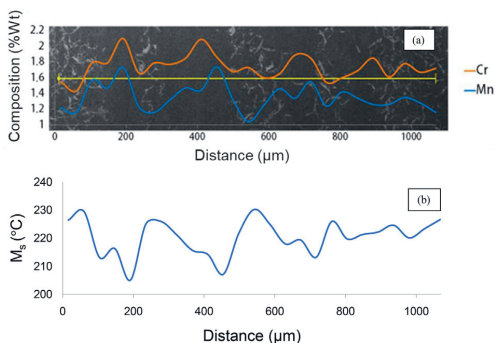


Figure 3. a) Line scan EDS on microstructural banding observed by SEM on QT190 sample. b) Calculated M_s along the distance corresponding to the measured segregation in a).

along the segregated bands considering the point by point data for Cr and Mn from Figure 3a and assuming that the other elements do not have a compositional variation (Figure 3b). Considering also the effect of C variation on the highest and lowest values in Figure 3b the difference in M_s temperature between the bands is extended up to 40 °C.

As mentioned previously, the segregation profile can be detected perpendicular to the rolling direction. So, the effect of segregation on hardness ($HV_{0.2}$) of the bands is compared with the volume fraction of retained austenite measured from the section transversal to the rolling direction and initial martensite formed during the first quenching in addition to the hardness ($HV_{0.5}$) of the same side, which does not have segregation in Table 1. Figure 1 illustrate that specimens quenched at a higher temperature (QT190 and QT165) have higher amount of fresh martensite, because the carbon partitioning is insufficient to stabilize the remained austenite after the first quenching. Hence, QT190 and QT165 show higher hardness in general, besides the difference between the hardness of the bands is also noticeable. On the other hand, by decreasing the quenching temperature the volume fraction of initial martensite increases and the amount of retained austenite and fresh martensite could not play a significant role. The effect of partitioning condition is always important to consider due to the fact that decreasing partitioning temperature or time can lead to an incomplete carbon partition process in both enriched and depleted regions. This can increase the amount of untempered martensite and, therefore, increase the microstructural banding.^[18]

Table 1. Hardness of Mn–Cr depleted and enriched regions and volume fraction of the phases in samples quenched at different temperatures.

QT [°C]	HV _{0.2} of Mn–Cr enriched region	HV _{0.2} of Mn–Cr depleted region	ΔHV _{0.2}	HV _{0.5}	%Austenite by XRD	%F _M (calculated initial martensite for the nominal composition)
190	845	703	142	719	9	38
165	845	774	71	762	17	56.7
100	742	726	16	730	18	83.1
25	720	747	27	725	15	94

4. Discussion

A schematic illustration emphasizing the effect of segregation in quenching and partitioning process is shown in **Figure 4**. Due to the sluggish diffusion of substitutional elements, segregation bands of Mn/Cr cannot be eliminated during austenitization.^[22] In the first quenching, a higher volume fraction of martensite is transformed in the Mn–Cr poor regions because of their higher M_s . During partitioning this initial martensite will temper and become softer and the final hardness is determined by partitioning conditions (temperature and time). Additionally, the carbon partitioning to the surrounding austenite is insufficient to stabilize all the austenite and thus, during final cooling more fresh martensite is formed in Mn–Cr rich regions because of their higher amount of austenite that can transform.

To calculate the volume fraction of martensite as a function of undercooling from M_s , Koistinen and Marburger equation^[23] (Equation (3)) can be used. T is the quenching temperature and

a_m is the rate parameter which is a function of chemical composition, as described in Equation (4) and (5).

$$f = 1 - e^{-a_m(M_s - T)} \quad (3)$$

$$a_m = 10^{-3} \left(27.2 - \sum_i S_i X_i - 19, 8(1 - e^{-1.56x_c}) \right) \quad (4)$$

And

$$\sum_i S_i X_i = 0.14x_{Mn} + 0.21x_{Si} + 0.11x_{Cr} + 0.08x_{Ni} + 0.05x_{Mo} \quad (5)$$

In Equation (5) is x_i the concentration in wt%.

Considering the highest and lowest M_s calculated based on EDS profiles for Cr and Mn (Figure 3a) and taking into account

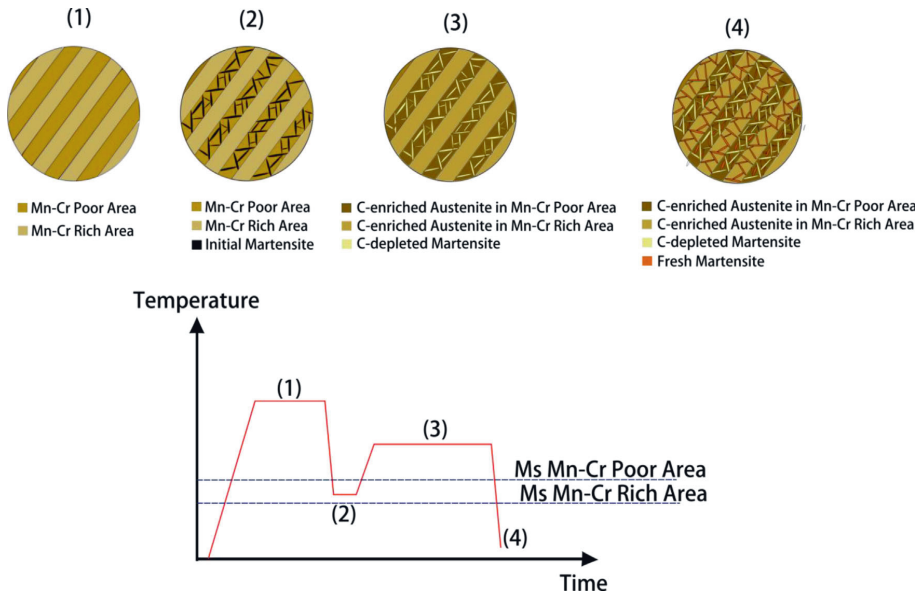


Figure 4. Schematic illustration of microstructure development during QP process, emphasizing the effect of segregation in the quenching and partitioning process.

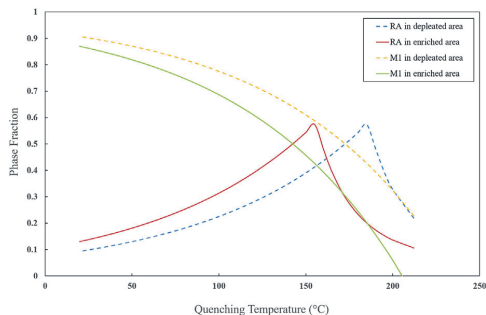


Figure 5. Calculated phase fraction of initial martensite (M_1) and retained austenite (RA) for segregated bands.

the C variations according to the simulation, the theoretical fraction of initial martensite and retained austenite of both Mn–Cr–C depleted and enriched regions are calculated based on a CCE model proposed^[24,25] and shown in **Figure 5**.

They illustrate that by decreasing the quenching temperature and proposing higher undercooling energy, the difference between volume fraction of initial martensite in Mn–Cr enriched and depleted regions will be reduced. In addition, based on the above-mentioned relationships, if the carbon content and amount of segregated elements (mainly Mn) decrease, the fraction of martensite in enriched and depleted region will be more similar. But it should be noticed that by decreasing the quenching temperature, the fraction of retained austenite in Mn–Cr depleted region decreases and it will be higher in enriched region which makes the difference to be negative from a certain point (in this case from 162 °C). Regarding to the fact that predicted data for retained austenite is higher than experimental results and the rest will transform to fresh

martensite at final quenching, finding the optimum point for having as similar structure and mechanical properties as possible to justify the effect of banding is not so simple. **Figure 6** shows the correlation between the predicted and experimental data according to the quenching temperature. Results indicate that in both cases, experimental results are much smoother than predicted as it is also shown by other researchers.^[26]

In both Table 1 and **Figure 7**, it is possible to notice that the difference in hardness between bands (ΔHV) decreases when the quenching temperature is lowered till a certain point and then it will increase but inversely which means the depleted region which was softer becomes harder than enriched region due to higher austenite fraction. Additionally, comparing the difference between the hardness of the bands (ΔHV) with the difference in the fraction of martensite (Δf_m) shows a linear relationship. As the carbon content is the preponderant parameter to define the hardness in steels and also the substitutional elements of alloys may affect, it is expected that the slope of this line depends on the chemical composition of the steel and degree of segregation, which could affect the volume fraction of different phases

Linear relation showed in **Figure 7** illustrates that the fraction of initial martensite is predominant parameter which controls the hardness but if the quenching temperature is low enough to make the structure between 80% and 90% martensitic ($\Delta f_m < 0.1$), the Mn–Cr rich regions include more retained austenite and it will result in the softest band. Optimizing the temperature to a slightly higher temperature, which could vary for different chemical compositions, will compensate the effect of softening of initial martensite during partitioning with the higher amount of austenite in the Mn–Cr rich region. On the other hand, by increasing the quenching temperature, the higher hardness of fresh martensite will dominate the average hardness and will result in a hardness increase in this region.

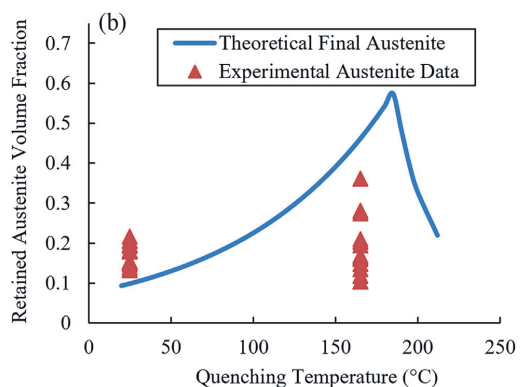
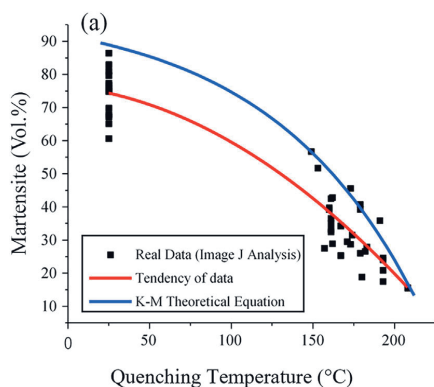


Figure 6. Comparison between theoretical and experimental data regarding the quenching temperature for different partitioning conditions. a) For martensite fraction. b) For retained austenite fraction.

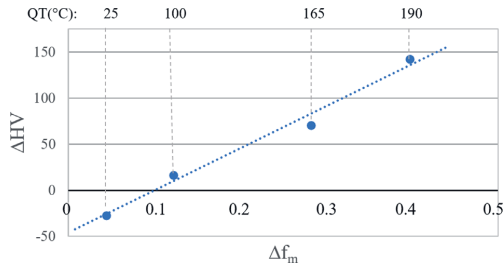


Figure 7. Relation between difference in fraction of martensite and hardness between bands.

5. Conclusion

In this study has the effect of micro-segregation of substitutional elements on microstructure and local hardness of an alloy after Q&P process been investigated and the following main conclusions can be made.

- 1) Micro-segregation of Mn and Cr is a common issue in all steels resulting in banding phenomena by changing the M_s temperature of the Mn–Cr depleted and enriched regions.
- 2) Difference in M_s temperature between the bands is extended up to 40 °C for the steel investigated.
- 3) Since a higher amount of Mn and Cr lowers the M_s temperature, the Mn–Cr depleted regions are imposed to a larger undercooling in comparison with the Mn–Cr enriched regions. This will result in a higher volume fraction of initial martensite in the first quenching stage for the Mn–Cr depleted region and this produces a softer final structure with higher fraction of tempered martensite and retained austenite in comparison with Mn–Cr enriched region.
- 4) The difference between the hardness of the bands at high quenching temperatures could be very high, depending on the chemical composition (150 HV at QT200 in this steel) but by decreasing the quenching temperature, the difference between the amounts of initial martensite will be very small and Mn–Cr enriched region becomes softer due to higher fraction of retained austenite.
- 5) Although a low quenching temperature leads to a decrease in the banding phenomenon, the optimum quenching temperature is represented by considering the balance between the banding formation and the possibility to retain a considerable fraction of austenite to improve the ductility. Thus, when bands with different level of alloying elements are present, the quenching temperature should not be close to the M_s temperature to prevent the banding formation. But, on the other hand, it must be high enough to obtain a significant amount of retained austenite after the heat treatment. For this reason, the optimum quenching temperature may be evaluated for each particular chemical composition and level of segregation.

Acknowledgement

The European Commission was acknowledged for funding through the projects: Erasmus Mundus Doctoral Programme, DocMASE, and Advanced Materials Science and Engineering, AMASE.

Conflict of Interest

The authors declare no conflict of interest.

Keywords

banding, hardness, microsegregation, microstructure, quenching and partitioning (Q&P)

Received: May 29, 2018

Revised: August 15, 2018

Published online:

- [1] D. K. Matlock, J. G. Speer, E. De Moor, P. J. Gibbs, *Jestech* **2012**, 15, 1.
- [2] J. G. Speer, E. De Moor, A. J. Clarke, *Mater. Sci. Technol.* **2015**, 31, 3.
- [3] F. Forouzan, E. Vuorinen, F. Mücklich, *Mater. Sci. Eng. A* **2017**, 698, 174.
- [4] R. Wu, W. Li, S. Zhou, Y. Zhong, L. Wang, X. Jin, *Metall. Mater. Trans. A* **2014**, 45, 1892.
- [5] G. Krauss, *Steels: Processing, Structure, and Performance*, 2nd ed., ASM International, Materials Park **2015**.
- [6] G. Krauss, *Metall. Mater. Trans. B* **2003**, 34, 781.
- [7] B. Wietbrock, M. Bambach, S. Seuren, G. Hirt, *Mater. Sci. Forum* **2010**, 638–642, 3134.
- [8] A. Grajcar, M. Kaminska, M. Opiela, P. Skrzypczyk, B. Grzegorzczak, E. Kalinowska-Ozgowicz, *Achievements in Mater. Manuf. Eng.* **2012**, 55, 256.
- [9] P. Andreas, T. Sandra, H. Thomas, S. Peter, E. A. Werner, *Steel Res. Int.* **2016**, 78, 216.
- [10] A. Grajcar, E. Kalinowska-Ozgowicz, M. Opiela, B. Grzegorzczak, K. Gołombek, *Arch. Mater. Sci. Eng.* **2011**, 49, 5.
- [11] A. S. Bor, *ISIJ Int.* **1991**, 31, 1445.
- [12] W. Spitzig, *Metall. Trans. A* **1983**, 14, 271.
- [13] L. Hellner, T. O. Norrman, *Jernkontorets Ann.* **1968**, 152, 269.
- [14] M. J. Santofimia, L. Zhao, R. Petrov, C. Kwakernaak, W. G. Sloof, J. Sietsma, *Acta Mater.* **2011**, 59, 6059.
- [15] M. E. De, J. G. Speer, D. K. Matlock, K. Jai-Hyun, L. Seung-Bok, *Steel Res. Int.* **2012**, 83, 322.
- [16] G. Miyamoto, J. C. Oh, K. Hono, T. Furuhashi, T. Maki, *Acta Mater.* **2007**, 55, 5027.
- [17] D. T. Pierce, D. R. Coughlin, K. D. Clarke, E. De Moor, J. Poplawsky, D. L. Williamson, B. Mazumder, D. L. Speer, A. Hood, A. J. Clarke, *Acta Mater.* **2018**, 151, 454.
- [18] F. HajyAkbari, J. Sietsma, R. H. Petrov, G. Miyamoto, T. Furuhashi, M. J. Santofimia, *Scr. Mater.* **2017**, 137, 27.
- [19] F. S. LePera, *Metallography* **1979**, 12, 263.
- [20] S. Van Bohemen, *Mater. Sci. Technol.* **2012**, 28, 487.
- [21] K. W. Andrews, *J. Iron Steel Inst.* **1965**, 203, 721.
- [22] J. D. Verhoeven, *J. Mater. Eng. Perform.* **2000**, 9, 286.
- [23] D. P. Koistinen, R. E. Marburger, *Acta Metall.* **1959**, 7, 59.
- [24] J. Speer, D. K. Matlock, B. C. De Cooman, J. G. Schroth, *Acta Mater.* **2003**, 51, 2611.
- [25] J. G. Speer, D. V. Edmonds, F. C. Rizzo, D. K. Matlock, *Curr. Opin. Solid State Mater. Sci.* **2004**, 8, 219.
- [26] D. V. Edmonds, K. He, F. C. Rizzo, B. C. De Cooman, D. K. Matlock, J. G. Speer, *Mater. Sci. Eng. A* **2006**, 438–440, 25.

Paper V

Process control maps to design an ultra-high strength-ductile steel

Farnoosh Forouzan ^{a,b}, Luciano Borasi^a, Esa Vuorinen^a and Frank Mücklich^b

^aDepartment of Engineering Sciences and Mathematics, Luleå University of Technology Luleå, Sweden; ^bDepartment for Materials Science, Functional Materials, Saarland University Saarbrücken, Germany

ABSTRACT

Steel with 2.4–2.5 GPa tensile strength and elongation to fracture of 4.8–5.7%, is produced by designing a novel heat treatment identical to quenching and tempering, in less than a few minutes. Since addition of Si to Fe–Mn steel promotes the austenite stabilisation by carbon enrichment, the elongation to fracture of 0.6C–1.6Si–1.2Mn (wt-%) steel treated by different quenching and partitioning (Q&P) routes is improved. Results demonstrated by process control maps give a good overview of the final microconstituents. By using higher partitioning temperatures, the tempering of martensite, stabilisation of austenite and improvement of the mechanical properties, could effectively be accelerated. This approach results in significant time and cost reduction which makes this heat treatment attractive for industries.

ARTICLE HISTORY

Received 29 January 2019
Revised 30 March 2019
Accepted 3 May 2019

KEYWORDS

Ultrahigh strength;
high-carbon low-alloy steel;
Q&P; ductility; map


Introduction

Ultra-high strength steels with good ductility are highly demanded and have been developed in recent years in order to design lighter components and decrease the energy consumption and environmental impact [1–5]. Increasing carbon content to medium or high level (> 0.5 wt-%) as the primary alloy for steels with higher strength and hardness is usually the most economical approach to achieve extreme properties. However, high-carbon martensitic steels are ‘as brittle as glass’ in the as-quenched or low-temperature-tempered state [6]. When the limited ductility and toughness can be tolerated, the excellent strength and hardness of high-carbon steels could be utilised. Common applications of high-carbon steels include rail steels, spring steels, wear resistant steels, forging grades, wire rope, tire reinforcement, pre-stressed concrete, and high strength bars [7].

Many attempts have been performed in order to develop such ultra-high strength steels without losing the ductility. The most typical class is ‘maraging’ steels which contain carbon-free martensitic matrix with nanoprecipitates, but these steels are highly alloyed with Ni (8–18), Co (4–15), Mo (1–5) wt-% and Ti, which limits their applicability due to their price. For instance, C530 in this group has the highest strength of 2.4 GPa and 7% ductility. On the other hand, tempering of martensitic steels has been widely studied during the last 50 years [8,9]. For example, a modified version of the 100Cr6 (AISI 52100, a 1C-1.5Cr wt-%

bearing steel) was developed in the late 1990s to exhibit higher retained austenite contents by adding Mn and Si to the chemical composition [10,11]. The original 100Cr6 has a high tensile strength of 2 GPa, but very low elongation of about 1–2% [12]. Basically, retained austenite is often undesirable in standard 100Cr6 steel because of its low thermal and mechanical stability which makes it susceptible to rapid decomposition (a few hours) at temperatures as low as 200°C [13–15]. By adding Mn, the martensite start temperature is lowered, while Si additions help further stabilisation of retained austenite. Previous investigations on low austempering temperatures (125–350°C) of high-carbon high-silicon steels provide comprehensive information on the kinetics of austenite decomposition into bainite [7,16–21]. The main purpose of using low temperature austempering is to allow the development of a mixture of very fine bainite laths with retained austenite but this requires tens of hours at 250°C or lower temperatures. Comparing yield strength of different microconstituents, the martensitic structure has the highest yield since strain-induced martensitic transformation from retained austenite relieves the stress within untransformed retained austenite and gives rise to stress redistribution also in its adjacent ferrite laths during deformation [22]. So, Quenching and Partitioning (Q&P) steels show one of the best mechanical properties among low carbon steels (C < 0.3 wt-%). However, the formation of brittle twin-type martensite [23–25], as well as the instability of carbon enriched

CONTACT Farnoosh Forouzan  farnoosh.forouzan@ltu.se  Department of Engineering Sciences and Mathematics, Luleå University of Technology, Luleå SE-97187, Sweden; Department for Materials Science, Functional Materials, Saarland University, Saarbrücken D-66041, Germany

 Supplemental data for this article can be accessed here. <https://doi.org/10.1080/02670836.2019.1615752>

© 2019 Institute of Materials, Minerals and Mining.

This is an Open Access article distributed under the terms of the Creative Commons Attribution-NonCommercial-NoDerivatives License (<http://creativecommons.org/licenses/by-nc-nd/4.0/>), which permits non-commercial re-use, distribution, and reproduction in any medium, provided the original work is properly cited, and is not altered, transformed, or built upon in any way.

retained austenite [22] are detrimental for the ductility and toughness of steels. In order to enhance the ductility of high-carbon martensitic steel, the basic approach is to utilise dispersed carbon enriched retained austenite to replace bulky retained austenite [25]. In addition, recent findings [6,26] showed that decreasing the number of coarse martensite plates can effectively increase the ductility. Wang et al. [27] have decreased the austenite grain size by applying severe plastic deformation ($\epsilon = 90\%$) above A_3 and quenching the sample to room temperature. Thereafter, heating the sample to 500°C and holding it there for 1 h, applying the second deformation ($\epsilon = 85\%$) followed by quenching and finally performing the heat treatment by austenitisation, water quench and low temperature tempering. Although this thermomechanical treatment is long and costly, ultra-fine austenite grains of $2.4\ \mu\text{m}$ and 2.6 GPa ultimate tensile strength (UTS) with 7% elongation is obtained.

Recently, Sourmail et al. [13] have designed a new heat treatment based on the fact that pre-existing martensite shortens the required duration for bainitic transformation [28–30]. So, the process is basically quenching and tempering of a high-carbon high-silicon steel (1C–1.25Si–0.96 Mn wt-%) but the tempering temperature is selected to be sufficient (300°C) to complete the bainite reaction in a few hours. In comparison with austempering, the quenching and partitioning (Q&P) treatment has much higher transformation rate. Basically, Q&P starts with a first controlled quenching to a temperature between M_s and M_f after fully or partially austenitisation. This quench defines a specific fraction of initial martensite, and then a holding of the component at a usually higher temperature for some time gives enough energy for tempering the ‘initial martensite’ and partitioning of carbon from martensite to retained austenite. Subsequently, the process finishes with a second quench which may lead to the formation of ‘secondary martensite’ (fresh martensite) [31,32]. Owing to weldability requirements, 90% of all steels used today are alloyed with less than 0.2 wt-% C [33]. Therefore, there is still a large lack of information on high-carbon steels in comparison with low carbon steels.

In this work, the concept of quenching and partitioning based on the understanding of the microstructural evolution of high-carbon high-silicon steel has been used to design a new heat treatment route. Owing to that fact that silicon retards the austenite decomposition into bainite by promoting carbon partitioning from martensite into austenite and increasing austenite stability during the partitioning stage [34,35], high partitioning temperatures for a few seconds have been compared with lower temperatures but longer times. The goal has been to compare the effect of different Q&P conditions and to provide a process map in order to elucidate the microstructural evolution and give the

opportunity for the consumer to select the heat treatment conditions based on the desired properties.

Experimental procedure

The chemical composition of the steel in this study, denominated 0.6CV, is shown in Table 1.

Gleeble 3800 has been used to perform different heat treatments on samples with the size of $10 \times 10 \times 75\ \text{[mm}^3\text{]}$. These were used to analyse the microstructure (Section ‘Microscopy’), fraction of phases (Section ‘XRD Analysis’), hardness (Section ‘Hardness’) and impact toughness (Section ‘Impact Toughness’). A fully austenitisation at 890°C for 5 min was performed for all samples, while different quenching and partitioning conditions were applied (Figure 1) Three different quenching temperatures ($190, 165, 25^\circ\text{C}$) were selected, which results approximately in 30, 50 and 85% of martensite after the first quench ($M_s = 223^\circ\text{C}$; $M_f = 99-195^\circ\text{C}$). Partitioning conditions in order to achieve similar levels of carbon enrichment of austenite, based on carbon diffusivity (discussed in section ‘Discussion’, Figure 12) were selected. So, a total number of 48 conditions were analysed as shown in Figure 1, where QT, PT, and Pt refer to the quenching temperature, partitioning temperature and partitioning time, respectively.

The terminology of the samples is QTX-PTX-PtY, where X and Y denote the temperature (in Celsius) and time (in seconds) used during the different steps of the heat treatment.

Concerning the process maps, the experimentally tested partitioning temperatures and times were used to construct each process map. Any other information outside these values is a result of a linear inter/extrapolation based on the experimental obtained values made with OriginPro 2017 (Colour Fill tool).

Table 1. The chemical composition of steel 0.6CV. Contents are in wt-%.

C	Si	Mn	Cr	Mo	V	Fe
0.6	1.6	1.25	1.75	0.15	0.12	bal.

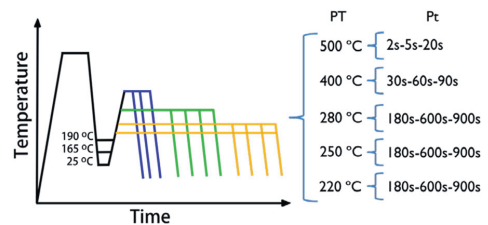


Figure 1. Schematic illustration of the Q&P conditions evaluated. PT and Pt refer to partitioning temperature and partitioning time, respectively.

Microstructure characterisation

A polished surface for each sample was prepared by conventional manual grinding and polishing step by step up to Colloidal silica of 0.06 μm for the final stage, to reveal the microstructure for optical microscopy, SEM, EBSD, XRD and to evaluate the microhardness.

Microscopy

The optical microscopy (OM) analysis was carried out using Nikon Eclipse MA200. LePera colour etching [36] was utilised to reveal and distinguish initial martensite (tinted in blue) from bainite (brown), while either retained austenite or fresh martensite do not etch and can be observed as white. Samples QT165 and QT190 were etched during 15–20 s, while 30 s was necessary for specimens quenched until room temperature based on the variation in the amount of initial martensite. JEOL JSM-IT300LV scanning electron microscopy (SEM) and FE-SEM Helios Nanolab 600 (FEI company) have been used for higher magnification microscopy and EBSD, respectively. The ARPGE [37] software was also used to post-process the EBSD results to construct the parent austenite grains.

XRD analysis

X-ray diffraction test to determine the fraction of phases and austenite carbon content has been performed on the transversal cut samples by using Panalytical Empyrean diffractometer, collecting data from 40° to 100° (2θ) with a step size of 0.013°, and a scan speed of 0.026796° s^{-1} , on the cross-section of the sample. HighScore Plus v. 4.7 software and PDF4 database were utilised to perform Rietveld analysis [38] to find the lattice parameters for calculation of the retained austenite carbon contents.

Mechanical properties

Hardness

A Matsuzawa MXT microhardness tester with a load of 5 N ($\text{HV}_{0.5}$) was utilised to study the Vickers hardness (HV) variations of the samples. This load was selected in order to obtain an indentation size with a diagonal larger than 25 μm , so that all microconstituents present in the microstructure could be covered by the indentation.

Impact toughness

Dimension of the samples is according to ASTM Standard E 23. The Charpy V-Notch Impact Tests were carried out at room temperature and the energy absorbed during the test is reported in joule (J).

Tensile test

The austenitisation was carried out at 890°C for 1 h based on NANOBAIN project results [17] using

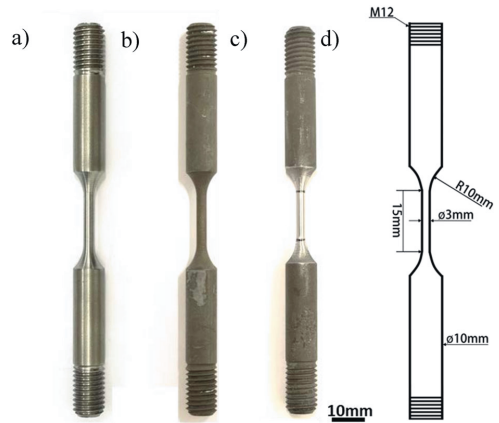


Figure 2. Shape and layout of tensile test samples (a) As-machined (b) After heat treatment (c) After grinding (d) Layout of specimens.

a Nabertherm N11/H batch furnace. The quenching stage was performed in either Therm Concept salt bath (for QT190 and QT165) or oil (for QT25).

Samples quenched until 190 and 165°C were held in the salt bath for 1 min, in order to stabilise the quench temperature in the sample and directly afterward, they were heated to the respective partitioning temperature by moving them to a second salt bath. On the other hand, for samples quenched until room temperature, the oil was removed from the sample surfaces before they were partitioned in the salt bath. All the samples were cooled down in calm air after the partitioning. Owing to austenitisation in an air atmosphere, the decarburised surface layer of samples was 400 μm , revealed by hardness ($\text{HV}_{0.1}$) as a function of the distance from the surface measurements. So, as shown in Figure 2, samples were ground to remove the decarburised layer before the test.

Tensile tests were carried out at room temperature using Gleeble 3800 and the strain rate applied was 0.005 s^{-1} .

Results

Phase fractions

Based on the quenching temperature, which implies the amount of initial martensite, the final content of retained austenite at room temperature changes. Figure 3 shows the ‘constrained carbon equilibrium’ (CCE) model [39] in order to illustrate the influence of QT on the phase fraction of different microconstituents of the final structure. Since the assumption in this model, is that all the trapped carbon in the initial martensite will diffuse out and dissolve evenly in the retained austenite during the partitioning stage, it will overestimate the amount of retained austenite. This will

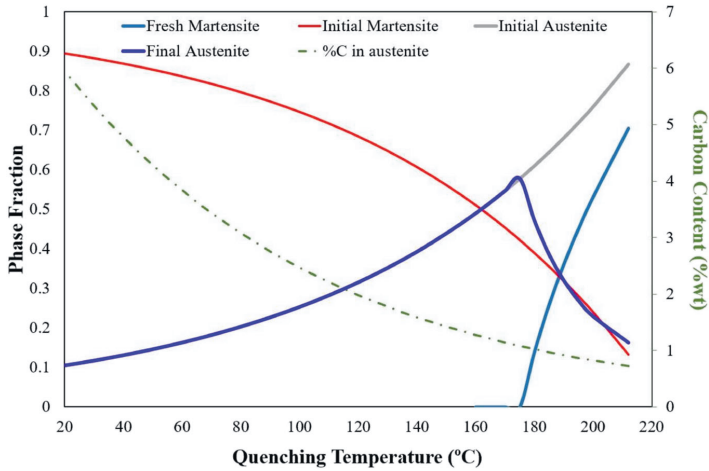


Figure 3. Theoretical evolution of the microstructure of the 0.6CV vs quenching temperature.

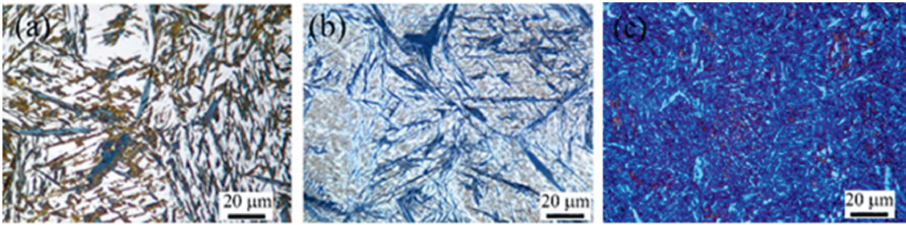


Figure 4. Example of the different microstructures according to the quenching temperature. (a) QT200-PT220-Pt600, (b) QT165-PT500-Pt5; and (c) QT25-PT400-Pt60 (Magnification: 1000x-Samples tint etched with Lepera method, to be able to see the phase colors please refer to digital version).

still be useful in order to find the optimum QT, which has the highest potential to result in the highest retained austenite content [40].

The importance of adequate characterisation technique for complex phase steels and their accuracy is obvious, and the quantitative measurement of phase fractions is not an easy task. The difference in the results achieved by established techniques like light microscopy, XRD and EBSD makes this more challenging. Comparisons between different techniques for determination of the RA have been performed for TRIP [41] and stainless steels [42]. No preferential technique has been found by round robin tests performed in these comparisons. Nevertheless light microscopy and EBSD systematically over- and under-estimate the amount of RA, respectively.

Light optical microscopy (LOM)

Figure 4 shows colour etched microstructures of different Q&P treated samples at different conditions. This method can well discriminate the phases based on their colours which subsequently will be used by the image processing software to quantify the fraction of phases.

Since both retained austenite and fresh martensite appear as white, high magnification EBSD with a very

small step size of the beam could clarify the difference between them and help to compare the image analysis results of LOM with EBSD.

Electron backscatter diffraction (EBSD)

Figure 5 shows the EBSD results of the sample shown in Figure 4(b). In this picture image quality (IQ) and phase map are superimposed on each other. All body-centred cubic (BCC) structures are coloured as red but higher tetragonality of BCT structure and dislocation density of martensite decreases the quality of the Kikuchi patterns [43,44]. Consequently, initial martensite is brighter than fresh martensite/bainite. So, Figure 5, shows that most of the austenite is located just around the tempered martensite and the lathes which are darker are fresh martensite. In this regard, image analysis of the LOM results should be performed at the highest magnification of the optical microscope (1000x) and with high consciousness not to overestimate the fraction of retained austenite [41].

It is clear in this picture (Figure 5) that initial martensite (bright red) is formed mostly as plate martensite. Figure 6(a) shows the Image quality map and Figure 6(b) the Kernel average misorientation

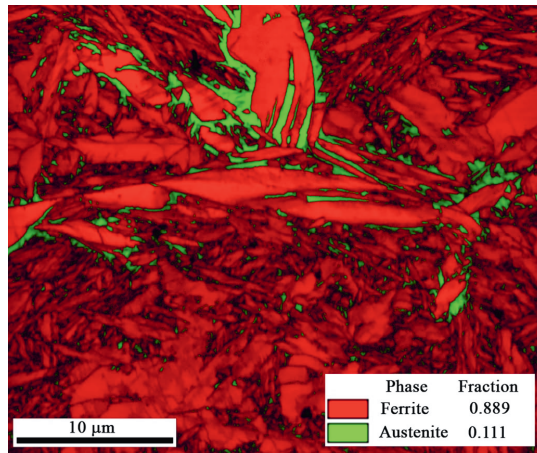


Figure 5. Superimposed image quality map and colour-coded phase map of sample QT165-PT500-Pt5. Austenite appears green. Regions of tempered or fresh martensite/bainite all appear red, but the brighter regions are likely tempered martensite while darker greyscale indicates regions are likely martensite/bainite (For interpretation of the references to color in this figure legend, please refer to the web version of this article).

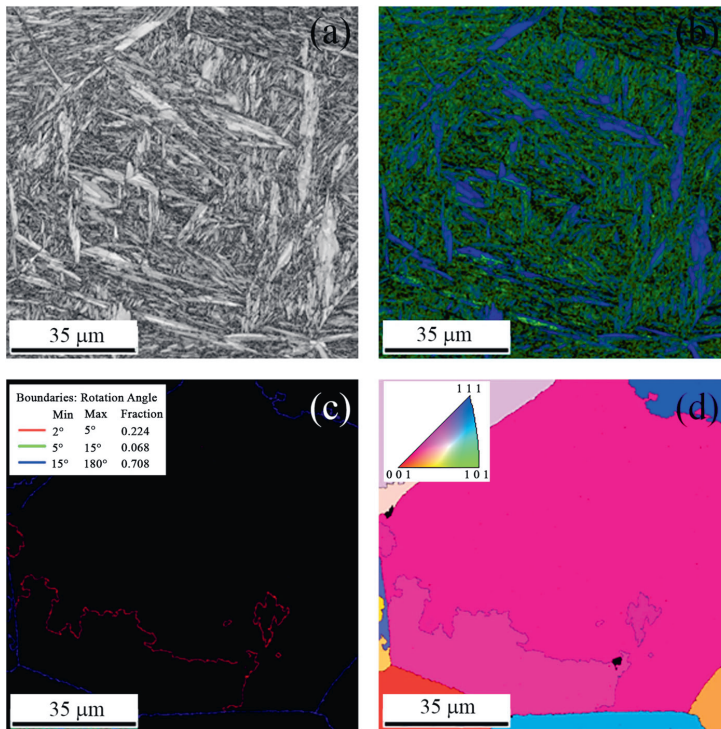


Figure 6. (a) Image quality map and (b) Kernel average map of sample QT165-PT250-Pt600 from its EBSD analysis. (c) Grain boundary map and (d) IPF of reconstructed parent austenite grain by post processing the above EBSD data by ARPGE software.

(KAM) map located on one parent austenite grain, which is reconstructed by ARPGE software. Figure 6(c) shows the grain boundaries of parent austenite grains and Figure 6(d) the inverse pole Figure of that austenite grain. Comparison between them shows that brighter parts of Figure 6(a) demonstrate lower stress level (blue

parts) in Figure 6(b) which represent smaller distortion of tempered martensite [45]. In addition, although there are a few lathes of initial martensite in the structure, most of them are plate martensite and oriented along the grain boundaries of parent austenite grains (compare Figure 6(b,c)).

Table 2. Equations for determination of the austenite carbon content.

No.	Equation	Reference
1	$a(\text{nm}) = 0.35467 + 0.00467\%C$	[46,47]
2	$a(\text{nm}) = 0.3556 + 0.00453\%C + 0.000095\%Mn$	[48]
3	$\%C_{\gamma} = \frac{(a(\text{nm}) - 0.3578)}{0.0033}$	[49]
4	$a(\text{Å}) = 3.556 + 0.0453\%C - 0.00095\%Mn - 0.0056\%Al$	[50]
5	$a(\text{nm}) = 0.03578 + 0.0033\%C + 0.000095\%Mn - 0.00002\%Ni + 0.00006\%Cr + 0.00031\%Mo + 0.00018\%V$	[51]
6	$a(\text{nm}) = 0.3556 + 0.00453\%C + 0.000095\%Mn + 0.00056\%Al + 0.0006\%Cr - 0.0002\%Ni$	[5]
7	$a = 0.3573 + 0.0033C + 0.000095Mn - 0.00002Ni + 0.00006Cr + 0.00031Mo + 0.00018V$	[52]

Table 3. Carbon content range of retained austenite in the samples quenched at a specific temperature but partitioned according to the 15 different routes mentioned in Figure 1.

Quenching temperature	Carbon content (wt-%)
QT25	0.99–1.44
QT165	0.6–1.32
QT190	0.67–0.89

X-ray diffraction (XRD)

Considering the tetragonality of the iron BCC and BCT, and by using PDF4 (2018) database, it is possible to separate fresh martensite from tempered martensite/bainitic ferrite in an integrated XRD-peak.

In order to measure the retained austenite, patterns were analysed via Rietveld simulation and austenite carbon content was calculated using different equations. By comparing the results from different equations (see Table 2) with the minimum amount of carbon to stabilise austenite at room temperature, the first equation is selected, because it was in accordance with the results.

As shown in Table 3, the carbon content range in austenite generally increases when the quenching temperature is reduced, regardless of the partitioning conditions. This is due to a higher chance for carbon enrichment of retained austenite when there is a higher fraction of initial martensite and smaller amount of austenite during the partitioning stage. Besides, the wide carbon content range of QT165, this shows the importance of partitioning condition to stabilise the RA.

Figure 7 shows the austenite fraction measured by XRD based on quenching temperature for different partitioning times and temperatures.

Mechanical properties

Hardness

The influence of different partitioning conditions on hardness is summarised in three different colour maps, one for each quenching temperature (see Figure 8). It is important to highlight that (i) even though samples quenched until room temperature (QT25-Figure 8(c)) have the highest amount of initial martensite, the highest levels of hardness are achieved in QT165 and QT190

(Figure 8(a,b)). (ii) Owing to the high-carbon content distorting the body centered tetragonal (BCT) unit cell of the martensite, plus the high dislocation density, the fresh martensite represents a hard phase in the microstructure. Therefore, higher level of hardness (approximately, 800 HV) confirms the presence of fresh martensite as the hardest microconstituent, in QT165 and QT190 samples. (iii) The location of the lowest levels of hardness has a clear tendency. For the three QT, the lowest levels of hardness are reached when the highest partitioning temperatures are applied. This behaviour can be seen in the lower-right corners of Figure 8(a–c).

Impact test

Results of the energy absorbed in Charpy V-Notch tests are presented in different colour maps according to the quenching temperature as a function of the partitioning time and temperature (Figure 9). Maps illustrate that the range of absorbed energy for QT25 is obviously higher than for the 2 other quenching temperatures and also the variation between the numbers is low for QT25. For example, the absorbed energy of QT165 could be as high as 10 J for high-temperature PTs while in lower PTs it is less than 3 J, while the changes of QT25 are around 2 J for all the partitioning conditions with PT higher than 280°C.

Tensile test

The tensile strength and elongation to fracture for the 11 selected Q&P conditions and one normal Q&T sample (QT25-PT280-Pt2h: quenched to RT and tempered at 280°C for 2 h) are shown in Figure 10. Samples quenched to room temperature achieve not only the highest tensile strength but also the largest elongation to fracture. Since no necking is observed in these samples, the maximum engineering tensile stress is almost the same as the fracture stress. The values of ultimate tensile strength (UTS) rise from 1.1–1.8 GPa for QT165 and QT190 samples and for the QT25 samples values up to 2.4–2.5 GPa are achieved. In addition, elongation to fracture increases up to 4.8–5.7% for these samples. This is mainly because there is no brittle fresh martensite, much finer structure of martensite lathes and a very small fraction of bulky retained austenite in QT25

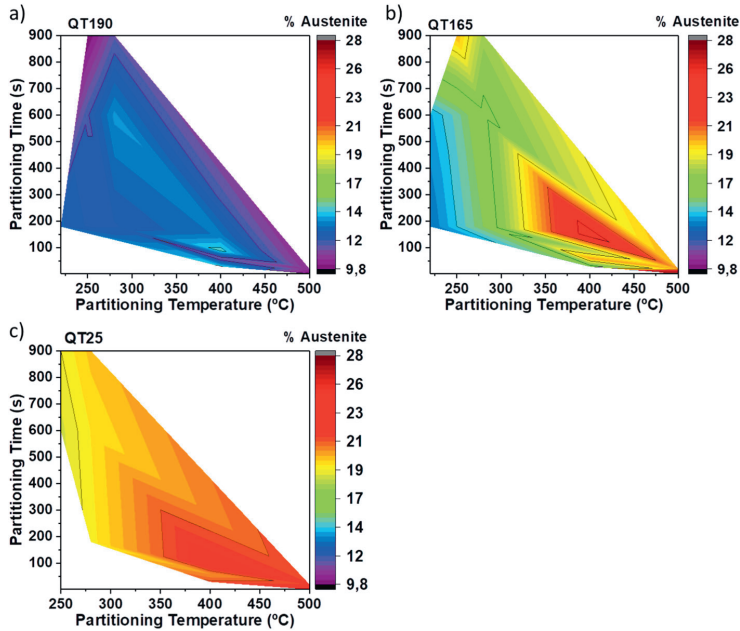


Figure 7. Colour maps of the changes in the amount of retained austenite (%) after different partitioning times and temperatures for each QT. Analysis via XRD.

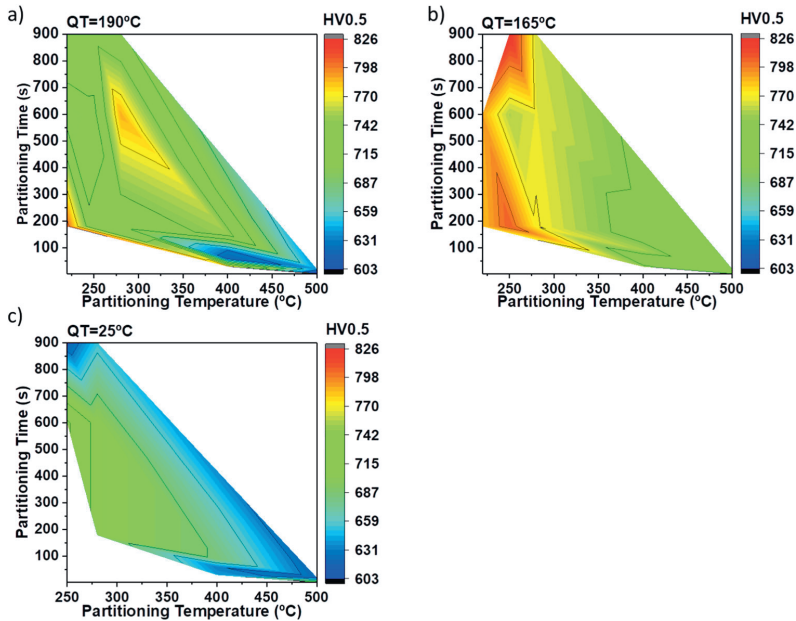


Figure 8. Colour maps of the hardness vs partitioning conditions for each QT.

samples. In addition, these samples show better properties in comparison with the Q&T sample, caused by the higher amount of retained austenite. The reason of such low strength and brittleness of samples quenched

at higher temperatures (QT165 and 190) goes back to the high notch-sensitivity of high-carbon fresh martensite, since all these samples had cleavage faceted fracture surfaces in tensile testing.

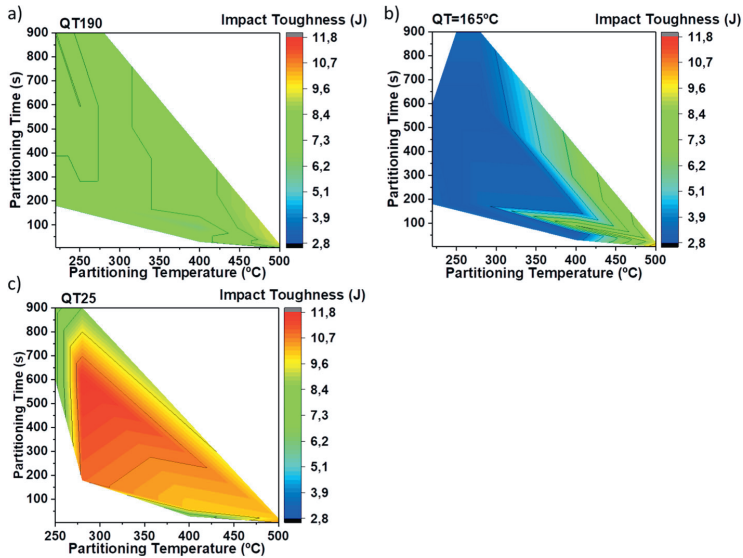


Figure 9. Colour maps of the impact toughness (J) for each QT. The change in energy absorbed is denoted by alterations in colours as a function of the partitioning time (s) and partitioning temperature ($^{\circ}\text{C}$).

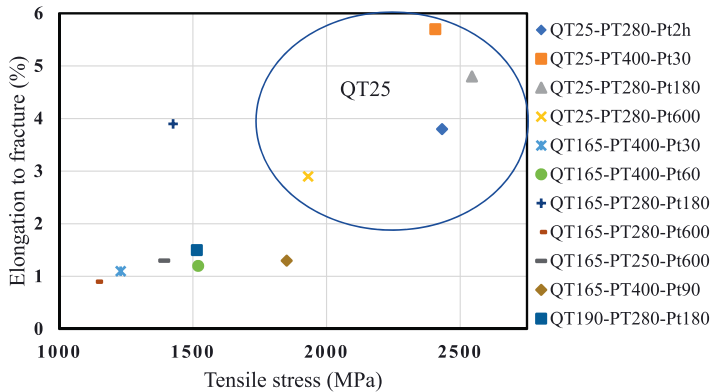


Figure 10. Results of elongation at fracture vs tensile strength achieved for the different Q&P conditions.

Discussion

In order to find the most accurate data for phase fractions in different samples, all results; image analysis of optical microscopy pictures; Rietveld simulation of XRD data and; EBSD have been compared.

The effect of partitioning duration on the final amount of retained austenite is shown in Figure 11. Results identified by using XRD method show that an increase in the partitioning time at a 'high partitioning temperature' (500°C) gives a significant austenite reduction by decomposition of austenite (Figure 11(a)). In contrast, prolonging the time at 'low partitioning temperatures' ($\leq 280^{\circ}\text{C}$) leads to an increase in the quantity of retained austenite (Figure 11(b)). There are 2 different possible explanation for this phenomenon. Depending on the chemical composition, transitional

carbide precipitates can be formed instantly after quenching in martensite before the partitioning stage. Nevertheless, as the formation of cementite is supposed to be inhibited, an increase in the partitioning time may lead to a resolution of these transitional carbides providing, a 'new' source of carbon to enrich the austenite carbon content during partitioning [53]. Another explanation about this behaviour is due to the difference between the carbon content of RA achieved after a short partitioning time and the longer time. Retained austenite after a short time partitioning at low temperature has low carbon content resulting in lower stability. By prolonging the holding time at low temperature, the carbon content of austenite increases so that less austenite will transform to martensite during final quenching to room temperature.

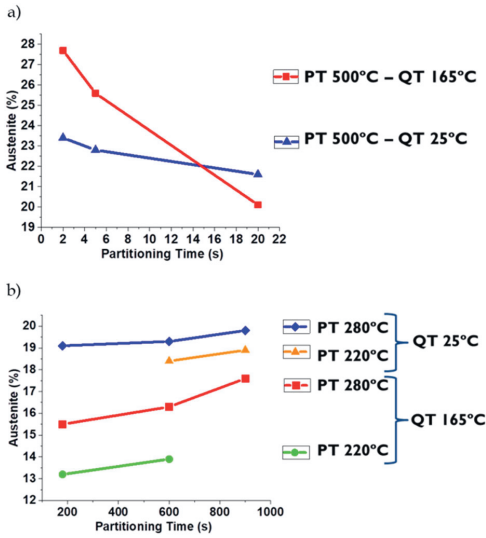


Figure 11. Effect of partitioning time on the final amount of retained austenite (a) At high partitioning temperatures (500°C) (b) At low partitioning temperatures (< 280°C). Analysis via XRD.

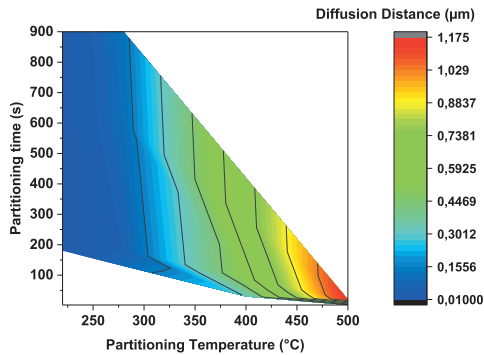


Figure 12. Diffusion distance of a carbon atom for the partitioning conditions analysed.

However, the minimum amount of achieved RA at high temperature (20%) is still higher than the highest amount of RA at low temperature. So, the rate of carbon diffusion out of martensite and enrichment of RA is calculated and correlated to partitioning time and temperature in Figure 12.

Since the rate of carbon diffusion out of martensite is much higher than the diffusion of carbon inside austenite, what will control the carbon diffusion rate and subsequent stabilisation of RA is mainly the rate of carbon diffusion in austenite [54]. An estimation of the distance (r) that a carbon atom can diffuse at a certain temperature and a given time (t) can be evaluated through Equation (1) [55]:

$$r = 2.4\sqrt{D \cdot t} \quad (1)$$

where D is the diffusion coefficient of carbon in austenite (Equation 2) [53]:

$$D \left(\frac{\text{cm}^2}{\text{s}} \right) = (0.04 + 0.08C) \exp \left(\frac{-31350}{R_c \cdot T} \right) \quad (2)$$

R_c and T are the ideal gas constant (1.987(cal/K.mol)) and the temperature in Kelvin, respectively.

Figure 12 describes the distance diffused by carbon atoms (r) for the partitioning conditions considered in this study. As can be seen in Equation (2), the diffusivity of carbon has an exponential relation with temperature. Subsequently, even though the time is a few seconds at high partitioning temperature, the carbon diffusion is at least two orders of magnitude higher.

Therefore, high partitioning temperatures lead to faster carbon depletion in martensite and, not only a larger amount of carbon is available to partition into austenite but also there is a faster carbon enrichment and carbon content homogenisation of the austenite. Consequently, due to the lower quantity of carbon atoms distorting the martensite unit cell and higher stability of austenite, high partitioning temperatures results in a lower hardness and higher amount of retained austenite. So, it is a question of seconds to control the partitioning time at higher temperatures to control the final microstructure and properties, because after this critical time an increment in time just leads to austenite consumption due to competing transformations (perlite/ferrite, upper bainite, and carbide precipitations).

Comparing the general effect of the partitioning conditions on microstructure and properties of samples quenched at the same QT in Figures 7–9, it can be observed that the partitioning conditions which lead to the lowest levels of hardness are almost the same as for highest levels of impact toughness and retained austenite.

Furthermore, the reduction of austenite amount is faster for higher quenching temperatures (Figure 11(a)), because the amount of initial martensite after quenching is not high enough to stabilise all available retained austenite after the first quench. In other words, a lower amount of carbon is available to stabilise austenite during partitioning and larger pools of austenite will remain for distribution of this carbon. The last two factors decrease the stability of the austenite and are the main reason for the faster reduction of austenite amount at higher quenching temperatures. So, if the carbon content of a RA pool is not high enough, it will transform to fresh martensite during final cooling, which is detrimental, and if carbon content is high enough to stabilise this bulky austenite after quench, it has a higher probability to transform to martensite during deformation [8,26,56]. Chen et al. [57] showed that it is possible to have 2 different carbon contents in RA in the microstructure, high carbon and low carbon bulky RA. Similarly, the higher carbon diffusivity

explains the increase in austenite fraction when the partitioning temperature is increased from 220°C up to 280°C.

On the other hand, poor impact toughness of high-carbon steels is mainly caused by large pools of blocky austenite and brittle martensite, since blocky austenite may easily transform to martensite under deformation, when its size is large and the tendency of the martensite to crack also increases with its size. Therefore, the size of austenite blocks should be reduced below the size of phases that can initiate a fracture, i.e. non-metallic inclusions [58].

Conclusions

- Formation of different types of martensite after the first quench in Q&P treatment has been compared and the effect of partitioning parameters have been described by analysing the results of hardness, impact toughness, and XRD measurements. These results are reported in several colour maps in order to assist in designing of heat treatments based on desired properties.
- The best heat treatment in order to achieve the highest hardness, tensile strength and elongation results from the quenching to room temperature (which implies over 80% of initial martensite) and partitioning at high temperatures (500, 400 or 280°C for a few seconds up to a few minutes).
- Although quenching to 25°C result in lower amount of retained austenite, very small amount of bulky austenite or coarse martensite (detrimental microconstituents) have been observed with this quenching temperature in comparison with QT190 or 165°C.
- The tensile strength of 2.4 GPa and 5.7% elongation, with around 20% RA and hardness above 730 Vickers was obtained by quenching to 25°C and partitioning at 400°C for 30 s, while other heat treatment conditions lead to a lower ductility but a higher hardness of up to around 800 Vickers.
- The steels treated by this method costs around 1/50 of maraging steels with similar properties, and the time used in this process is only 1/10th of the best austempering/Q&T treatments resulting in similar properties [13,27].

Acknowledgements

The support of the EUSMAT – European School of Materials via Ph.D. program ‘DOCMASE’ and supports and useful discussions with Dr. Flavio Soldera and Johannes Webel at FUWE, UDS is gratefully acknowledged by the authors.

Disclosure statement

No potential conflict of interest was reported by the authors.

Data availability

The raw/processed data required to reproduce these findings cannot be shared at this time as the data also forms part of an ongoing study. But it could be available upon request.

ORCID

Farnoosh Forouzan  <http://orcid.org/0000-0002-5390-7701>

References

- [1] Speer JG, De Moor E, Clarke AJ. Critical assessment 7: quenching and partitioning. *Mater Sci Technol.* 2015;31(1):3–9.
- [2] Opbroek E. Ultralight steel: a global consortium changes the future of automotive steel. *Bloomington: XLIBRIS; 2013.*
- [3] Caballero FG, García-Mateo C, Cornide J, et al. 2013. New advanced ultra high strength bainitic steels: ductility and formability (DUCTAFORM). DOI:10.2777/14158
- [4] Halfa H. Recent trends in producing ultrafine grained steels. *J Minerals Mater Charact Eng.* 2014;2(05): 428–469.
- [5] Santofimia MJ, Zhao L, Petrov R, et al. Microstructural development during the quenching and partitioning process in a newly designed low-carbon steel. *Acta Mater.* 2011;59(15):6059–6068.
- [6] Sun J, Liu Y, Zhu Y, et al. Super-strong dislocation-structured high-carbon martensite steel. *Sci Rep.* 2017: Article number: 6596. DOI:10.1038/s41598-017-06971-w
- [7] Vuorinen E, Ojala N, Heino V, et al. Erosive and abrasive wear performance of carbide free bainitic steels – comparison of field and laboratory experiments. *Tribol Int.* 2016;98:108–115.
- [8] Krauss G. Tempering of lath martensite in low and medium carbon steels: assessment and challenges. *Steel Res Int.* 2017;87:9999.
- [9] Hutchinson B, Hagström J, Karlsson O, et al. Microstructures and hardness of as-quenched martensites (0.1–0.5%C). *Acta Mater.* 2011;59(14):5845–5858.
- [10] Bellus J, Baudry G, Dudragne G, et al. 2000. Steel for bearings. *Google Patents; 2000.*
- [11] Daguier P, Baudry G, Bellus J, et al. Improved bearing steel for applications involving debris, higher loads and temperatures. In: Beswick J, editor. *Bearing steel technology.* West Conshohocken (PA): ASTM International; 2002. p. 320–329.
- [12] Bhadeshia HKDH. Steel for bearings. *Prog Mater Sci.* 2012;57:268–435.
- [13] Sourmail T, Caballero FG, Moudian F, et al. High hardness and retained austenite stability in Si-bearing hypereutectoid steel through new heat treatment design principles. *Mater Des.* 2018;142:279–287.
- [14] Perez M, Sidoroff C, Vincent A, et al. Microstructural evolution of martensitic 100Cr6 bearing steel during tempering: from thermoelectric power measurements to the prediction of dimensional changes. *Acta Mater.* 2009;57(11):3170–3181.
- [15] Sourmail T, Millot-Méheux M. Thermal and mechanical stability of retained austenite in 1%C bearing steels with varying Si contents. *Mater Sci Technol.* 2016;32(11):1126–1132.

- [16] Garcia-Mateo C, Caballero FG. Ultra-high-strength bainitic steels. *ISIJ Int.* 2005;45(11):1736–1740.
- [17] Sourmail T, Smanio V, Ziegler C, et al. Novel nanostructured bainitic steel grades to answer the need for high-performance steel components (Nanobain), Research and Innovation, ed. 2013.
- [18] Soliman M, Palkowski H. Ultra-fine bainite structure in hypo-eutectoid steels. *ISIJ Int.* 2007;47(12):1703–1710.
- [19] Sourmail T, Smanio V, Auclair G. Kinetics of bainite formation in 100Cr6 and similar high-carbon steel grades. Bearing steel technologies: 10th volume, Advances in steel technologies for rolling bearings, 2014; p. 1–11.
- [20] Garcia-Mateo C, Caballero FG, Bhadeshia HKDH. Acceleration of low-temperature bainite. *ISIJ Int.* 2003; 43(11):1821–1825.
- [21] Kabirmohammadi M, Avishan B, Yazdani S. Transformation kinetics and microstructural features in low-temperature Bainite after ausforming process. *Mater Chem Phys.* 2016;184:306–317.
- [22] Zhang K, Zhang M, Guo Z, et al. A new effect of retained austenite on ductility enhancement in high-strength quenching-partitioning-tempering martensitic steel. *Mater Sci Eng A.* 2011;528(29–30):8486–8491.
- [23] Qin S, Liu Y, Hao Q, et al. High carbon microalloyed martensitic steel with ultrahigh strength-ductility. *Materials Science and Engineering: A.* 2016;663: 151–156.
- [24] Qin S, Liu Y, Hao Q, et al. The mechanism of high ductility for novel high-carbon quenching-partitioning-tempering martensitic steel. *Metall Mater Trans A.* 2015;46(9):4047–4055.
- [25] Bhadeshia HKDH, Edmonds DV. Bainite in silicon steels: new composition-property approach. *Met Sci.* 1983;17(9):420–425.
- [26] Wang M, Hell J, Tasan CC. Martensite size effects on damage in quenching and partitioning steels. *Scr Mater.* 2017;138(Supplement C):1–5.
- [27] Wang Y, Sun J, Jiang T, et al. A low-alloy high-carbon martensite steel with 2.6 GPa tensile strength and good ductility. *Acta Mater.* 2018;158:247–256.
- [28] Ravi AM, Sietsma J, Santofimia MJ. Exploring bainite formation kinetics distinguishing grain-boundary and autocatalytic nucleation in high and low-Si steels. *Acta Mater.* 2016;105:155–164.
- [29] Smanio V, Sourmail T. Effect of partial martensite transformation on bainite reaction kinetics in different 1% C steels. *Sol State Phenomena.* 2011;172:821–826.
- [30] HajyAkbari F, Sietsma J, Miyamoto G, et al. Interaction of carbon partitioning, carbide precipitation and bainite formation during the Q&P process in a low C steel. *Acta Mater.* 2016;104:72–83.
- [31] Santofimia MJ, Zhao L, Sietsma J. Overview of mechanisms involved during the quenching and partitioning process in steels. *Metall Mater Trans A.* 2011;42(12):3620–3626.
- [32] Forouzan F, Gunasekaran S, Hedayati A, et al. Micro structure analysis and mechanical properties of low alloy high strength quenched and partitioned steel. *Sol State Phenomena.* 2017;258:574–578.
- [33] Vuorinen E. Structure and properties of advanced fine grained steels produced using novel thermal treatments [dissertation]. Luleå: Luleå tekniska universitet; 2012.
- [34] Toji Y, Matsuda H, Raabe D. Effect of Si on the acceleration of bainite transformation by pre-existing martensite. *Acta Mater.* 2016;116:250–262.
- [35] Kim B, Sietsma J, Santofimia MJ. The role of silicon in carbon partitioning processes in martensite/austenite microstructures. *Mater Des.* 2017;127(Supplement C): 336–345.
- [36] LePera FS. Improved etching technique for the determination of percent martensite in high-strength dual-phase steels. *Metallography.* 1979;12(3):263–268.
- [37] Cayron C. ARPGE: a computer program to automatically reconstruct the parent grains from electron backscatter diffraction data. *J Appl Crystallogr.* 2007;40:1183–1188.
- [38] Rietveld HM. A profile refinement method for nuclear and magnetic structures. *J Appl Crystallogr.* 1969;2: 65–71.
- [39] Speer J, Matlock DK, De Cooman BC, et al. Carbon partitioning into austenite after martensite transformation. *Acta Mater.* 2003;51(9):2611–2622.
- [40] Forouzan F, Borasi L, Vuorinen E, et al. Optimization of quenching temperature to minimize the micro segregation induced banding phenomena in quenching and partitioning (Q&P) steels. *Steel Res Int.* 2019;90:1800281.
- [41] Jacques PJ, Allain S, Bouaziz O, et al. On measurement of retained austenite in multiphase TRIP steels – results of blind round robin test involving six different techniques. *Mater Sci Technol.* 2009;25(5): 567–574.
- [42] Talonen J, Aspegren P, Hänninen H. Comparison of different methods for measuring strain induced α -martensite content in austenitic steels. *Mater Sci Technol.* 2004;20(12):1506–1512.
- [43] Thomas G, Speer J, Matlock D, et al. Application of electron backscatter diffraction techniques to quenched and partitioned steels. *Microsc Microanal.* 2011;17(03):368–373.
- [44] Forouzan F, Vuorinen E, Mücklich F. Post weld-treatment of laser welded AHSS by application of quenching and partitioning technique. *Mater Sci Eng A.* 2017;698:174–182.
- [45] Sakakibara Y, Kubushiro K. Stress evaluation at the maximum strained state by EBSD and several residual stress measurements for plastic deformed austenitic stainless steel. *World J Mech.* 2017;7:195–210.
- [46] Yan S, Liu X, Liu WJ, et al. Comparison on mechanical properties and microstructure of a C–Mn–Si steel treated by quenching and partitioning (Q&P) and quenching and tempering (Q&T) processes. *Mater Sci Eng A.* 2015;620:58–66.
- [47] Sugimoto K, Usui N, Kobayashi M, et al. Effects of volume fraction and stability of retained austenite on ductility of TRIP-aided dual-phase steels. *ISIJ Int.* 1992;32(12):1311–1318.
- [48] Lee S, Matlock DK, Van Tyne CJ, et al. An empirical model for carbon diffusion in austenite incorporating alloying element effects. *ISIJ Int.* 2011;51(11): 1903–1911.
- [49] Yakubtsov IA, Purdy GR. Analyses of transformation kinetics of carbide-free bainite above and below the athermal martensite-start temperature. *Metall Mater Trans A.* 2012;43(2):437–446.
- [50] van Dijk NH, Butt AM, Zhao L, et al. Thermal stability of retained austenite in TRIP steels studied by synchrotron X-ray diffraction during cooling. *Acta Mater.* 2005;53(20):5439–5447.
- [51] Chen X, Vuorinen E, Grahm J. In-situ SEM observation on fracture behavior of austempered silicon alloyed steel. *China Foundry.* 2009;6(3):185–190.

- [52] Li HY, Lu XW, Li WJ, et al. Microstructure and mechanical properties of an ultrahigh-strength 40SiMnNiCr steel during the one-step quenching and partitioning process. *Metall Mater Trans A*. 2010;41(5):1284–1300.
- [53] Edmonds DV, He K, Rizzo FC, et al. Quenching and partitioning martensite – a novel steel heat treatment. *Mater Sci Eng A*. 2006;438–440:25–34.
- [54] Forouzan F, Guitart M, Vuorinen E, et al. Effect of carbon partitioning, carbide precipitation, and grain size on brittle fracture of ultra-high-strength, low-carbon steel after welding by a quenching and partitioning process. *Metals*. 2018;8(10):747.
- [55] Porter D, Easterling K, Sherif M. Phase transformations in metals and alloys (revised reprint). Boca Raton: CRC press; 2009.
- [56] Blondé R, Jimenez-Melero E, Zhao L, et al. Mechanical stability of individual austenite grains in TRIP steel studied by synchrotron X-ray diffraction during tensile loading. *Mater Sci Eng A*. 2014;618:280–287.
- [57] Chen X, Vuorinen E. In situ x-ray observation of bainitic transformation of austempered silicon alloyed steel. *J Mater Res*. 2009;24(4):1559–1566.
- [58] Caballero FG, Bhadeshia HKDH. Very strong bainite. *Curr Opin Solid State Mater Sci*. 2004;8(3):251–257.

